

97580

AISC E&R Library



8935

RR3186



**STRUCTURAL SYSTEMS
RESEARCH PROJECT**

Report No.
SSRP-2003/08

**DEVELOPMENT OF TESTING PROTOCOL
FOR SHORT LINKS IN ECCENTRICALLY
BRACED FRAMES**

by

**PAUL RICHARDS
CHIA-MING UANG**

Final Report Submitted to the American Institute of Steel
Construction

May 2003

Department of Structural Engineering
University of California, San Diego
La Jolla, California 92093-0085

University of California, San Diego
Department of Structural Engineering
Structural Systems Research Project

Report No. SSRP-2003/08

**Development of Testing Protocol for Short Links
in Eccentrically Braced Frames**

by

Paul Richards
Graduate Research Assistant

Chia-Ming Uang
Professor of Structural Engineering

Final Report Submitted to the American Institute of Steel Construction

Department of Structural Engineering
University of California, San Diego
La Jolla, California 92093-0085

May 2003

00929

ACKNOWLEDGEMENTS

The American Institute of Steel Construction provided funding for this research; Mr. Tom Schlafly was the project manager. Mr. James Malley and the AISC Solutions Center developed designs for the prototype structures. Professor Helmut Krawlinkler provided guidance and insight in the selection of ground motions and the development of the loading protocol. Professors Michael Engelhardt and Subhash Goel also provided helpful input on the project.

ABSTRACT

An analytical study was conducted to develop a loading protocol to be used for experimental testing of short links in eccentrically braced frames (EBFs). Past experimental studies have demonstrated that link rotation capacity is dependent on the loading protocol that is used in testing. There has been a shear link loading protocol specified in the AISC Seismic Provisions since 1997; however, it is a modified version of the SAC moment frame loading protocol without any study to justify it.

Three eccentrically braced frames with short shear links ($eV_p/M_p < 1.6$) were designed for the study. Models were developed for these frames and nonlinear time-history analysis was performed using Los Angeles ground motions scaled to match the design spectral acceleration for each frame. Critical links were identified from the models and analysis results from these links were used to establish parameters for a new loading protocol.

The analysis results indicated that the loading sequence in the AISC Seismic Provisions for testing links is too conservative for short shear links. It has 1.5 times the cumulative rotation demand and a higher percentage of large cycles than the analysis results indicate is necessary.

A new protocol was developed following the same methodology as used in creating the SAC moment frame loading history. The proposed loading protocol has more total cycles than the current AISC protocol; however, there are fewer large inelastic cycles and the cumulative rotation demand is significantly less.

00931

TABLE OF CONTENTS

ACKNOWLEDGEMENTS.....	i
ABSTRACT.....	ii
TABLE OF CONTENTS.....	iii
LIST OF TABLES.....	iv
LIST OF FIGURES.....	v
1 INTRODUCTION.....	1
1.1 Statement of Problem.....	1
2 MODEL DEVELOPMENT AND ANALYSIS.....	3
2.1 Prototype Buildings.....	3
2.2 Models.....	4
2.2.1 Beam, Column, and Brace Elements.....	4
2.2.2 Shear Link Elements.....	4
2.2.3 Gravity Loads and Seismic Masses.....	7
2.2.4 Damping.....	7
2.3 Modal and Pushover Analysis.....	7
2.4 Time-History Analysis.....	8
2.4.1 Earthquake Records.....	8
2.4.2 Analysis and Data Reduction.....	9
3 LOADING PROTOCOL DEVELOPMENT.....	28
3.1 Cumulative Damage Model.....	28
3.2 Response Parameters for Link Loading Protocol.....	29
3.3 Target Values for Demand Parameters.....	30
3.3.1 Governing Principles in Selecting Target Values.....	30
3.3.2 Determining Target Values.....	30
4 PROPOSED LINK LOADING PROTOCOL.....	41
4.1 Proposed Testing Protocol.....	41
4.2 Comparing the Proposed and Current Loading Protocols.....	41
5 SUMMARY AND CONCLUSIONS.....	46
REFERENCES.....	47
APPENDIX A—Results from Time-History Analyses Using Simplified Models.....	49
APPENDIX B—Results from Time-History Analyses Using SAC LA 10/50 Records.....	56
APPENDIX C—Rainflow Cycle Counting Procedure.....	67

LIST OF TABLES

Table 2.1 Summary of Link Design Values.....	10
Table 2.2 Gravity Loads Used for Building Models.....	11
Table 2.3 Seismic Masses Used for Building Models	11
Table 2.4 Modal Analysis Results	11
Table 2.5 LMSR (PEER) Ground Motion Records.....	12
Table 3.1 Summary of Demand Parameter Target Values	34
Table 4.1 Proposed Short Link Loading Protocol	43
Table 4.2 Comparing Protocol Demands with Target Values	43
Table B.1 Comparing Protocol Demands with Target Values	56
Table C.1 Rainflow Counting Results	70

LIST OF FIGURES

Figure 1.1 Failure Mode Observed in UTA Short Links.....	2
Figure 2.1 Plan Views of Prototype Buildings	13
Figure 2.2 Elevations of Eccentrically Braced Frames in 3-Story Building.....	14
Figure 2.3 Elevation of Frame 10	15
Figure 2.4 P-M Interaction Curve for Beam-Column Elements.....	16
Figure 2.5 Shear Link Element Proposed by Rahmadan and Ghoborah (1994).....	16
Figure 2.6 Comparing Methods of Modeling Beam Flexural Stiffness.....	17
Figure 2.7 Shear Link Element Used in Study	17
Figure 2.8 Representative Results from Correlation Study	18
Figure 2.9 Push-Over Analysis Results for Frame 3L.....	19
Figure 2.10 Push-Over Analysis Results for Frame 3T	20
Figure 2.11 Push-Over Analysis Results for Frame 10	21
Figure 2.12 Acceleration Time Histories of Unscaled Ground Motions	22
Figure 2.13 Design Spectra for 2 percent Damping	24
Figure 2.14 Response Spectra and Scaling Factors	25
Figure 2.15 Representative Link Data (First Story Link, Frame 3T, P04 Record).....	27
Figure 3.1 Demand Parameter Values for Links in Frame 3L.....	35
Figure 3.2 Demand Parameter Values for Links in Frame 3T.....	36
Figure 3.3 Demand Parameter Values for Links in Frame 10	37
Figure 3.4 Percentile Placing of the Total Number of Cycles, N_t	38
Figure 3.5 Percentile Placing of the Number of Inelastic Cycles, N_p	38
Figure 3.6 Percentile Placing of the Sum of the Rotation Ranges, $\Sigma\Delta\gamma_i$	38
Figure 3.7 Percentile Placing of the Maximum Rotation Range, $\Delta\gamma_{max}$	39
Figure 3.8 Percentile Placing of the Maximum Rotation, γ_{max}	39
Figure 3.9 Percentile Placing of the Second Largest Rotation Range, $\Delta\gamma_2$	39
Figure 3.10 Percentile Placing of the Third Largest Rotation Range, $\Delta\gamma_3$	40
Figure 3.11 Cumulative Distribution Function of Cycle Ranges, $\Delta\gamma_i$	40
Figure 4.1 Proposed Shear Link Loading Protocol.....	44

Figure 4.2	Comparing Loading Protocol CDFs with those from Frame 3T Links.....	45
Figure 4.3	Comparing Cumulative Ranges for Proposed and 2002 AISC Protocols.....	45
Figure A.1	Demand Parameter Values for Links in Frame 3L.....	50
Figure A.2	Demand Parameter Values for Links in Frame 3T.....	51
Figure A.3	Demand Parameter Values for Links in Frame 10.....	52
Figure A.4	Percentile Placing of the Total Number of Cycles, N_t	53
Figure A.5	Percentile Placing of the Number of Inelastic Cycles, N_p	53
Figure A.6	Percentile Placing of the Sum of the Rotation Ranges, $\Sigma\Delta\gamma_i$	53
Figure A.7	Percentile Placing of the Maximum Rotation Range, $\Delta\gamma_{\max}$	54
Figure A.8	Percentile Placing of the Maximum Rotation, γ_{\max}	54
Figure A.9	Percentile Placing of the Ratio of $\Delta\gamma_2$ to $\Delta\gamma_{\max}$	54
Figure A.10	Percentile Placing of the Ratio of $\Delta\gamma_3$ to $\Delta\gamma_{\max}$	55
Figure A.11	Cumulative Distribution Function of Cycle Ranges, $\Delta\gamma_i$	55
Figure B.1	SAC Los Angeles 10/50 Ground Motion Acceleration Time Histories.....	57
Figure B.2	Response Spectra for SAC Los Angeles Ground Motions (2 percent damping).....	59
Figure B.3	Demand Parameter Values for Links in Frame 3L.....	61
Figure B.4	Demand Parameter Values for Links in Frame 3T.....	62
Figure B.5	Demand Parameter Values for Links in Frame 10.....	63
Figure B.6	Percentile Placing of the Total Number of Cycles, N_t	64
Figure B.7	Percentile Placing of the Number of Inelastic Cycles, N_p	64
Figure B.8	Percentile Placing of the Sum of the Rotation Ranges, $\Sigma\Delta\gamma_i$	64
Figure B.9	Percentile Placing of the Maximum Rotation Range, $\Delta\gamma_{\max}$	65
Figure B.10	Percentile Placing of the Maximum Rotation, γ_{\max}	65
Figure B.11	Percentile Placing of the Ratio of $\Delta\gamma_2$ to $\Delta\gamma_{\max}$	65
Figure B.12	Percentile Placing of the Ratio of $\Delta\gamma_3$ to $\Delta\gamma_{\max}$	66
Figure B.13	Cumulative Distribution Function of Cycle Ranges, $\Delta\gamma_i$	66
Figure C.1	Example Rotation Time History.....	68
Figure C.2	Reordering Rotation Time History.....	68
Figure C.3	Identification of Peaks and Valleys.....	69
Figure C.4	Counting Cycles in Record.....	69

Figure C.5 Counting Final Cycle..... 70
Figure C.6 Resulting Symmetric Cycles from Rainflow Counting..... 70

1 INTRODUCTION

1.1 Statement of Problem

Steel eccentrically braced frames, EBFs, have been a popular alternative to moment frames and concentrically braced frames since their introduction to practice in the early 1980's. EBFs provide high initial elastic stiffness as well as ductile response under extreme loading (Roeder and Popov 1977). The successful performance of EBFs under seismic loading depends on stable inelastic rotation of active links while other frame components remain essentially elastic. Current design provisions (AISC 2002) for active links are based primarily on a series of experimental studies conducted at the University of California, Berkeley (UCB) in the 1980's with links of A36 steel (Hjelmstad and Popov 1983; Malley and Popov 1983; Kasai and Popov 1986; Ricles and Popov 1987; Engelhardt and Popov 1989).

In 2001-2002, AISC sponsored a study to investigate the effects of higher strength steel ($F_y = 50$ ksi) on the performance of rolled section links in eccentrically braced frames. Experimental work was conducted at the University of Texas, Austin (UTA) and analytical work was performed at the University of California, San Diego (UCSD). During the experimental testing, most of the short links ($eV_p/M_p < 1.6$) failed to reach 0.08 rad inelastic rotation, which is the design value permitted in the AISC Seismic Provisions based on UCB studies. The most common failure mode of the UTA short links was one not previously observed in link testing, where horizontal fractures propagated out from the termination of stiffener-to-web fillet welds as shown in Figure 1.1 (Arce 2002).

An analytical investigation of the failures found that close stiffener spacing may explain this mode of failure, while the loading protocol may have been responsible for links failing to reach 0.08 rad inelastic rotation prior to failure (Richards and Uang 2002). The UCB links from the 1980's were tested under a variety of loading protocols. The UTA links (Arce 2002) were tested with a protocol, first specified in the 1997 AISC Seismic Provisions, which requires more cycles and more cumulative rotation to reach 0.08 rad inelastic rotation than did any of the earlier UCB protocols.

The objecting of this study was to investigate the rotation demands on short links in eccentrically braced frames under design earthquake loading and develop a loading protocol for experimental link testing that reflects those demands. Additional work remains to be conducted to determine rotation demands for longer links ($eV_p/M_p > 1.6$).

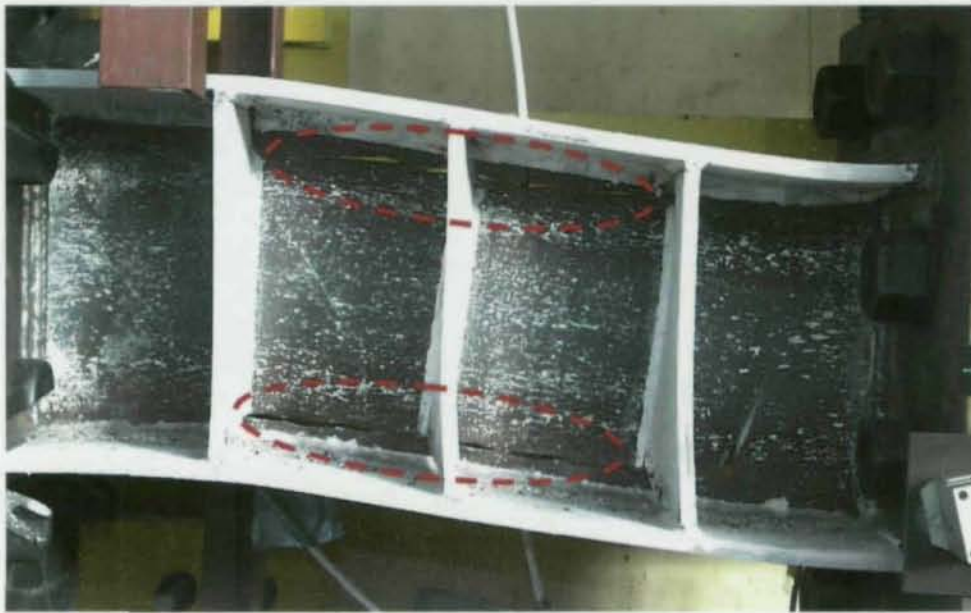


Figure 1.1 Failure Mode Observed in UTA Short Links
(Specimen 4a, Arce 2002)

2 MODEL DEVELOPMENT AND ANALYSIS

2.1 Prototype Buildings

Two prototype eccentrically braced buildings, one 3 stories and one 10 stories, were designed by the AISC Steel Solution Center with direction from Mr. James Malley. Figure 2.1 shows the plan views of the two buildings with the bay dimensions, column orientation, and EBF bays indicated. These buildings were similar in dimension and gravity loading to buildings used for moment frame analysis in the SAC project (Gupta and Krawinkler 1999).

The 3-story building had two different EBFs, one for longitudinal loading ("Frame 3L") and the other for transverse loading ("Frame 3T"). The elevations of these two frames are shown in Figure 2.2 with the member sizes and support conditions indicated. A few of the column sections in Frame 3L were modified from the prototype design for the analysis. The original column sections are indicated in parentheses (see Section 2.3 for explanation). Column bases in both 3-story frames were considered as pinned. The 10-story building had the same EBF in both directions, resulting in one prototype 10-story frame ("Frame 10"). The elevation of Frame 10 is shown in Figure 2.3. The column bases in the 10-story frame were considered as fixed.

The links in the EBFs of each frame were sized to have similar demand/capacity ratios under the design earthquake load to encourage distributed rather than concentrated link yielding (Popov et al. 1992). Table 2.1 summarizes the links sizes, non-dimensional lengths, and demand/capacity ratios. The nature of EBF design tends to result in low shear demand/capacity ratios. This is because the link shear under the design seismic loading, dictates a required web area, but in order to provide a short link, a section with a large M_p/V_p must be selected. Many sections with large M_p/V_p are disqualified by the current flange width/thickness requirement in the provisions (AISC 2002). The challenge to find suitable sections can result in actual web areas somewhat greater than the required. Recent studies suggest the flange width/thickness requirement for links can be relaxed (Arce 2002; Richards and Uang 2002).

2.2 Models

Models for the three frames (3L, 3T, and 10) were developed and analyzed with DRAIN-2DX (Prakash et al. 1993). Beam and column centerlines were used to define model geometry. Panel zone shears in EBFs are typically much lower than those in moment resisting frames, therefore panel zones were not modeled explicitly and panel zone rotations neglected. Connections in the eccentrically braced bays were considered as rigid while connections in the other bays were modeled as simple (see Figures 2.2 and 2.3). Rigid zones were included at the ends of beams and links to account for column depth.

2.2.1 Beam, Column, and Brace Elements

Beams, beam segments outside of the shear links, braces, and columns were all modeled as beam-columns. The beam-column element used consists of an elastic beam, two rigid-plastic hinges, and rigid end zones. The axial force-moment yield surface used for the beam-columns is illustrated in Figure 2.4. A yield stress of 55 ksi was used throughout in the model. Beam, column, and brace elements had post-yield stiffness equal to 5 percent of the elastic stiffness. Significant yielding in members other than the links was not anticipated or realized during the time-history analyses.

2.2.2 Shear Link Elements

Shear links were modeled using a technique similar to that proposed by Ramadan and Ghobarah (1995) but with some modifications. Ramadan and Ghobarah's approach is based on theory developed by Ricles and Popov (1994) and results in a simplified version of the element created by Ricles and Popov, which can be incorporated in general analysis programs. Modifications had to be made to Ramadan and Ghobarah's method to correctly model the elastic stiffness of the links.

Element Proposed by Ramadan and Ghobarah (1995)

Figure 2.5(a) illustrates the link element proposed by Ramadan and Ghobarah (1995) which consists of an elastic beam with translational and rotational springs at either end. Two nodes at each end of the link, referred to as the external and internal nodes, are defined to have the same coordinates. The elastic beam connects the internal nodes on either end of the link. Moment and shear hinging in the link is modeled by rotational and translational springs that couple the rotational and vertical translational degrees of freedom of the external and

internal nodes. Three translational and three rotational springs operate in parallel at each end in order to achieve multi-linear force deformation relationships using bilinear spring elements. The horizontal displacement of each internal node is constrained to equal that of the corresponding external node. Link rotation is calculated as the vertical distance between the external nodes divided by the length of the link.

Individual spring properties are calculated such that the combined force-deformation relationships of the springs at either end correspond to those indicated in Figure 2.5(b). The yield points and post-yield stiffnesses, which define the shear-force-deformation and bending-moment-rotation relationships shown in the figure, were calibrated using results from UCB tests on A36 links. Post-yield stiffness is modeled with kinematic hardening in the rotational springs, and both isotropic and kinematic hardening in the translational springs.

Conceptually, the element proposed by Ramadan and Ghobarah is sound. However the elastic shear and flexural stiffness is accounted for twice in the model, once in the elastic beam and again in the elastic stiffness of the rotational and translational springs, resulting in inaccurate elastic stiffness.

Modified Element Used in This Study

Since the elastic stiffness is accounted for twice in the Ramadan and Ghobarah's element, the element should be modified by removing elastic stiffness from either the beam or the springs. The elastic *shear* stiffness can easily be removed from the beam element, by specifying no shear deformation. Some modification of the springs is still needed, though. Ramadan and Ghobarah (1995) gives an elastic stiffness for the translational springs of GA_{shear}/e [Figure 2.5(b)]. However, the springs on either end should have a stiffness, K_{VI} , of $2GA_{shear}/e$ because the translational springs on either end of the link operate in series with each other, and the combined elastic stiffness of the springs on both ends becomes GA_{shear}/e .

In contrast to the elastic *shear* stiffness, the elastic *flexural* stiffness cannot be removed from the beam and lumped in the rotational springs without introducing errors. Figure 2.6 compares the stiffness matrix of a standard elastic beam element (neglecting shear and axial deformations) with that of a rigid beam with flexural stiffness modeled using rotational springs on either end. The four terms that are different in the two cases are highlighted. Under shear loading or loading with equal end moments, the two elements give identical results. However, under unequal or opposite end moments (typical under gravity loads)

discrepancies arise and the rigid-beam-with-springs element does not have the correct stiffness.

In light of difficulties associated with removing the elastic stiffness from the beam, it is more reasonable to keep the beam elastic in bending and remove the elastic stiffness from the rotational springs. Since the standard beam element already has rigid-plastic hinges built in, the rotational springs can be eliminated altogether. Multi-linear hardening for the moment hinges was not deemed necessary, because this study is concerned only with short links which experience only minor flexural hinging, so a single standard beam element was sufficient.

Figure 2.7(a) illustrates the link element used in this studied, which is a modified version of the concept proposed by Ramadan and Ghobarah (1995). The translational spring force-deformation behavior on either end is illustrated in Figure 2.7(b). The yield points and post-yield stiffnesses were calibrated based on the recent UTA link tests with A992 steel. The flexural hinges were defined to yield at M_p of the link (calculated using the expected yield strength, 55 ksi). The post-yield *flexural* stiffness of the link was equal to 5 percent of the elastic flexural stiffness.

To verify this link modeling approach, the UTA link test set-up (Arce 2002) was modeled in DRAIN2DX and a correlation study was performed. Each of the UTA tests was simulated, with the links modeled as described above. Figure 2.8 compares the analytical and experimental results for some of the UTA links. Similar correlation was observed for all of the links and validates the link modeling technique. The correlation study indicated that link behavior can be reasonably modeled with only kinematic hardening in the translational springs (rather than combined isotropic and kinematic), although some accuracy is lost in small initial cycles.

Simplified Modeling Technique

Whittaker et al. (1987) used a much simpler approach in modeling a six-story EBF frame with links in the chevron-braced configuration. In the model, shear links were standard beam elements with the moment hinges calibrated to yield when the nominal shear strength was reached. This approach is theoretically sound if the end moments of the link are equal and the post-yield stiffness of the moment hinges is properly calibrated.

The equal end moment assumption is reasonable for links in the chevron-braced configuration, but unequal end moments tend to occur in links adjacent to columns. Although the end moments were not initially equal for the frames in this study, they did tend to balance after minor yielding. To investigate the effect of modeling links in this simplified way, additional models were developed using this approach (see Appendix A) and analyzed for comparison with the more refined modeling techniques. Overall results using this simplified technique were very close to those obtained with the more precise modeling.

2.2.3 Gravity Loads and Seismic Masses

The gravity loads and seismic masses used in the models were the same as those used for the models in the SAC moment frame study (Gupta and Krawinkler 1999). Un-factored loads and masses are given in Tables 2.2 and 2.3. A gravity load combination of $1.2D+0.5L$ (ICC 2000) was applied to the structures during the static nonlinear pushover, or time-history analyses (Sections 2.3 and 2.4). The gravity loads for the half of the structure associated with each frame, but not acting directly on it, were applied to a P-delta column.

2.2.4 Damping

Ricles and Popov (1994) demonstrated that viscous damping in link elements may result in unrealistically high brace forces and suggested that nonproportional damping may be more appropriate for eccentrically braced frames than traditional Rayleigh damping. Nonproportional viscous damping was used in the models, where all elements except for the links had viscous damping. Damping coefficients were based on 2 percent damping in the first mode (see Section 2.3) and at a period of 0.2 seconds for each frame.

2.3 Modal and Pushover Analyses

Natural periods determined from modal analyses are indicated in Table 2.4. For reference, the period calculated using an empirical formula (Equation 16-39) in the International Building Code (ICC 2000) is also indicated.

A pushover analysis was performed for each of the three frames. The base shear was distributed as specified in the IBC (ICC 2000). Part (a) in Figures 2.9-2.11, shows the base shear versus roof displacement for each of the frames. The formation of hinges is indicated on the load-displacement curves. An abscissa on the top of each plot indicates the drift at the

roof. An ordinate on the right indicates the base shear normalized by the weight of the building associated with each frame (one half the total building weight). Labels in Part (b) of Figures 2.9-2.11 indicate the sequence of shear and flexural hinge formation.

The initial pushover analyses of Frame 3L indicated some undesirable column yielding, prior to the development of significant link rotation, in the first and second story columns of the right EBF bays. Yielding was the result of high axial forces and bending moments in the columns. It should be noted that during the pushover analysis all of the links eventually yield and reach ultimate strength, representing a worst-case situation. Since the purpose of this study was to investigate link rotations and it is generally presumed that the columns will not experience significant yielding, the column sizes were simply increased in the models to preclude any premature column yielding. Although only two of the columns had problems, all of the large columns were increased in size for consistency. The results shown in Figure 2.9 are for the model that has the modified columns.

For all of the buildings the base shear at yield was greater than the design base shear, by a degree that might be expected from the demand/capacity ratios of the links (see Table 2.1). Links began to reach 0.08 rad inelastic rotation at roof drifts between 1.0 and 1.3 percent in the models. Frame 3L, with significant gravity loads as compared to the others, had links reach design rotation at the lowest roof drift.

2.4 Time-history Analysis

2.4.1 Earthquake Records

The suite of ground motions used for the development of the loading protocol consisted of twenty LMSR (large magnitude, M, small distance, R) Los Angeles records that have been used in recent PEER projects (Krawinkler et al. 2003; Medina 2003). The motions are referred to as P01-P20 herein. Table 2.5 provides information on these time histories. Figure 2.12 shows the acceleration time histories of the un-scaled records.

Each record was scaled differently for each frame. Scale factors were calculated to make the spectral acceleration of each record, with 2 percent damping, equal to the design spectral acceleration, with 2 percent damping, at the period of each frame. The 2 percent damping design spectra was obtained by adjusting the 1997 UBC, Soil Type D spectra (ICBO 1997), which is for 5 percent damping, using the scaling procedure in FEMA 356

(FEMA 2000). Figure 2.13 illustrates the original and scaled design spectra. Figure 2.14 shows the response spectra of the un-scaled records with the 2 percent damping design spectra and the calculated values of the scaling factors for each frame.

A separate group of analyses were also performed with the twenty Los Angeles ground motions used in the SAC project, representing events with 10 percent probability of exceedance in 50 years (Somerville et al. 1997); this set of records contained some near-source ground motions. These ground motions and results from those analyses are presented in Appendix B. Results were similar to those obtained using the PEER records.

2.4.2 Analysis and Data Reduction

Each of the models was analyzed using each of the twenty specially scaled ground motion records. Link rotations were calculated at each step of the time-history analysis using the coordinates of the link ends. Rotation time histories were generated for the links in all three frames under all 20 ground motions. Figure 2.15(a) shows a typical link rotation time history from a first story link of Frame 3T under the P04 ground motion. Figure 2.15(b) shows the link shear versus rotation hysteresis for the same link. The link rotation histories were the only necessary data for the development of the loading protocol.

The link rotation time histories needed to be converted into series of cycles, before they could be used for loading protocol development. The simplified rainflow cycle counting method, used by Krawinkler et al. (2000) in the SAC study, was used. This technique is described in Appendix C. When mean effects are not considered, the rainflow cycle counting process results in a number of symmetric cycles defined by their range (change in deformation from peak to peak). Figure 2.15(c) shows cycles calculated from the rotation time history in Figure 2.15(a). All of the link rotation time history data was reduced in this way, so that for each link in each frame under each seismic event there was an associated sequence of symmetric cycles ordered with decreasing rotation range.

Table 2.1 Summary of Link Design Values

Frame	Story	Section	Non-Dimensional Length (eV_p/M_p)	$\frac{V_u}{\phi_v V_n}$
3L	1 st	18×86	1.07	0.55
	2 nd	14×82	1.15	0.59
	3 rd	10×68	1.21	0.55
3T	1 st	16×77	1.13	0.68
	2 nd	14×74	1.13	0.70
	3 rd	10×45	1.41	0.77
10	1 st	14×74	1.08	0.72
	2 nd	18×106	1.03	0.77
	3 rd	16×77	1.11	0.74
	4 th	14×82	1.13	0.79
	5 th	14×82	1.15	0.75
	6 th	14×74	1.12	0.80
	7 th	14×68	1.14	0.77
	8 th	10×68	1.21	0.80
	9 th	12×45	1.43	0.73
	10 th	10×45	1.41	0.50

Table 2.2 Gravity Loads Used for Building Models

Load Type	Load (psf)
Floor dead load for weight calculations	96
Floor dead load for mass calculations	86
Roof dead load	83
Reduced live load per floor and for roof	20

Table 2.3 Seismic Masses Used for Building Models

Location	Seismic Mass ^a (kip-sec ² /ft)
3-story Structure: 1 st and 2 nd Stories	65.53
3-story Structure: 3 rd Story	70.90
10-story Structure: 1 st Story	38.62
10-story Structure: 2 nd -9 th Story	67.86
10-story Structure: 10 th Story	73.10

^aValues for entire building

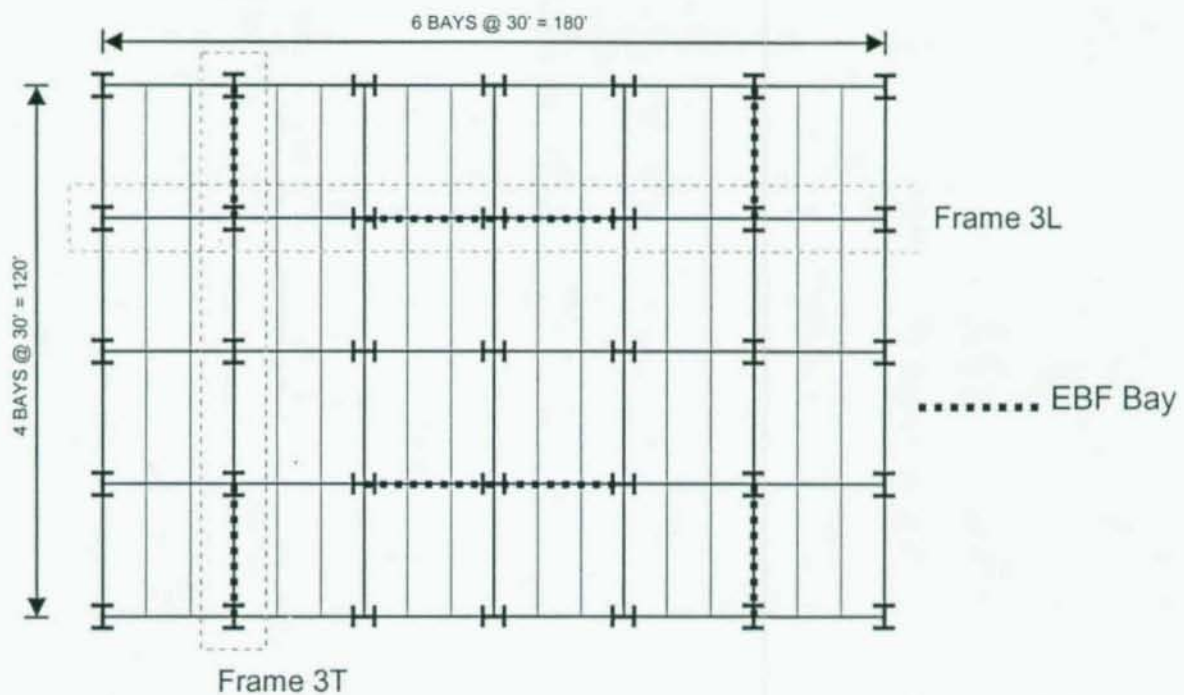
Table 2.4 Modal Analysis Results

Frame	T ₁ (sec)	T ₂ (sec)	T ₃ (sec)	T ₄ (sec)	T ₅ (sec)
3L	0.514 (0.468) ^a	0.209	0.190	-	-
3T	0.617 (0.468)	0.239	0.172	-	-
10	2.100 (1.182)	0.673	0.354	0.248	0.211

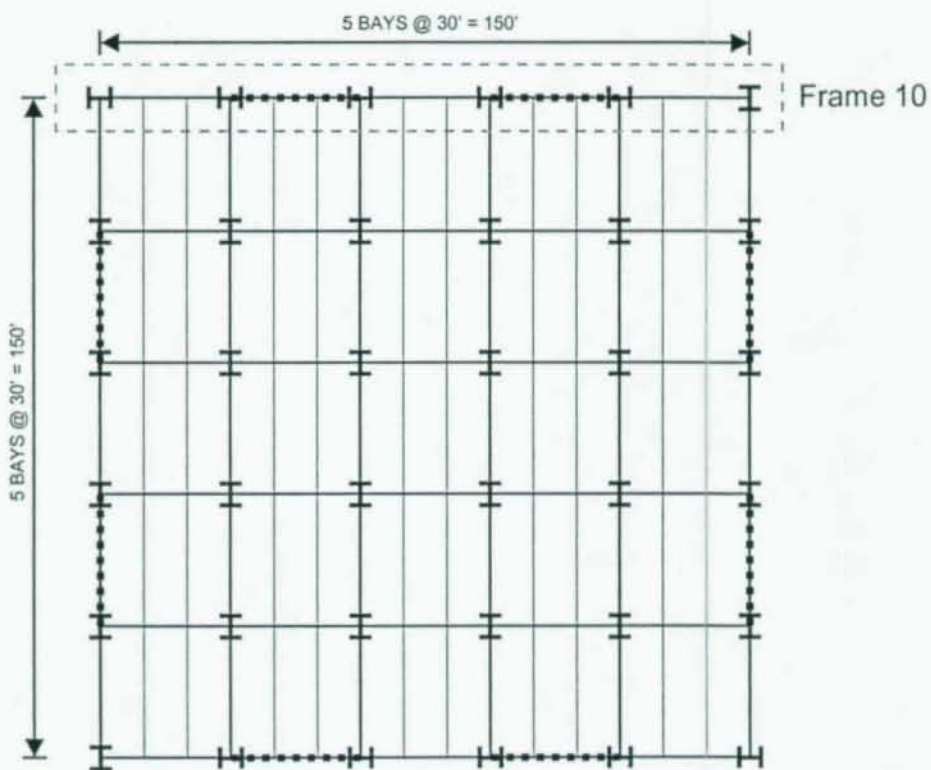
^aValues in parentheses calculated using $T_a = (0.030)h_n^{3/4}$

Table 2.5 LMSR (PEER) Ground Motion Records

Name	Event	Year	Station	R (km)	PGA (g)	Duration (sec)
P01	Loma Prieta	1989	Agnews State Hospital	28.2	0.172	40.0
P02	Loma Prieta	1989	Capitola	14.5	0.443	40.0
P03	Loma Prieta	1989	Gilroy Array # 3	14.4	0.367	39.9
P04	Loma Prieta	1989	Gilroy Array # 4	16.1	0.212	40.0
P05	Loma Prieta	1989	Gilroy Array # 7	24.2	0.226	40.0
P06	Loma Prieta	1989	Hollister City Hall	28.2	0.247	39.1
P07	Loma Prieta	1989	Hollister Differential Array	25.8	0.279	39.6
P08	Loma Prieta	1994	Sunnyvale-Colton Ave.	28.8	0.207	39.3
P09	Northridge	1994	Canoga Park – Topanga Can.	15.8	0.420	25.0
P10	Northridge	1994	LA – N Faring Rd	23.9	0.237	30.0
P11	Northridge	1994	LA – Fletcher Dr.	29.5	0.240	30.0
P12	Northridge	1994	Glendale – Las Palmas	25.4	0.206	30.0
P13	Northridge	1994	LA – Hollywood Store FF	25.5	0.231	40.0
P14	Northridge	1994	La Crescenta – New York	22.3	0.159	30.0
P15	Northridge	1994	Northridge – 17645 Saticoy St.	13.3	0.368	30.0
P16	San Fernando	1971	LA – Hollywood Store Lot	21.2	0.174	28.0
P17	Superstition Hills	1987	Brawley	18.2	0.156	22.1
P18	Superstition Hills	1987	El Centro Imp. Co. Cent	13.9	0.358	40.0
P19	Superstition Hills	1987	Plaster City	21.0	0.186	22.2
P20	Superstition Hills	1987	Westmoreland Fire Station	13.3	0.172	40.0

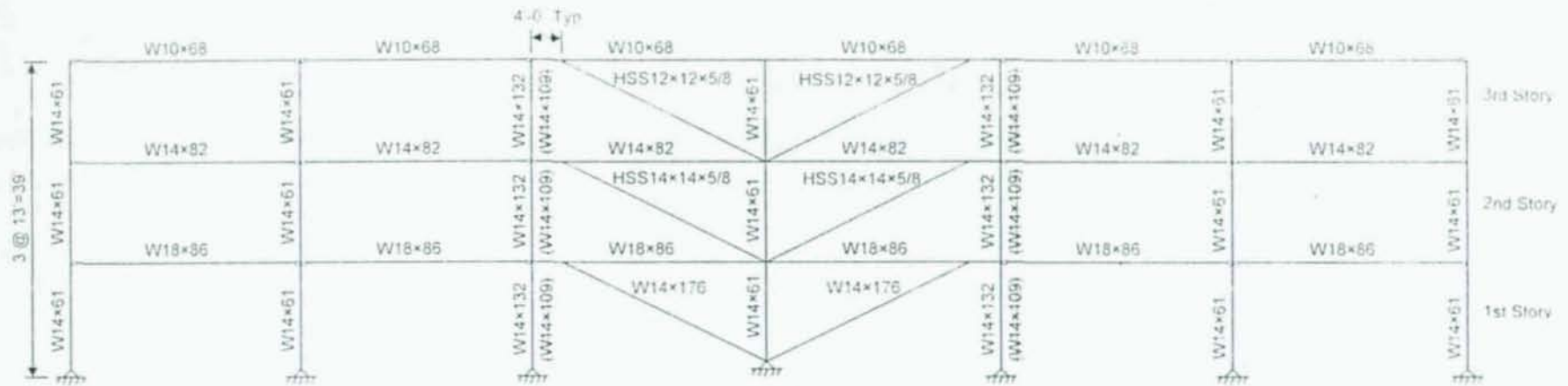


(a) 3-Story Building

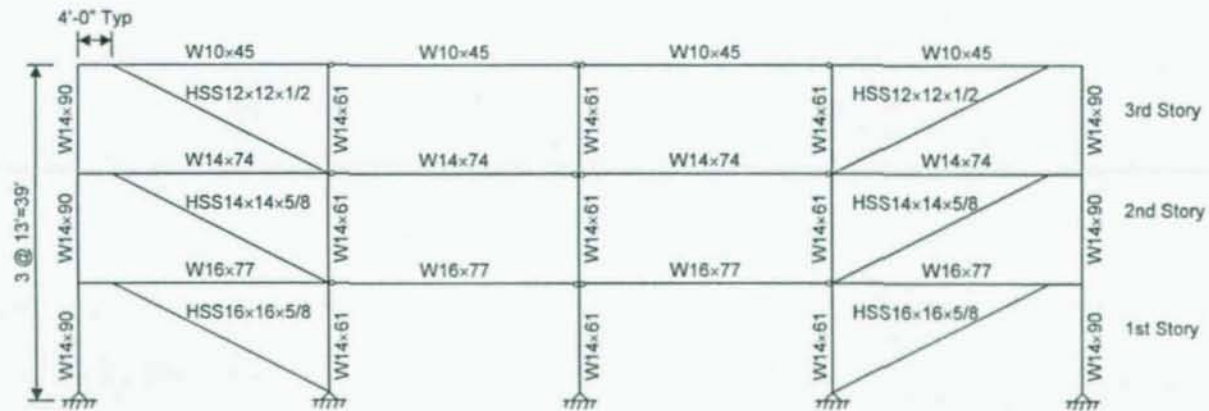


(b) 10-Story Building

Figure 2.1 Plan Views of Prototype Buildings



(a) Frame 3L



(b) Frame 3T

Figure 2.2 Elevations of Eccentrically Braced Frames in 3-Story Building

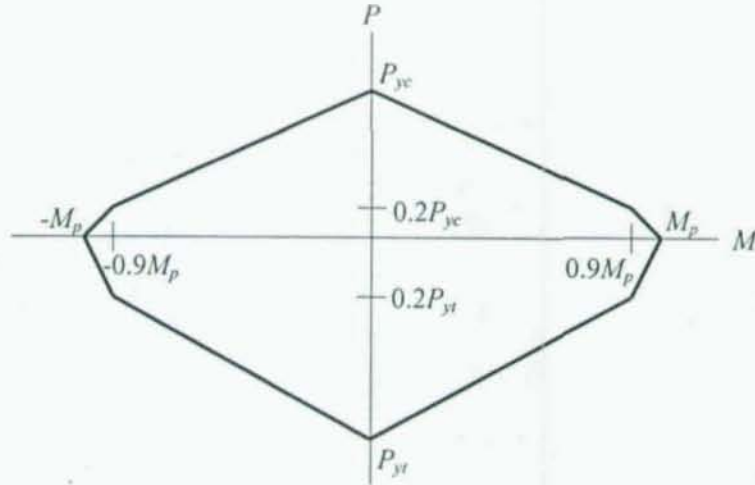
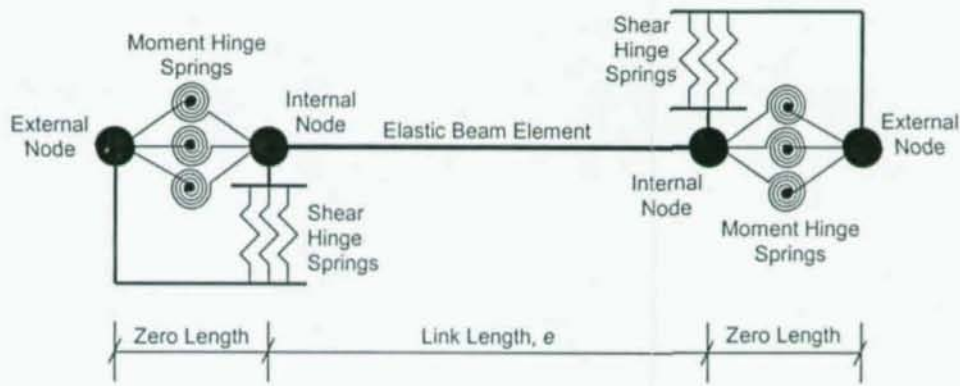
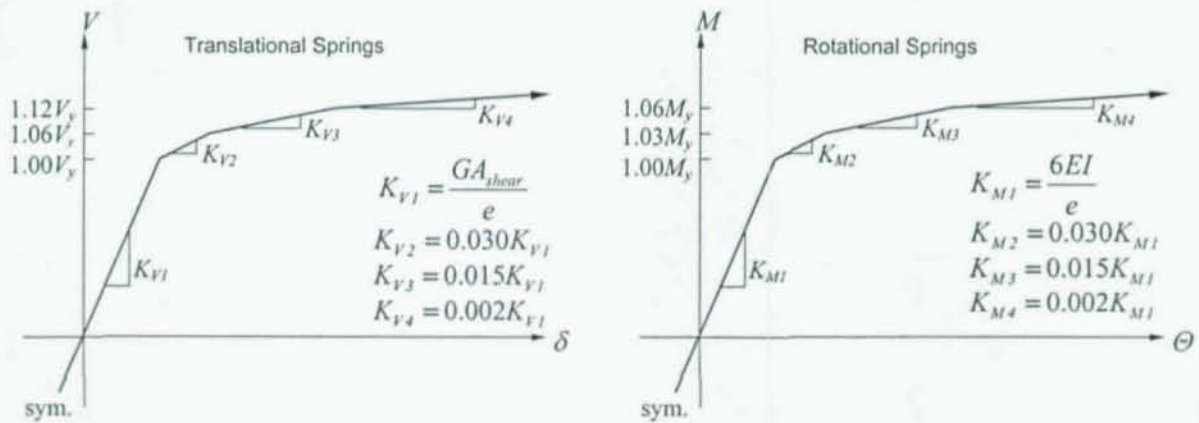


Figure 2.4 P-M Interaction Curve for Beam-Column Elements

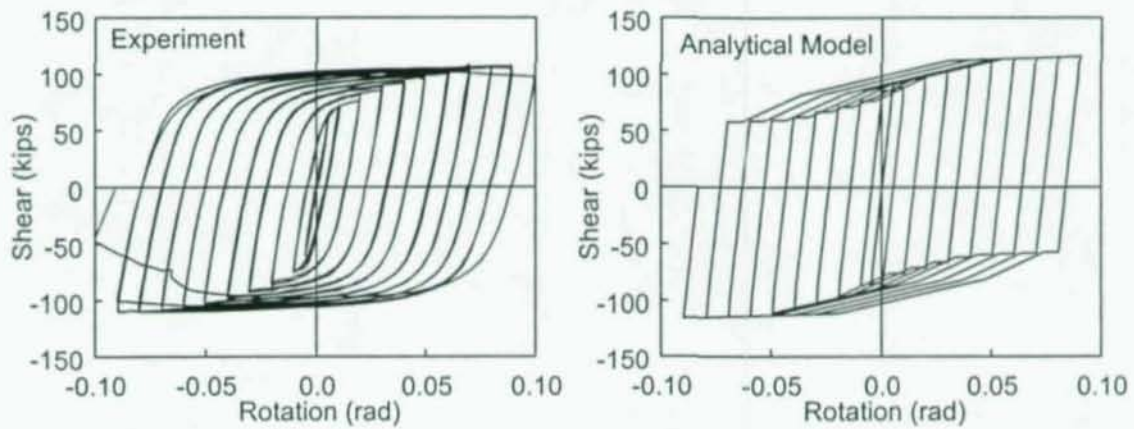


(a) Schematic

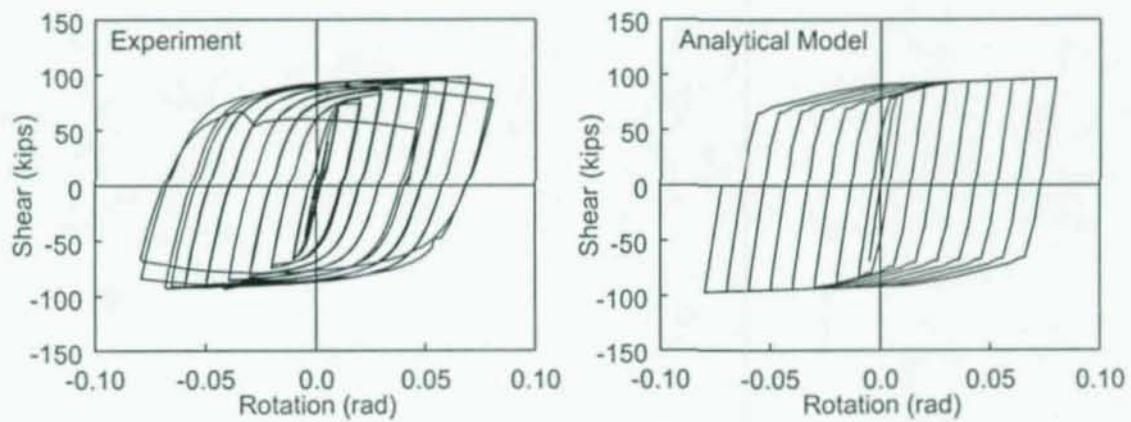


(b) Combined Spring Action at Each End

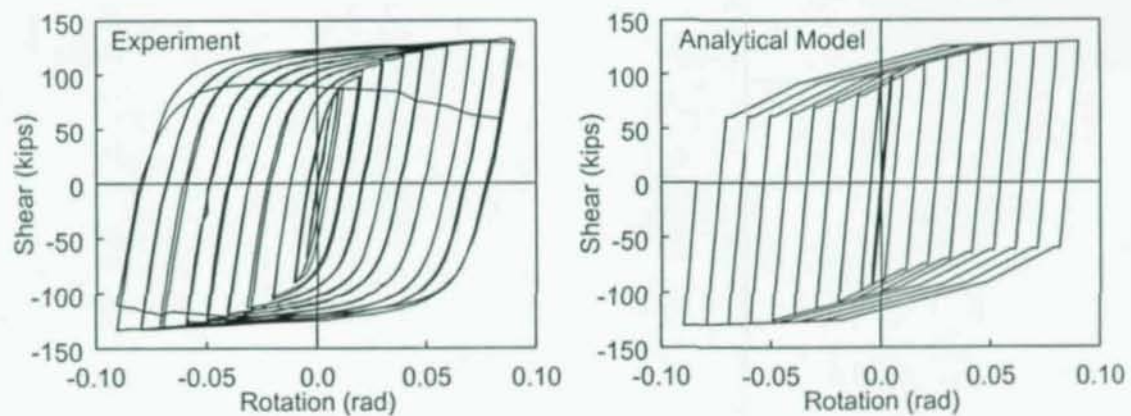
Figure 2.5 Shear Link Element Proposed by Rahmadan and Ghorah (1995)



(a) UTA Specimen 1C

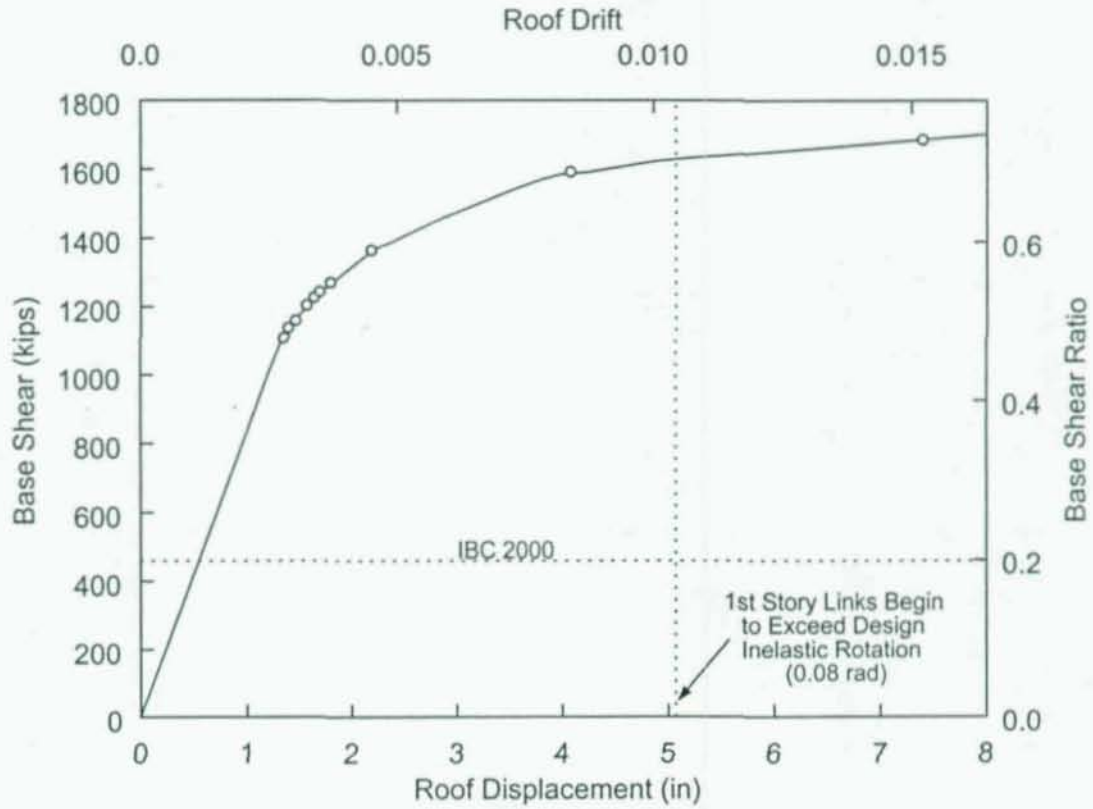


(b) UTA Specimen 2

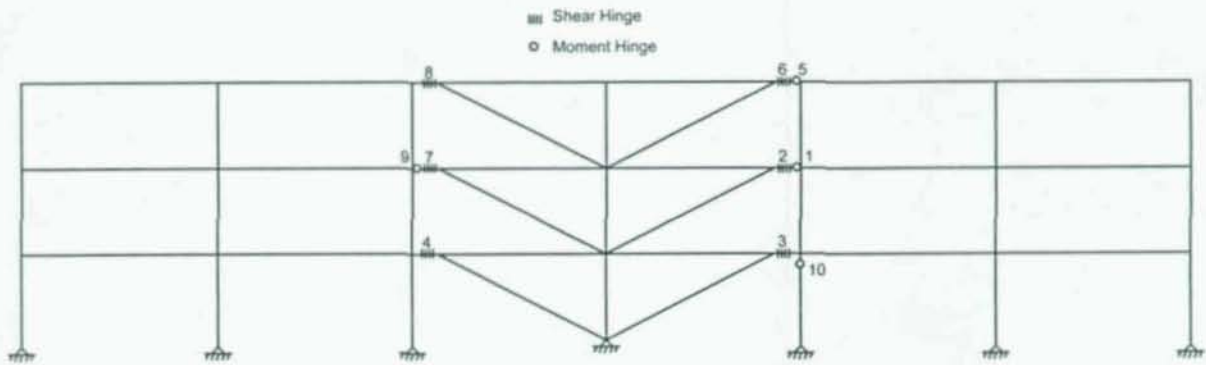


(c) UTA Specimen 4C

Figure 2.8 Representative Results from Correlation Study

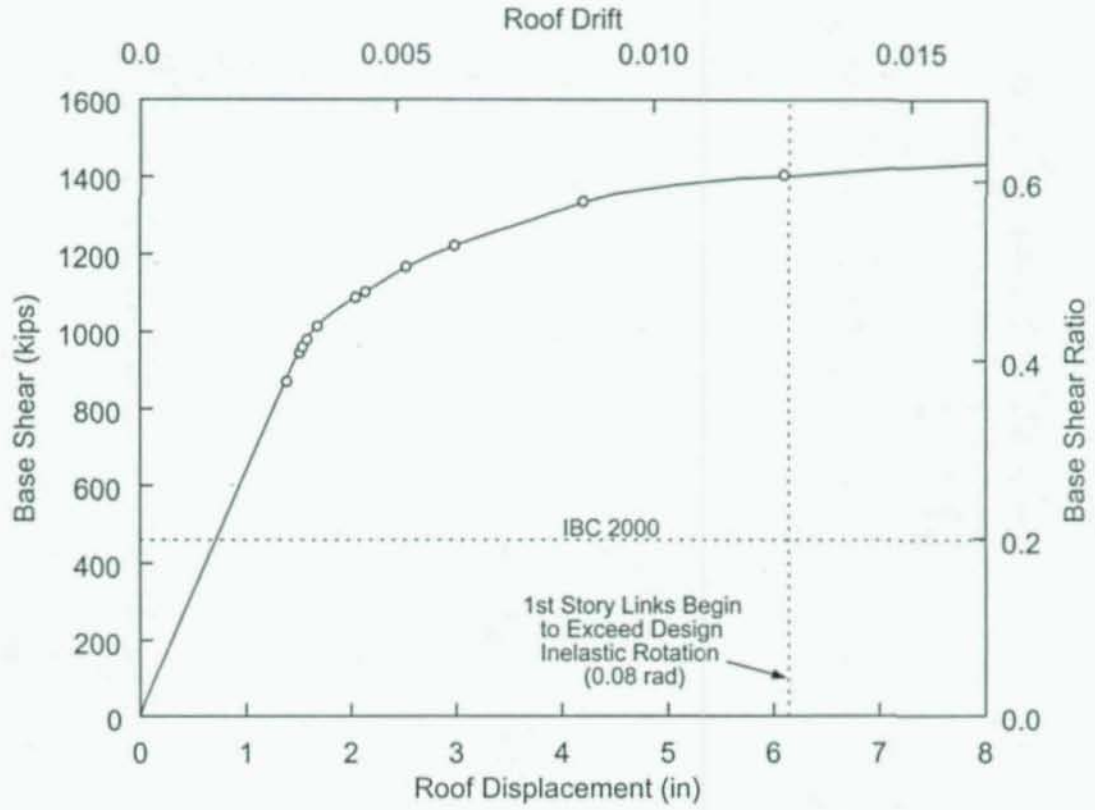


(a) Base Shear versus Roof Displacement

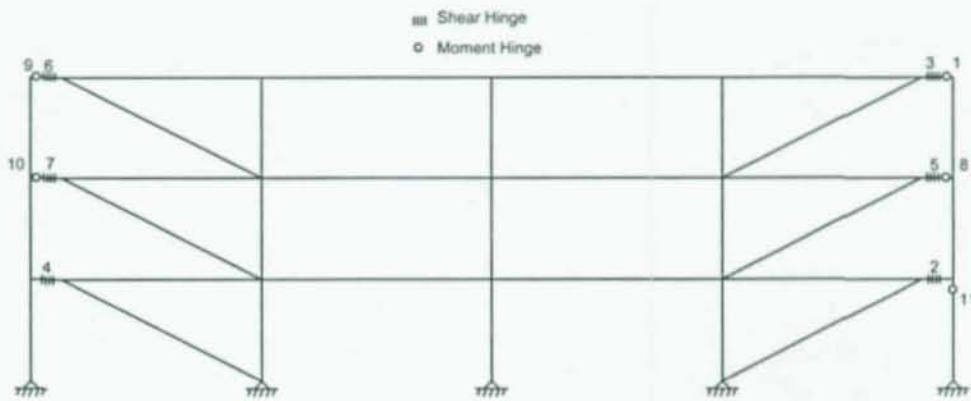


(b) Sequence of Plastic Hinge Formation

Figure 2.9 Push-Over Analysis Results for Frame 3L

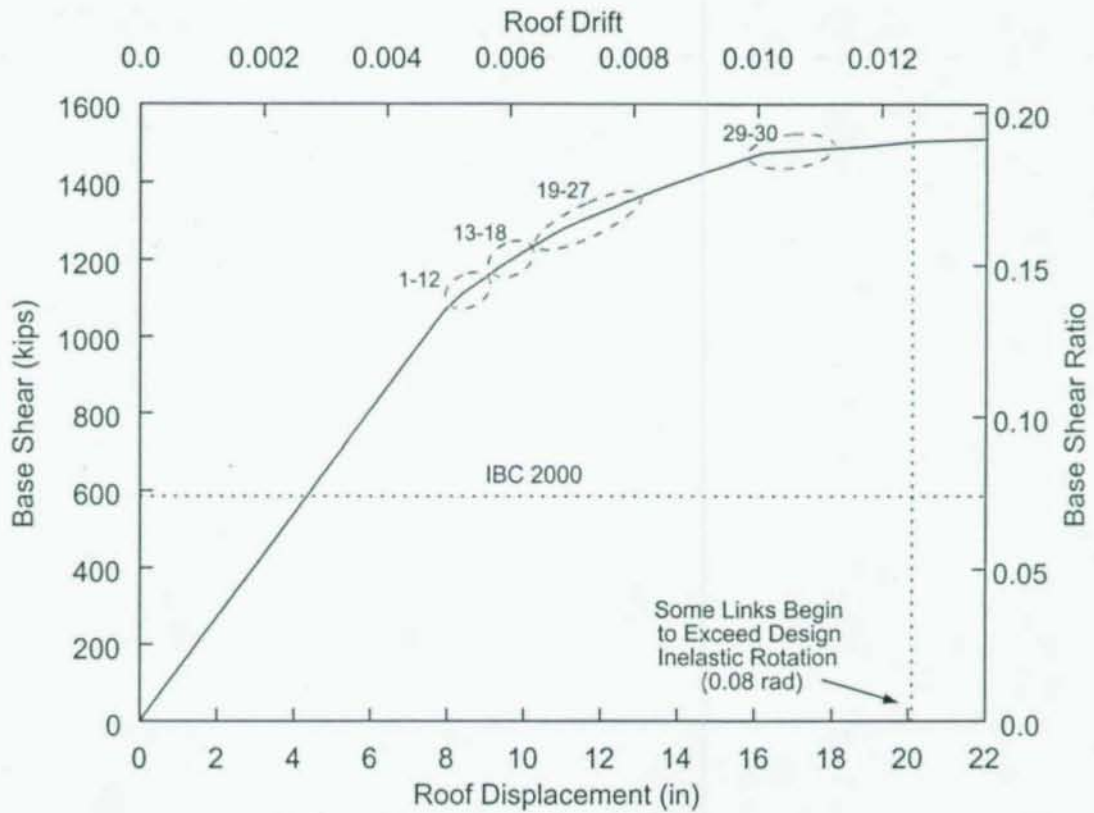


(a) Base Shear versus Roof Displacement



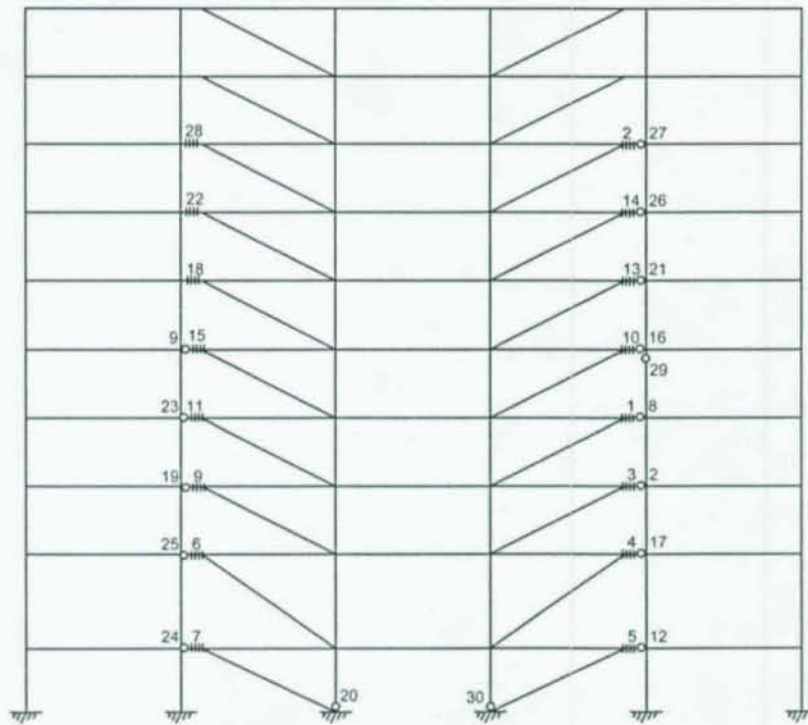
(b) Sequence of Plastic Hinge Formation

Figure 2.10 Push-Over Analysis Results for Frame 3T



(a) Base Shear versus Roof Displacement

▤ Shear Hinge
○ Moment Hinge



(b) Sequence of Plastic Hinge Formation

Figure 2.11 Push-Over Analysis Results for Frame 10

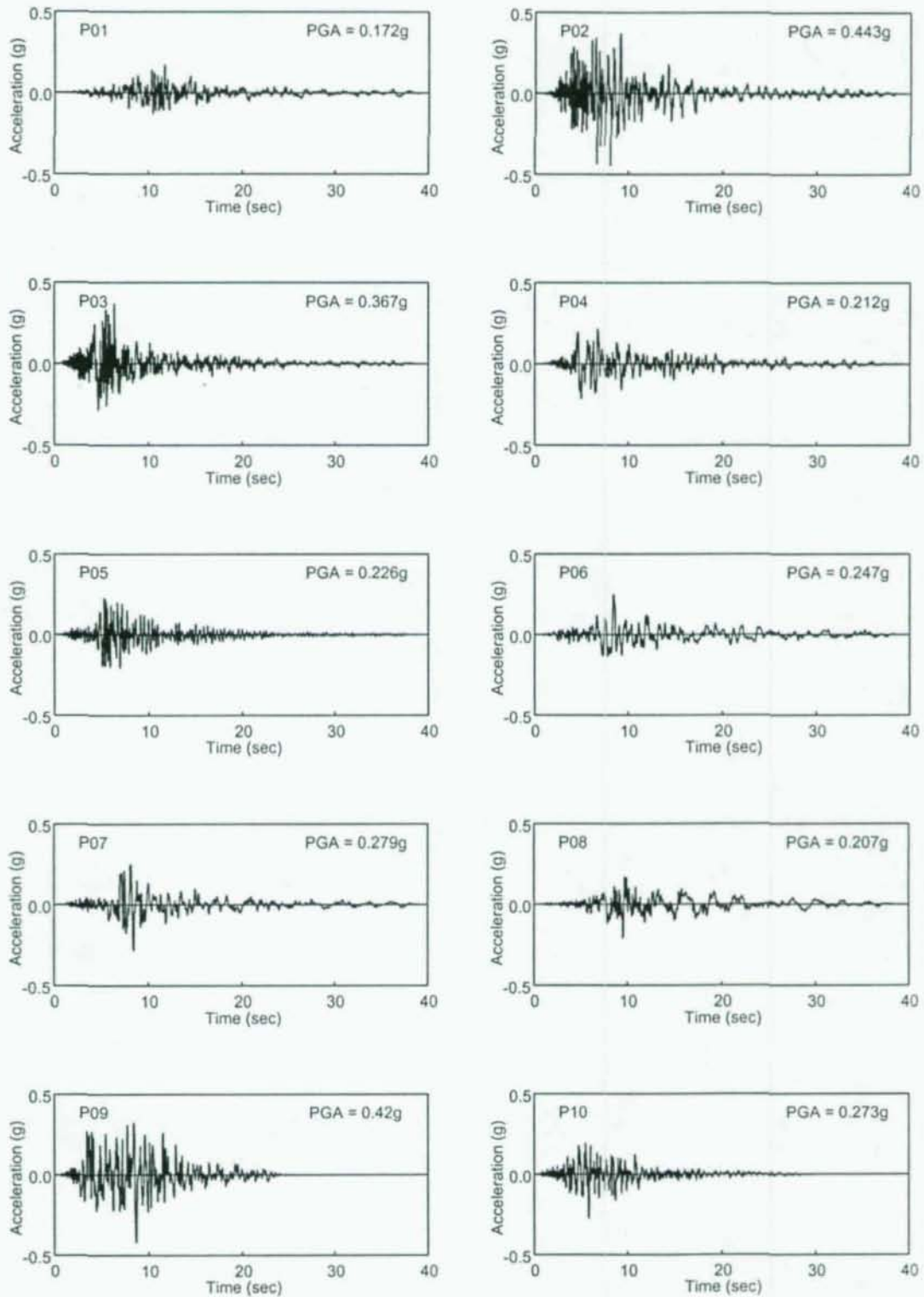


Figure 2.12 Acceleration Time Histories of Unscaled Ground Motions

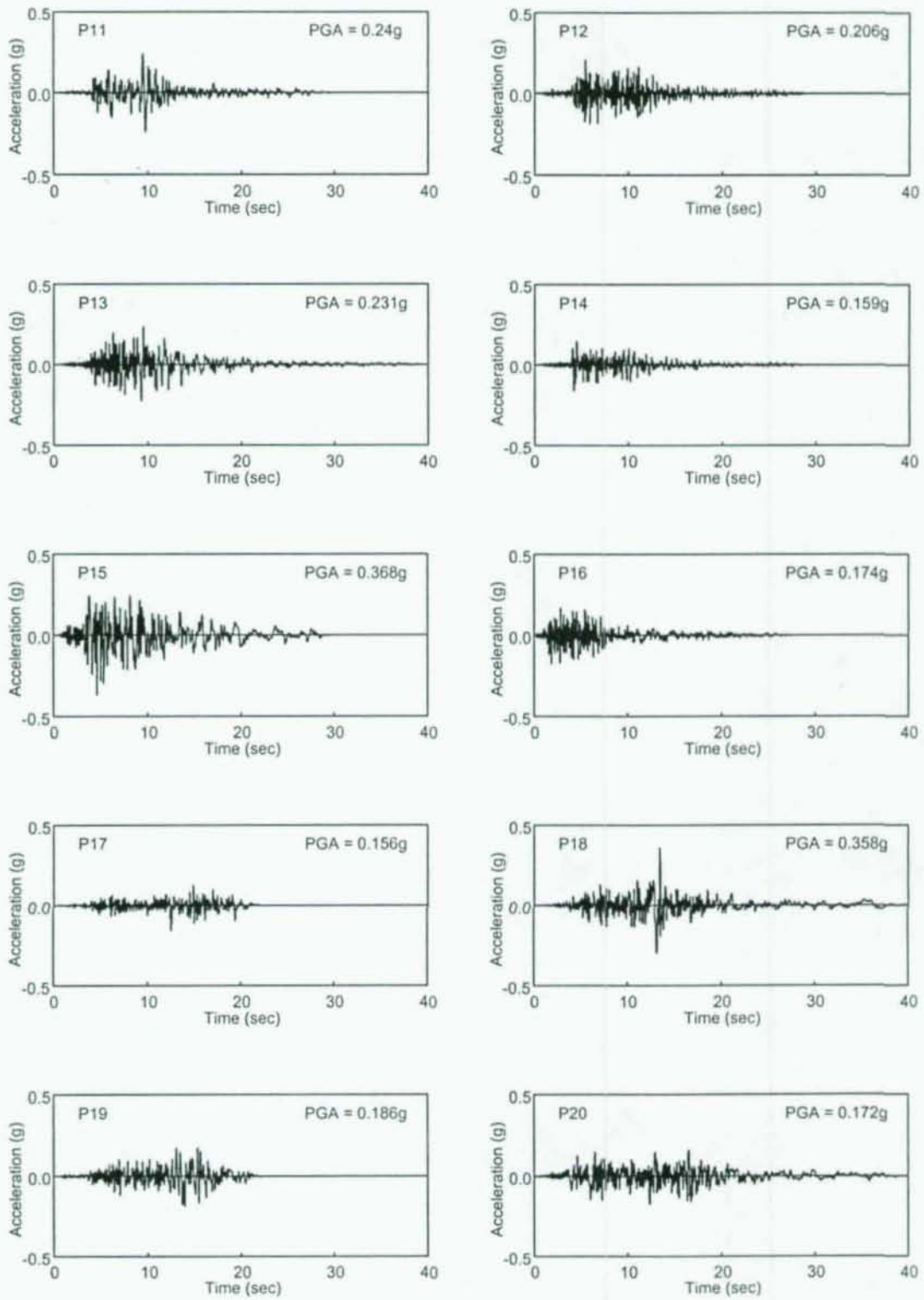


Figure 2.12 Acceleration Time Histories of Unscaled Ground Motions (con't)

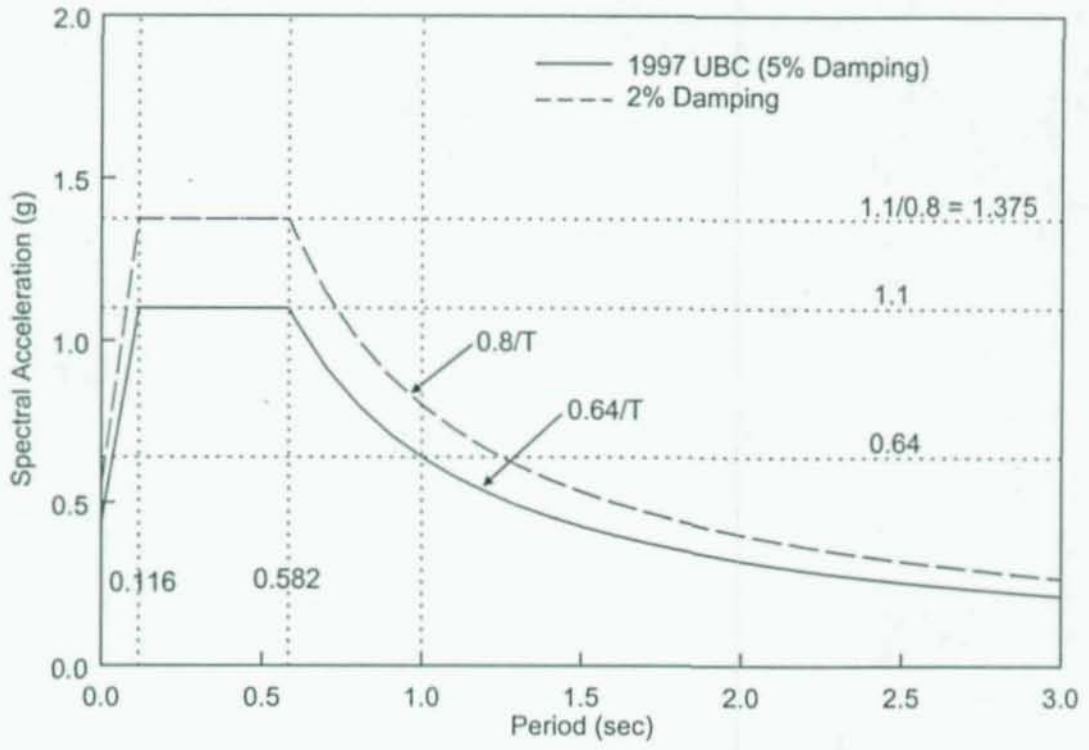


Figure 2.13 Elastic Design Spectra for 2 Percent Damping

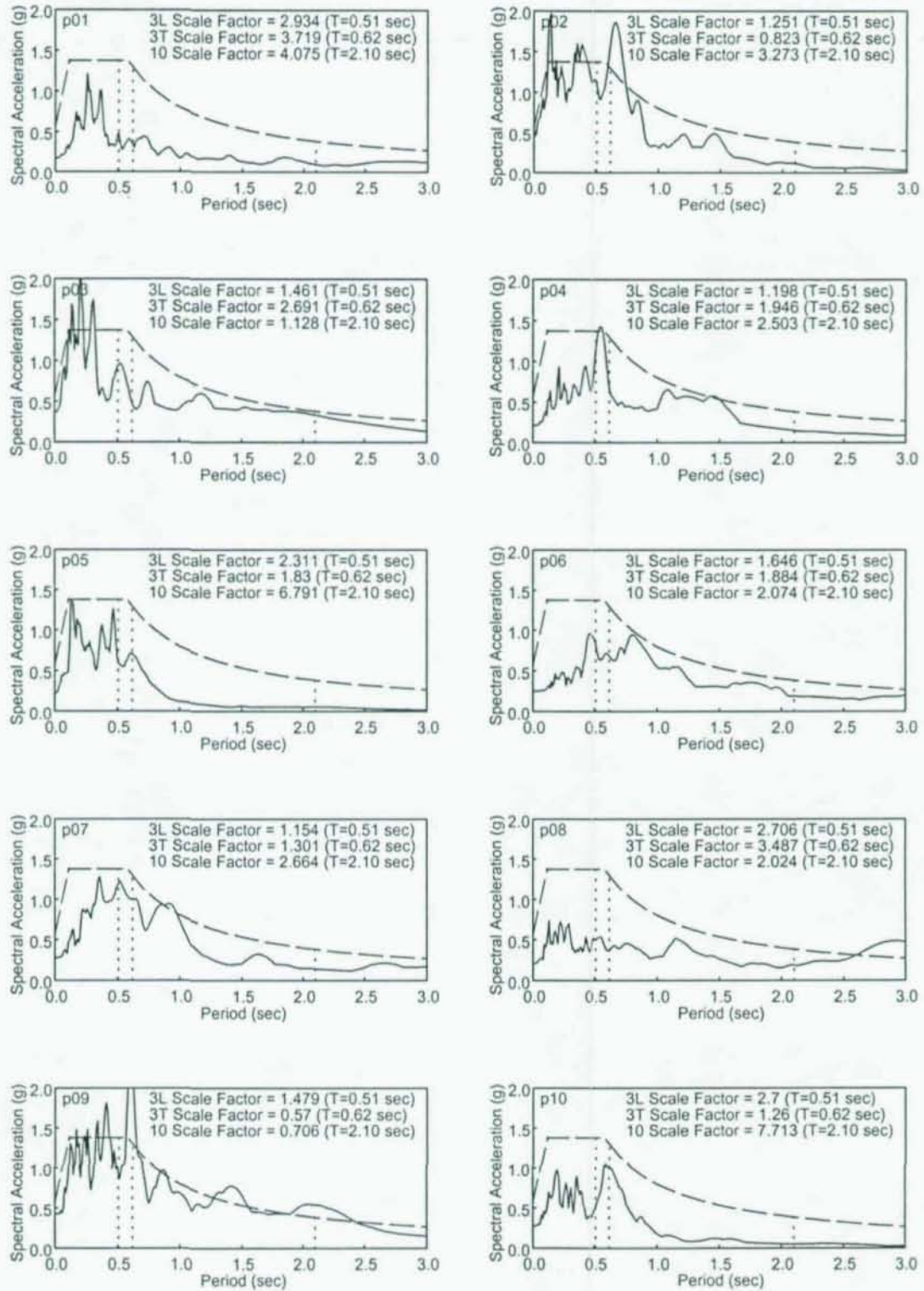


Figure 2.14 Response Spectra and Scaling Factors

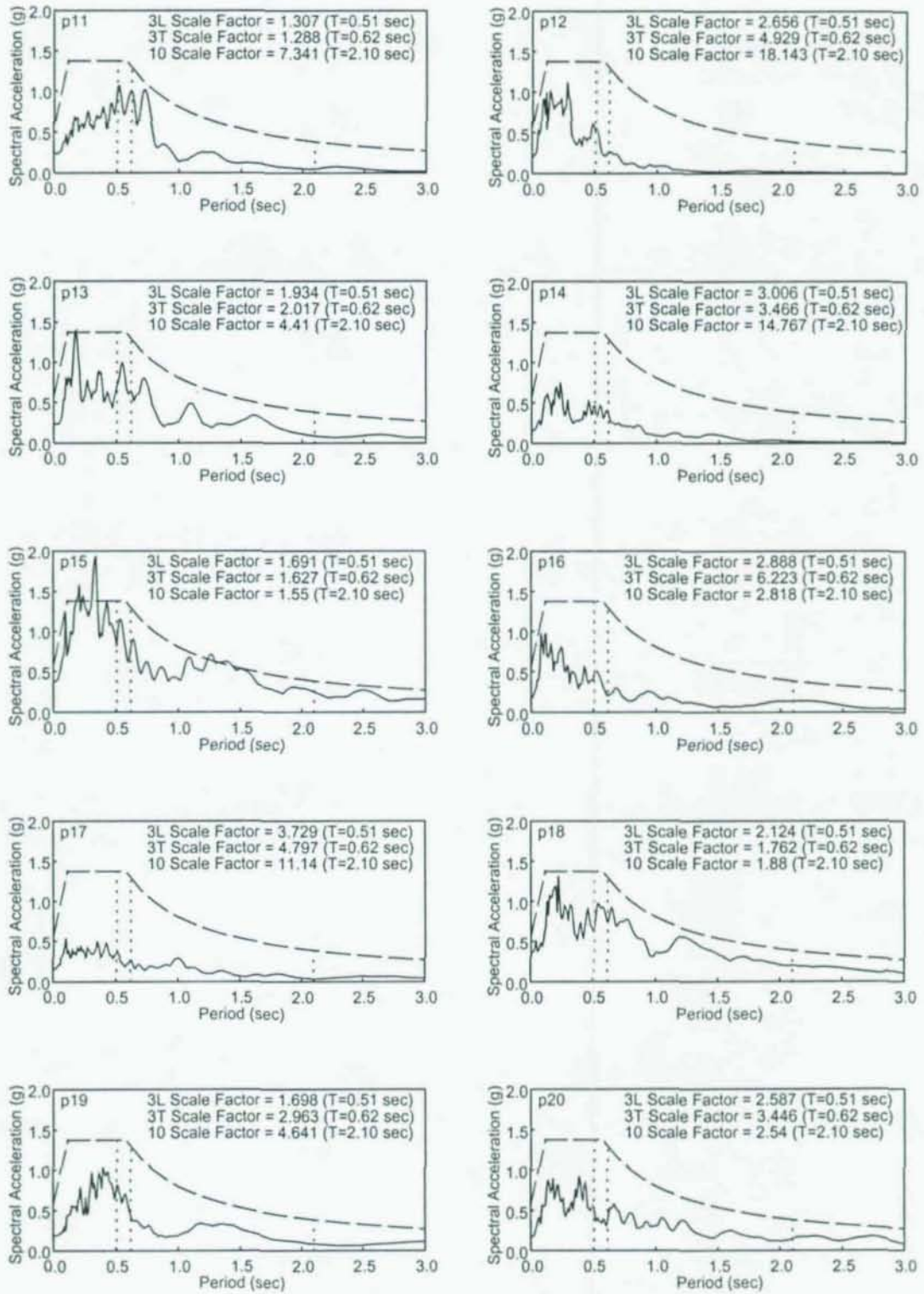
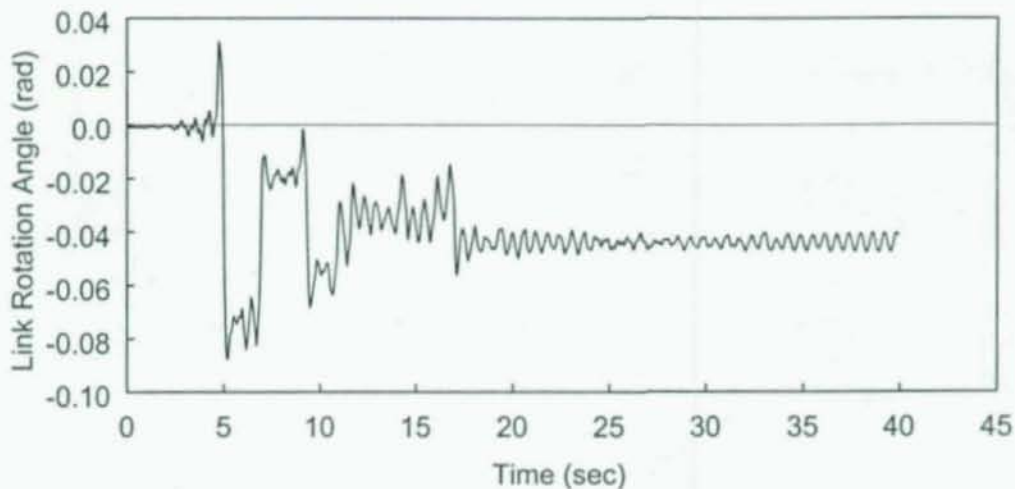
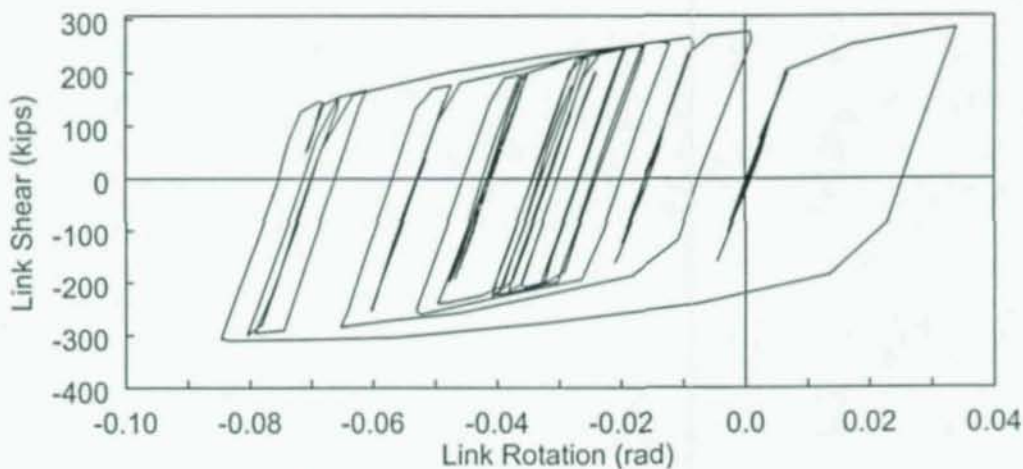


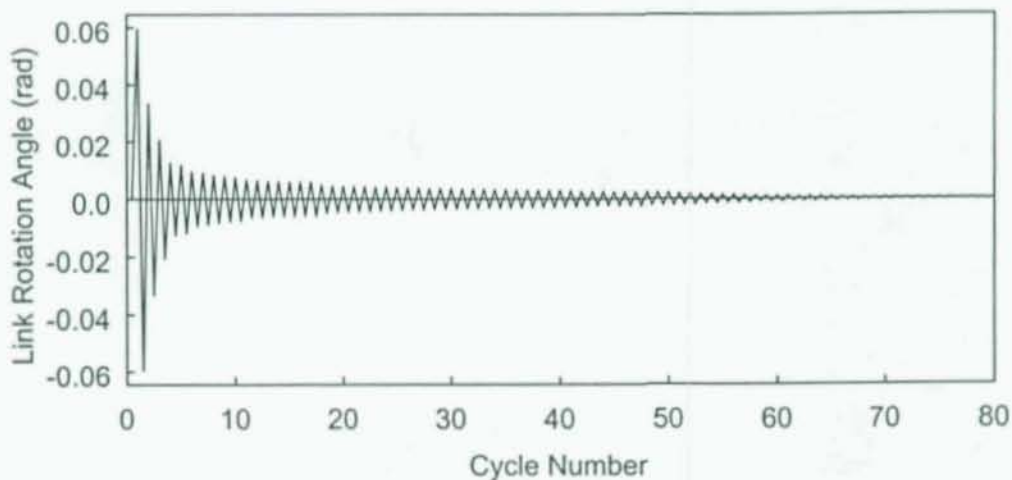
Figure 2.14 Response Spectra and Scaling Factors (con't)



(a) Rotation Time History



(b) Shear versus Rotation Hysteresis



(c) Ordered Cycles from Rainflow Counting Procedure

Figure 2.15 Representative Link Data (First Story Link, Frame 3T, P04 Record)

3 LOADING PROTOCOL DEVELOPMENT

3.1 Cumulative Damage Model

The development of the shear link protocol followed the same methodology used in developing the basic SAC moment frame loading history (Krawinkler et al. 2000). The basic premises of that methodology will be reviewed here.

Under cyclic loading, the damage to the link, D , is assumed to be described by a cumulative damage model of the type:

$$D = C \sum_{i=1}^N (\Delta\delta_i)^c \quad (3.1)$$

where:

- $\Delta\delta_i$ = deformation range of cycle i ,
- N = number of damaging excursions (cycles),
- C = a structural performance parameter that may depend strongly on the type of component and failure mode, and
- c = a structural performance parameter that is usually greater than 1.

From this model come several important principles of cumulative damage that should be considered in loading protocol development. Among these are, first, the damage from inelastic excursions is cumulative. Component capacity is expected to decrease as the number of cycles increases. Second, large cycles cause *much* more damage than small cycles ($c > 1$). For steel components experiencing plastic deformations, c is likely between 1.5 and 2 (Krawinkler et al. 2002). Finally, the model indicates that, for a simple loading history, the primary parameters should be the number of cycles (N), the deformation ranges of the cycles ($\Delta\delta_i$), and the sum of the deformation ranges ($\Sigma\Delta\delta_i$). Recall that the deformation range for a cycle is the change in deformation from peak positive deformation to peak negative deformation.

3.2 Response Parameters for Link Loading Protocol

For the SAC moment frame loading protocol, the basic deformation parameter was the interstory drift angle θ . For shear link loading protocols, however, the link rotation angle γ has typically been used as the deformation parameter.

In terms of γ , the primary demand parameters discussed in Section 3.1 are:

$$N_i = \text{Total Number of Cycles (cycles with rotation range } > 0.0075 \text{ rad)}$$

Rotations greater than half the yield rotation are considered damaging.

The range of 0.0075 rad was selected because a link rotation of 0.00375 rad (half of that range) corresponds to an estimate of half the yield rotation. Cycles with range < 0.0075 rad are not considered damaging.

$$\Delta\gamma_i = \text{Rotation Range of Cycle } i$$

Recall that cycles are arranged in descending order so that cycle 1 has the largest range, cycle 2 as the second largest, and so forth.

$$\Sigma\Delta\gamma_i = \text{Cumulative Deformation Range (cycles with rotation range } > 0.0075 \text{ rad)}$$

This is the sum of all the cycle ranges.

In addition to these primary demand parameters, secondary parameters considered in protocol development are:

$$N_p = \text{Number of Inelastic Cycles}$$

Link yield rotation varies somewhat depending on section geometry and link length, but is generally close to 0.0075 rad for short shear links. Inelastic cycles can be roughly defined as those with $\Delta\gamma_i > 0.015$ rad (2×0.0075).

$$\Delta\gamma_{\max} = \text{Maximum Rotation Range}$$

$$\gamma_{\max} = \text{Maximum Rotation}$$

$$\Delta\gamma_2 = \text{Second Largest Rotation Range}$$

$$\Delta\gamma_3 = \text{Third Largest Rotation Range}$$

These demand parameters parallel those used by Krawinkler et al. (2002). Values for these primary and secondary demand parameters were calculated for each link in each frame under each earthquake using the cycle data obtained from the rainflow counts (Section 2.4).

3.3 Target Values for Demand Parameters

A loading protocol can be characterized by the primary and secondary demand parameters discussed in Section 3.2. In developing a new protocol, "target values" for each of the demand parameters were selected based on statistical analysis of the values calculated from the model link data.

3.3.1 Governing Principles in Selecting Target Values

Krawinkler et al. (2002) outlined some guiding principles in determining appropriate target values for the demand parameters. These principles (re-written in terms of γ) are:

1. *The loading history should represent a "reasonable and generally conservative" demand on N_i , $\Delta\gamma_i$, and $\Sigma\Delta\gamma_i$ for the full range of anticipated link rotations (i.e., for links in EBFs of all periods, all stories in a structure, all reasonable designs, all seismic regions, all types of ground motions, etc.)*
2. *"Reasonable and generally conservative" implies that the total number of damaging cycles, N_i , should be represented in average, and that the cumulative deformation range, $\Sigma\Delta\gamma_i$, should be represented conservatively. Consideration should also be given to the fact that small cycles are much more frequent to large ones, and that small elastic cycles contribute very little to damage.*
3. *Primary consideration should be given to the cycles with relatively large deformation ranges, which will dominate damage accumulations.*
4. *Additional consideration should be given to conservative representation of the plastic deformation ranges.*
5. *Even though it is desirable (see item 1), it will not be possible to separate the loading history fully from the maximum deformation range, $\Delta\gamma_{\max}$, at which acceptability is to be evaluated. This cannot be done because $\Sigma\Delta\gamma_i$ depends strongly on $\Delta\gamma_{\max}$ and $\Sigma\Delta\gamma_i$ is the most important parameter to be represented in the loading history.*

3.3.2 Determining Target Values

Figures 3.1 shows values for three of the demand parameters (N_i , $\Sigma\Delta\gamma_i$, and $\Delta\gamma_{\max}$) for Frame 3L. Information is shown for links from each story for all of the ground motions. For reference, each plot also has the parameter value from the current AISC link loading protocol indicated by a dashed line. Results are shown in the same format for Frames 3T and 10 in Figures 3.2 and 3.3. Note that the AISC protocol has a significantly higher cumulative range

demand than that experienced by any of the links under any of the earthquakes [plot (b) in Figures 3.1 through 3.3].

In the development of the SAC moment frame protocol, a “critical story” was identified from the structures, and final statistical analysis and loading protocol development was based on the data from the critical story (Krawinkler et al. 2000). A similar approach was used in this study. Comparing the results from the three frames, the 3-story frames have higher values than the 10-story frame. Of the two 3-story frames, Frame 3T has slightly higher overall values for the three parameters and represents the critical frame. In Frame 3T the third story links have the highest cumulative range, while the first story links have greatest maximum range. For the remaining analysis, data from the first and third story links from Frame 3T was used since these represent the “critical links”.

Statistics were used to characterize the demand parameters for the critical links. For each parameter and link (e.g., $\Sigma\Delta\gamma_i$ at third story) several probabilistic distributions were tested to describe the variation of that parameter for the twenty earthquake records. Lognormal distributions tended to provide the best fit for most of the parameters. With a distribution assigned, percentile values were computed for each parameter.

Figures 3.4 through 3.10 show the percentile values for the parameters for the first and third story links in Frame 3T. These results were used to determine target demand parameter values for the proposed loading protocol. A brief discussion about the selection of the target values for each parameter follows.

Total Number of Cycles, N_t

Figure 3.4 indicates that the number of damaging cycles ($\Delta\gamma > 0.0075$ rad) was greatest for the third story links. Since the total number of cycles should be represented in average (see Section 3.3.1), a target value of 36 was reasonable.

Number of Inelastic Cycles, N_p

Figure 3.5 shows that the third story links experienced more inelastic cycles than the first story links. A target of 18 inelastic cycles, corresponding to the 90th percentile value, was selected. It was decided to conservatively represent the number of inelastic cycles, to account for buildings shorter than 3 stories which were not addressed specifically in the study. The two parameters, 36 total cycles and 18 inelastic cycles, provide a rough initial framework for the protocol.

Sum of Rotation Ranges, $\Sigma\Delta\gamma_i$

This parameter is one of the most important as it represents the cumulative rotation demand. From Figure 3.6, the third story links have higher values for $\Sigma\Delta\gamma_i$ than the first story links. Since this parameter should be represented conservatively, the 90th percentile value for the third story links, 1.10 rad, was used as the target value.

Maximum Rotation Range, $\Delta\gamma_{\max}$

The maximum rotation range in a protocol indicates the point at which the cumulative rotation should be accomplished, and usually represents the acceptance criteria. Since the current AISC Seismic Provisions specify a design inelastic rotation of 0.08 rad for short links (total rotation of about 0.09 rad assuming elastic rotation of about 0.0075 rad), an appropriate maximum rotation range in terms of that value would be 0.18 rad (2×0.09 rad). From Figure 3.7, the target value of 0.18 rad is higher than the 90th percentile value of the third story links, but a little lower than the 90th percentile value for the first story links.

Maximum Rotation, γ_{\max}

Since a simple protocol consists of symmetric cycles, the target maximum rotation was constrained by the target maximum rotation range to be 0.09 rad ($\Delta\gamma_{\max}/2$). Figure 3.8 indicates this corresponds well with the 90th percentile value for the third story links. The 90th percentile value for the first story links is somewhat greater, but this is not considered a problem for two reasons. First, damage is proportional to the range and not amplitude, and the results in Figure 3.7 indicate that rotation ranges remain reasonable even though large one-sided excursions sometimes occur. Second, links that experience a large maximum rotation generally have lower cumulative rotations (recall lower sum of rotation ranges for the first story links in Figure 3.6). Testing of several links has demonstrated that large, one-sided rotations are achievable as long as cumulative rotations are not high (Malley and Popov 1983; Kasai and Popov 1986).

These results (Figure 3.8) suggest that links in EBFs, designed according to the provisions (AISC 2002), will generally not exceed the design rotation of 0.08 rad inelastic rotation under design earthquake loading. Those that do will likely have lower cumulative rotations. Note that near fault records were not included in the ground motion suite used to generate the data. Such records result in higher maximum rotations, but again, cumulative range demands and maximum range values are still reasonable (see Appendix B).

Magnitudes of $\Delta\gamma_2$ and $\Delta\gamma_3$

From Figures 3.9 and 3.10, the target values of the second and third largest ranges were selected to be 0.10 rad and 0.08 rad based on the 90th percentile values.

Rotation Range of Cycle i , $\Delta\gamma_i$

This is one of the primary demand parameters and relates to the proper distribution of cycle ranges within a protocol. The model data for $\Delta\gamma_i$ is most useful in the form of the cumulative distribution function¹ (CDF) for all the cycles from all the records, for a given link. Figure 3.11 shows the CDF for the first and third story links. The CDFs are similar and both indicate that the majority of cycles have small ranges.

Table 3.1 summarizes all the target demand parameter values obtained from the time-history analysis data, as discussed above.

¹ The cumulative distribution function (CDF) should not be confused with cumulative rotation demand. The cumulative distribution function indicates the percentage of cycles having a range less than some given range. The cumulative rotation demand has units of rad and is the sum of the cycle ranges.

Table 3.1 Summary of Demand Parameter Target Values

Demand Parameter	Target Value
N_t	36 cycles
N_p	18 cycles
$\Sigma\Delta\gamma_i$	1.10 rad
$\Delta\gamma_{\max}$	0.18 rad
γ_{\max}	0.09 rad
$\Delta\gamma_2$	0.10 rad
$\Delta\gamma_3$	0.08 rad
$\Delta\gamma_i$	CDF (Figure 3.11)

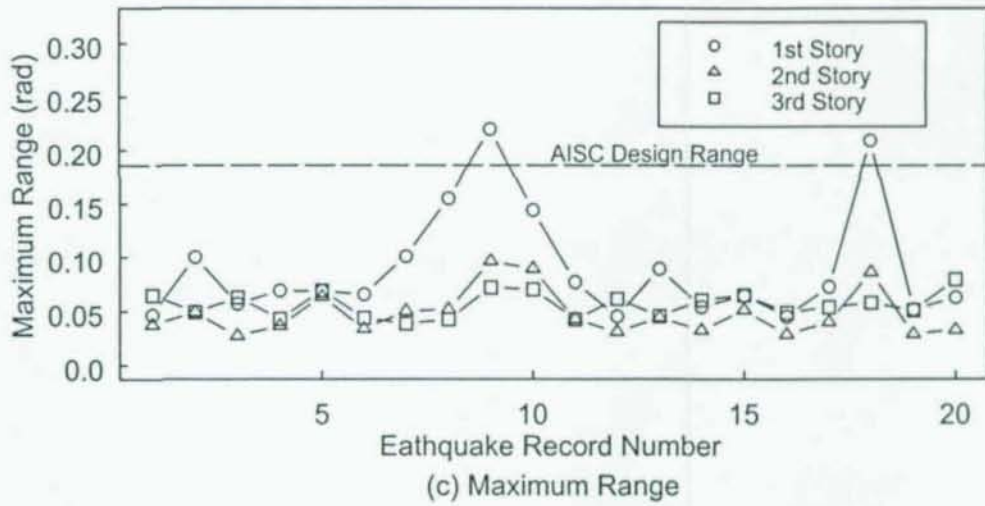
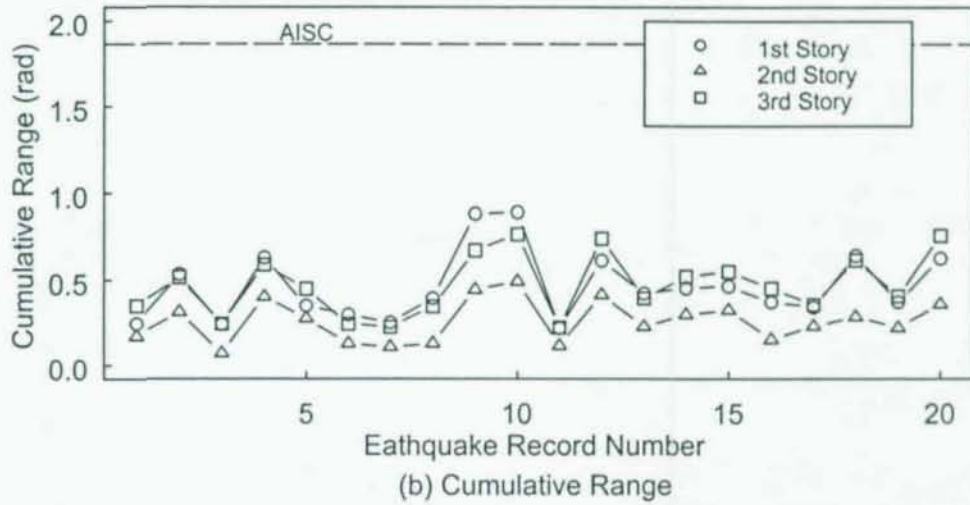
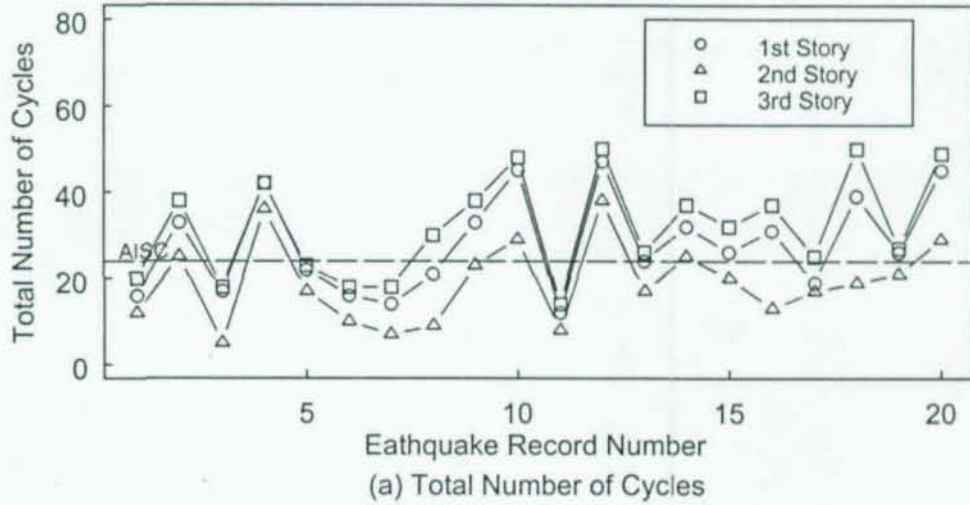


Figure 3.1 Demand Parameter Values for Links in Frame 3L
(Cycles with Range > 0.0075 rad Considered)

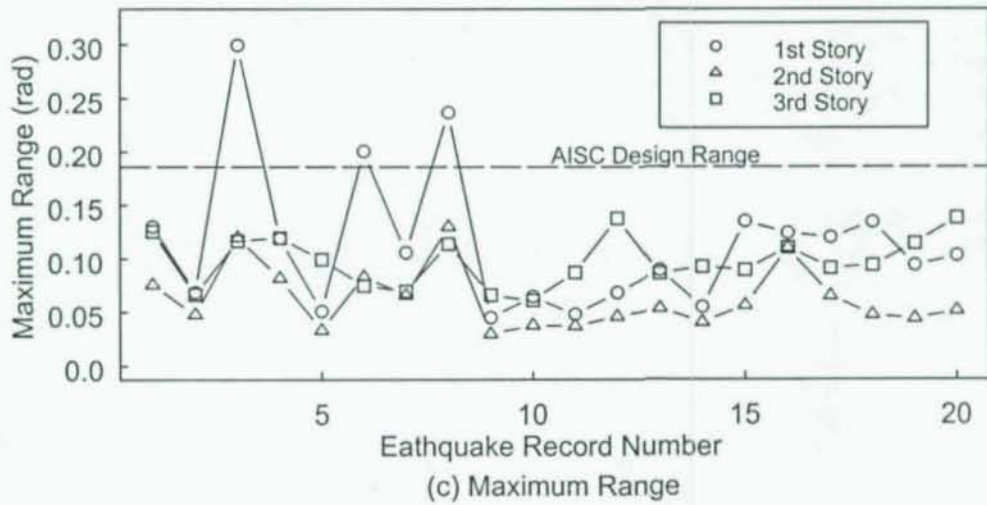
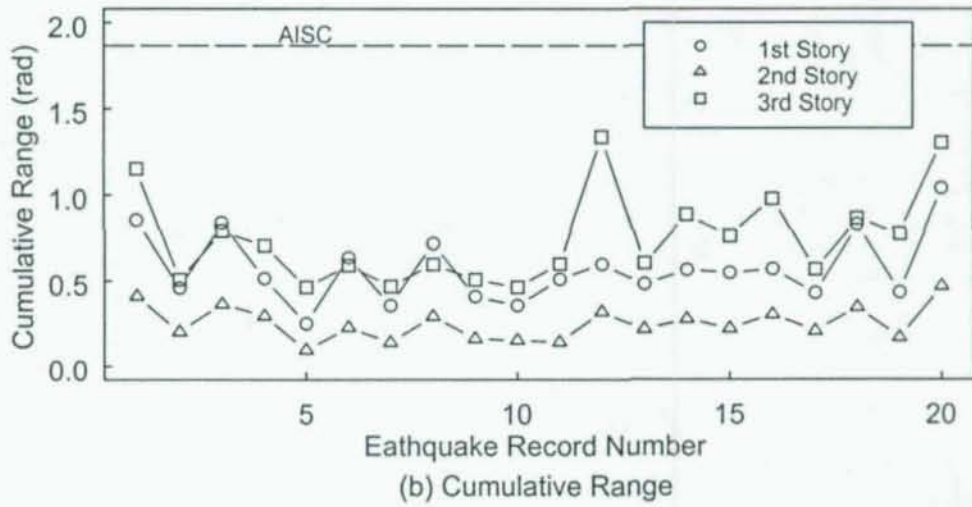
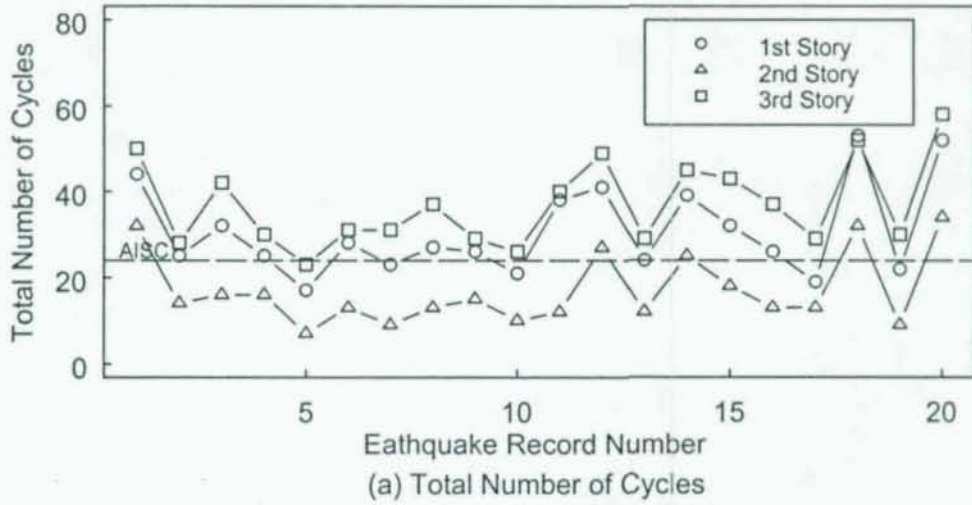


Figure 3.2 Demand Parameter Values for Links in Frame 3T
(Cycles with Range > 0.0075 rad Considered)

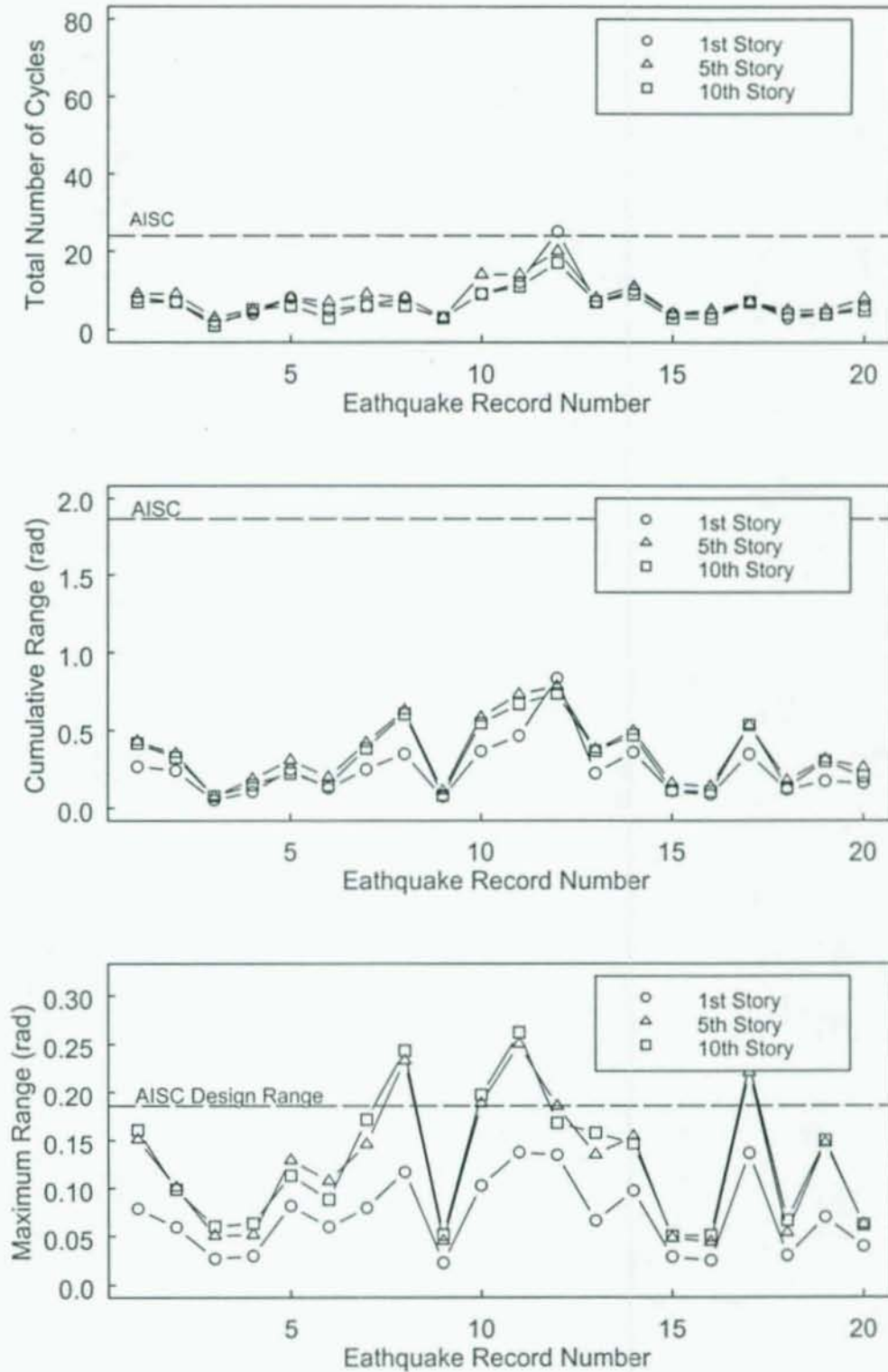


Figure 3.3 Demand Parameter Values for Links in Frame 10
(Cycles with Range > 0.0075 rad Considered)

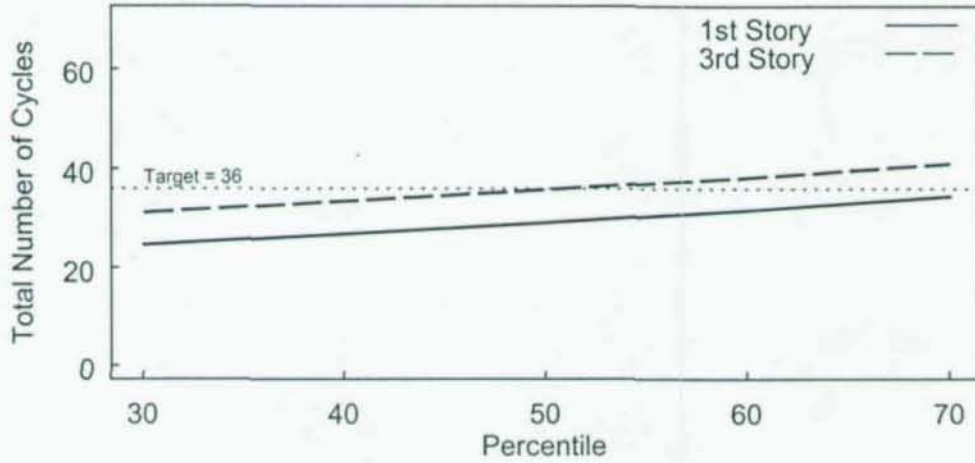


Figure 3.4 Percentile Placing of the Total Number of Cycles, N_r
(Cycles with Range > 0.0075 rad)

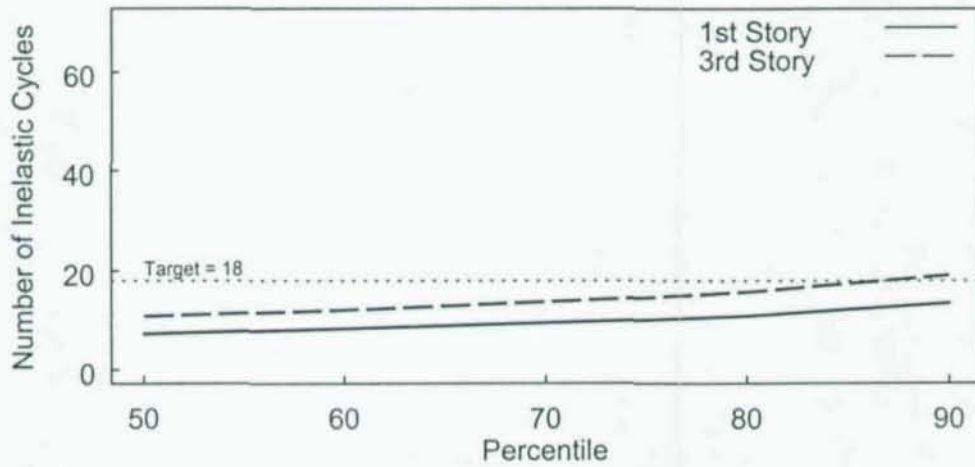


Figure 3.5 Percentile Placing of the Number of Inelastic Cycles, N_p
(Cycles with Range > 0.015 rad)

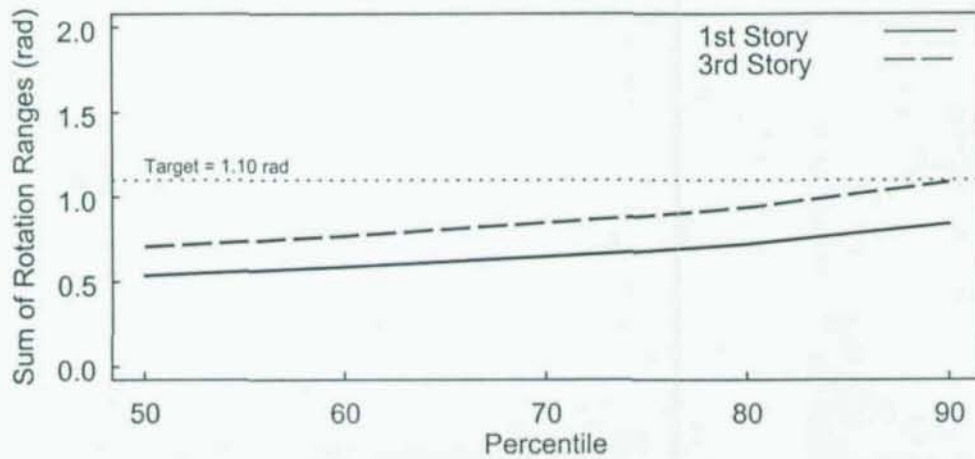


Figure 3.6 Percentile Placing of the Sum of the Rotation Ranges, $\Sigma\Delta\gamma_i$
(Cycles with Range > 0.0075 rad)

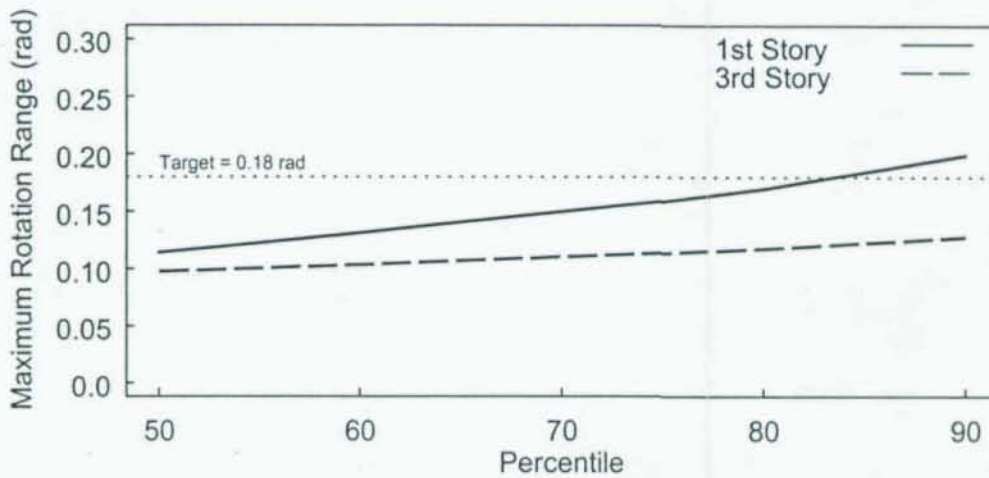


Figure 3.7 Percentile Placing of the Maximum Rotation Range, $\Delta\gamma_{\max}$

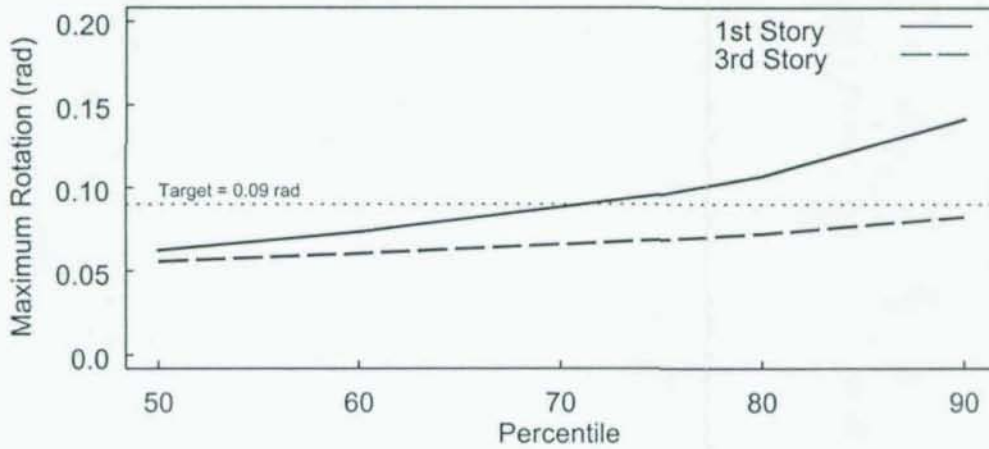


Figure 3.8 Percentile Placing of the Maximum Rotation, γ_{\max}

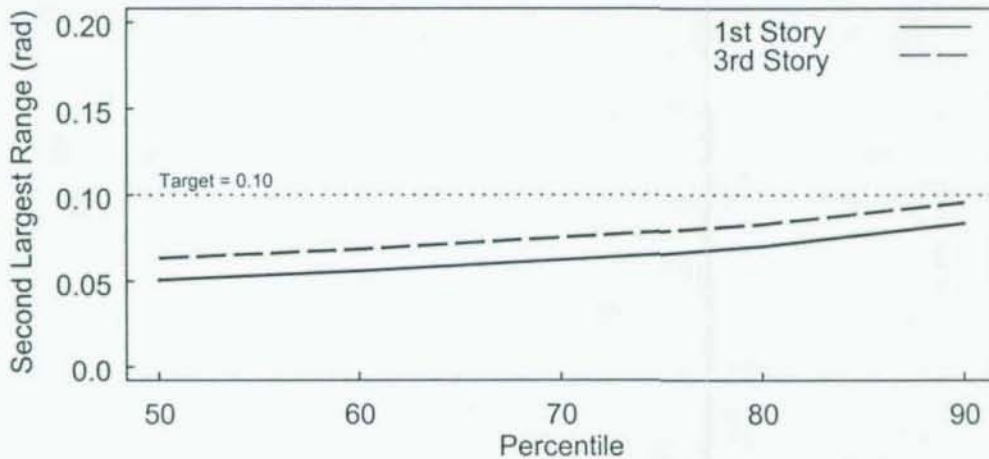


Figure 3.9 Percentile Placing of the Second Largest Rotation Range, $\Delta\gamma_2$

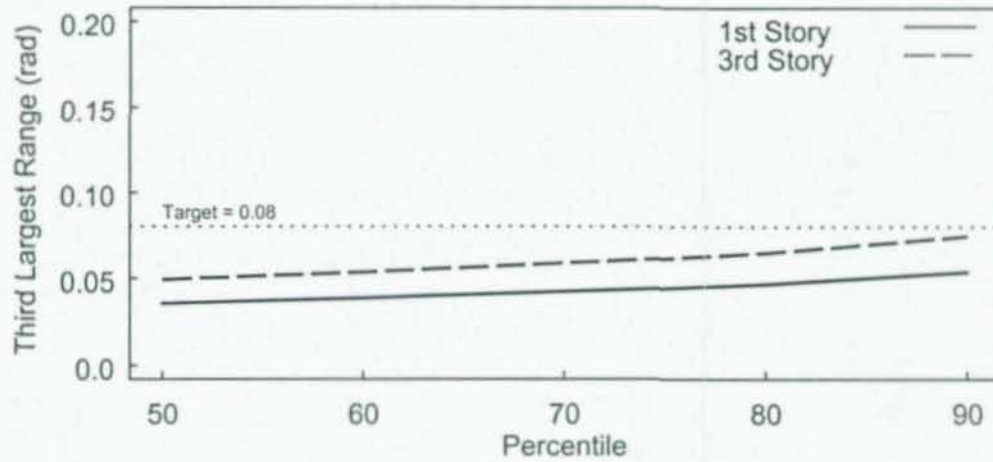


Figure 3.10 Percentile Placing of the Third Largest Rotation Range, $\Delta\gamma_3$

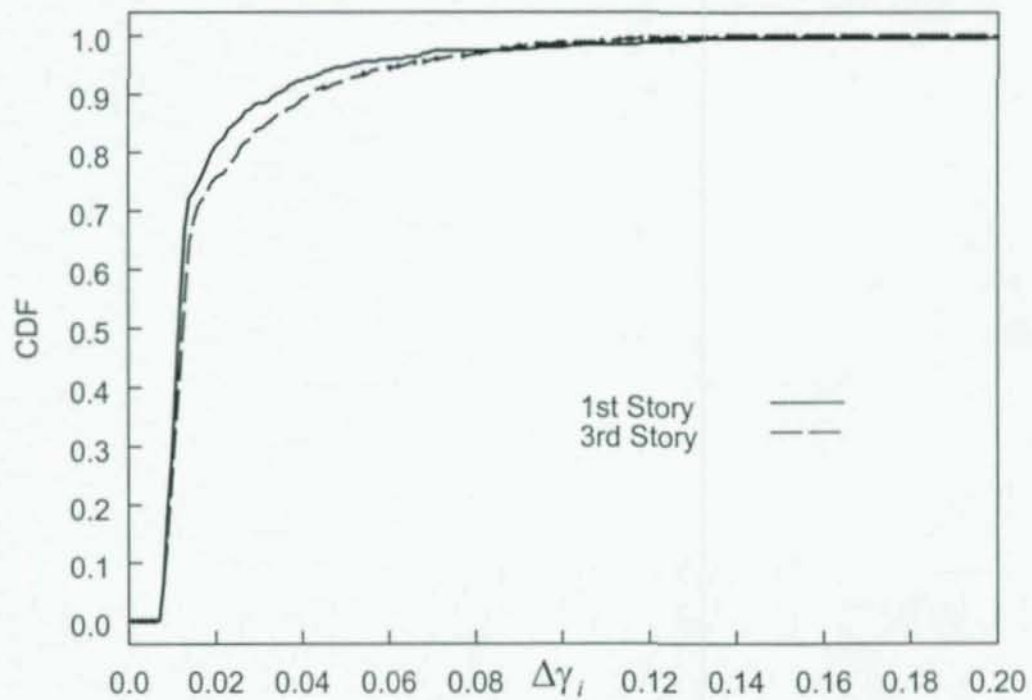


Figure 3.11 Cumulative Distribution Function of Cycle Ranges, $\Delta\gamma_i$
(Cycles with Range > 0.0075 rad, for Links in Frame 3T with all Ground Motions)

4 PROPOSED SHORT LINK LOADING PROTOCOL

4.1 Proposed Testing Protocol

A proposed loading protocol for short links was developed, based on the demand parameter values described in Section 3.3. The protocol consists of several rotation amplitude steps, each consisting of a number of symmetric cycles. The protocol is summarized in Table 4.1 and illustrated in Figure 4.1(a). The 2002 AISC protocol is shown in Figure 4.1(b) for comparison. Table 4.2 compares the demand parameter values of the proposed loading protocol with the target values. The target values are conservatively represented in the new protocol. The values of the 2002 AISC protocol are also shown in the table for comparison.

Figure 4.2 compares the discrete CDF of the proposed protocol with those of the links from Frame 3T (see Section 3.3.2). The CDF of the AISC protocol is also shown for comparison. Note that a protocol CDF "below" the data is conservative, indicating the protocol has a greater percentage of large amplitude cycles than the data. The proposed protocol is reasonable in comparison with the data.

4.2 Comparison of the Proposed and AISC Loading Protocols

The proposed protocol differs from the AISC link protocol, and the AISC moment frame loading protocol, in that the deformation increment changes for the latter steps and only one cycle is applied at the latter steps rather than two. These characteristics were necessary to provide a distribution of cycles consistent with the data.

From Table 4.2, the proposed protocol has more total cycles, the same number of inelastic cycles, and lower cumulative range demand as compared with the 2002 AISC protocol. Figure 4.3 illustrates the cumulative range demands of the two protocols plotted against cycle range. The AISC protocol requires 48% more cumulative rotation than the new protocol. In addition, and perhaps more significant, 72% of the total cumulative range demand in the AISC protocol comes from cycles with *ranges* greater than 0.1 rad. In comparison, only 37% of the total cumulative range demand comes from cycles with ranges greater than 0.1 rad in the proposed protocol. Recall from the damage model that large excursions cause *much* more damage than small excursions (see Section 3.1). This higher

percentage of large range cycles in the AISC protocol is also illustrated by the CDF (see Figure 4.2)

Based on the demand parameters and the assumed damage model, the proposed protocol is significantly less severe than the AISC protocol. It is anticipated that a short shear link would reach a greater rotation level prior to failure with the proposed protocol than it would with the AISC protocol.

Table 4.1 Proposed Short Link Loading Protocol

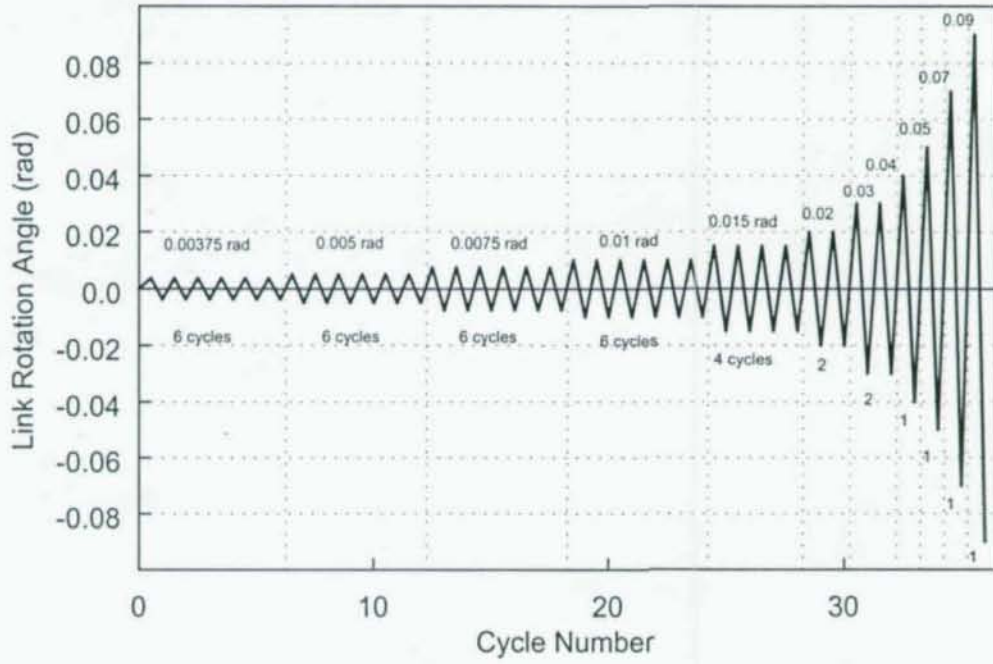
Load Step	Peak Link Rotation Angle, γ	Number of Cycles
1	0.00375	6
2	0.005	6
3	0.0075	6
4	0.01	6
5	0.015	4
6	0.02	2
7	0.03	2
8	0.04	1
9	0.05	1
10	0.07	1
11 ^a	0.09	1

^a Continue with increments in γ of 0.02, and perform 1 cycle at each step until failure

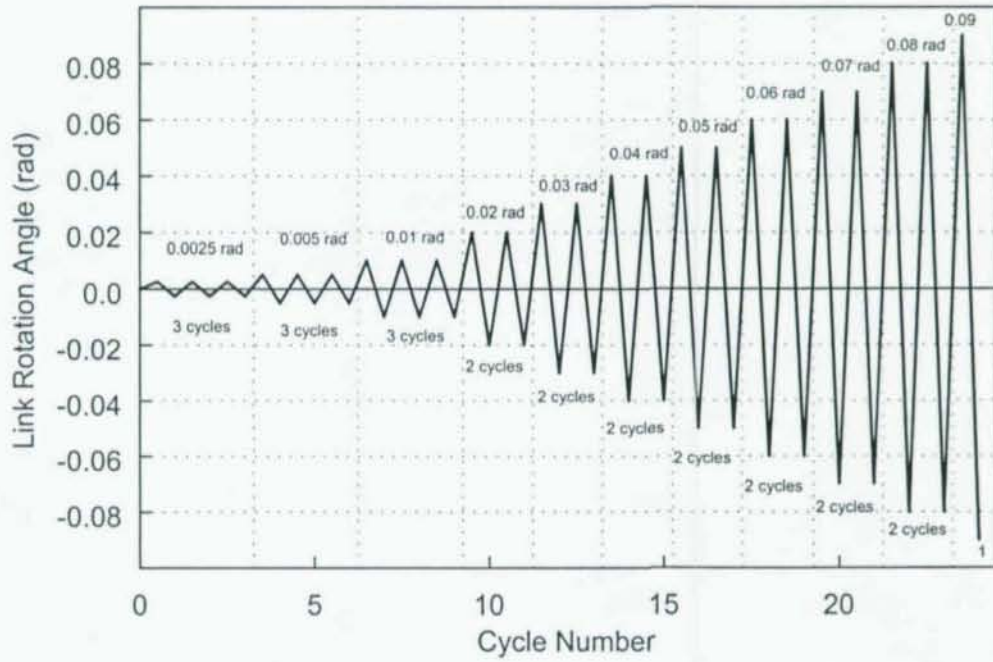
Table 4.2 Comparing Protocol Demands with Target Values

Demand Parameter	Target Value	Proposed Protocol	AISC Protocol
N_t	36 cycles	36 cycles	24 cycles
N_p^a	18 cycles	18 cycles	18 cycles
$\Sigma\Delta\gamma_i$	1.10 rad	1.14 rad	1.69 rad
$\Delta\gamma_{\max}$	0.18 rad	0.18 rad	0.18 rad
γ_{\max}	0.09 rad	0.09 rad	0.09 rad
$\Delta\gamma_2$	0.10 rad	0.14 rad	0.16 rad
$\Delta\gamma_3$	0.08 rad	0.10 rad	0.16 rad
$\Delta\gamma_i$	See Figure 4.2	See Figure 4.2	See Figure 4.2

^a Assuming $\gamma_y \approx 0.0075$ rad



(a) Proposed



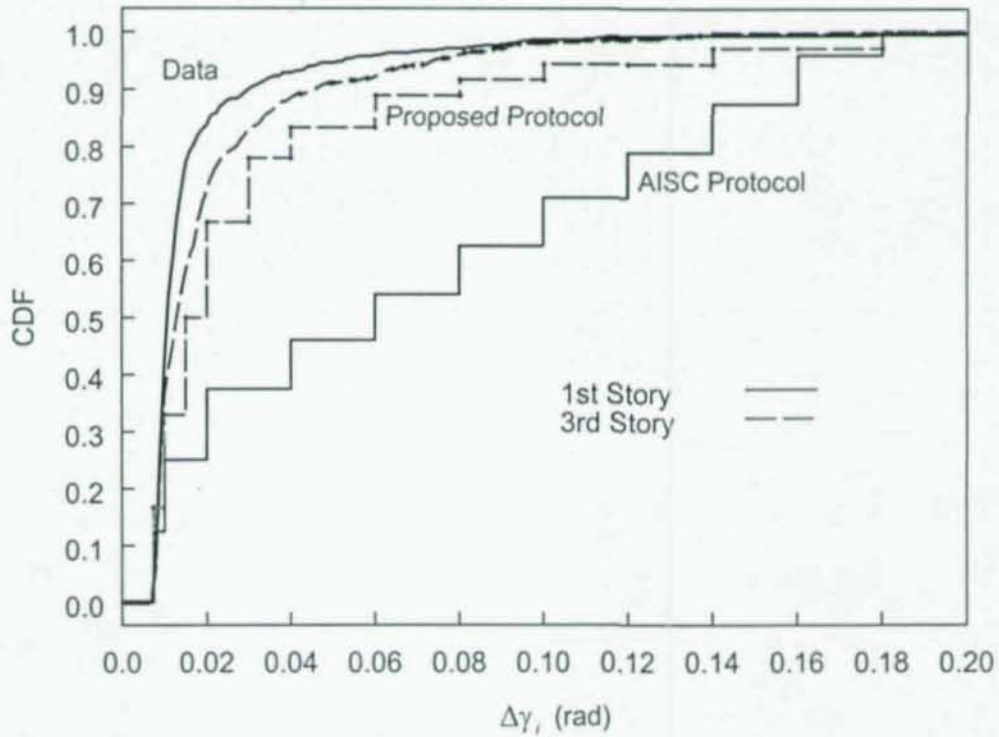


Figure 4.2 Comparing Loading Protocol CDFs with those from Frame 3T Links

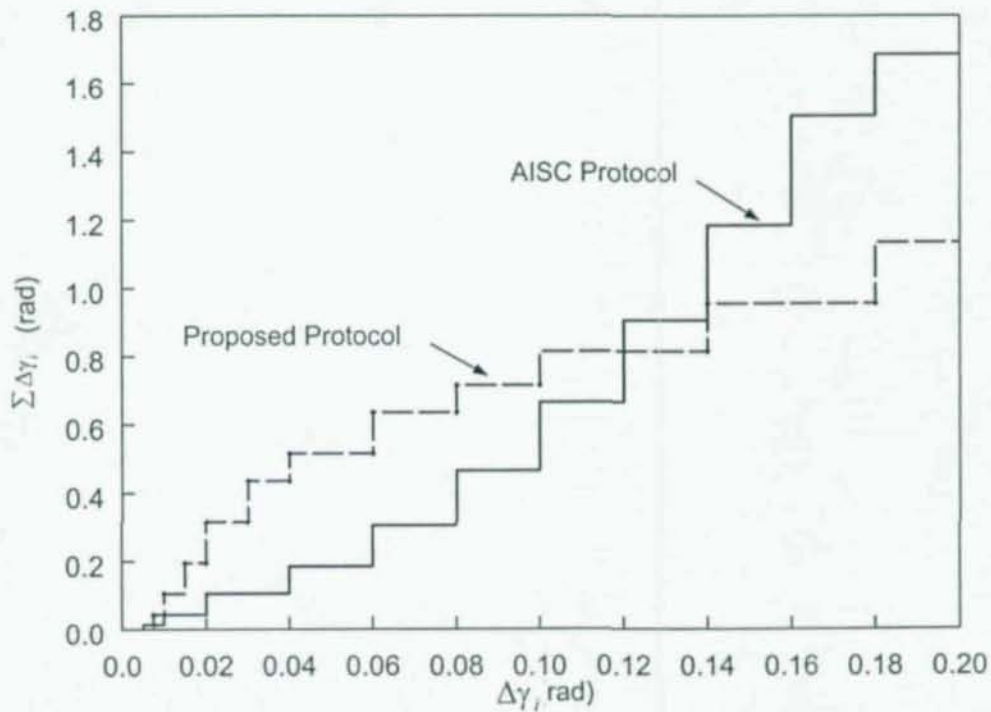


Figure 4.3 Comparing Cumulative Ranges for Proposed and 2002 AISC Protocols

5 SUMMARY AND CONCLUSIONS

There has been a shear link loading protocol specified in the AISC Seismic Provisions since 1997; however, it is a modified version of the SAC moment frame loading protocol without any study to justify it. The objective of this study was to investigate the rotation demands on short links in eccentrically braced frames under design earthquakes and develop a loading protocol for link testing. One 3-story building and one 10-story building, with a total of three unique eccentrically braced frames, were designed by the AISC Solutions Center. The designs called for links in configurations where one end of each link was connected to a column. Models were developed for each of the frames, and nonlinear time-history analysis was performed using a suite of Los Angeles earthquakes scaled to match the 1997 UBC design spectra.

The model results indicated that the protocol in the AISC Seismic provisions is overly conservative in representing design earthquake demands. A new loading protocol was developed following the same general procedure as was used in developing the SAC moment frame loading protocol. The proposed protocol requires only 67% of the cumulative rotation specified by the AISC protocol in order to reach the link design inelastic rotation for short links (0.08 rad). The proposed protocol also requires fewer large inelastic cycles as compared to the AISC protocol. According to the assumed damage model, the proposed protocol is significantly less severe than the current AISC protocol and links would achieve higher maximum rotation when tested with the proposed protocol.

It is recommended that the proposed protocol be used for future testing of short shear links. Additional work needs to be completed to address loading for longer links ($eV_p/M_p > 1.6$).

18680

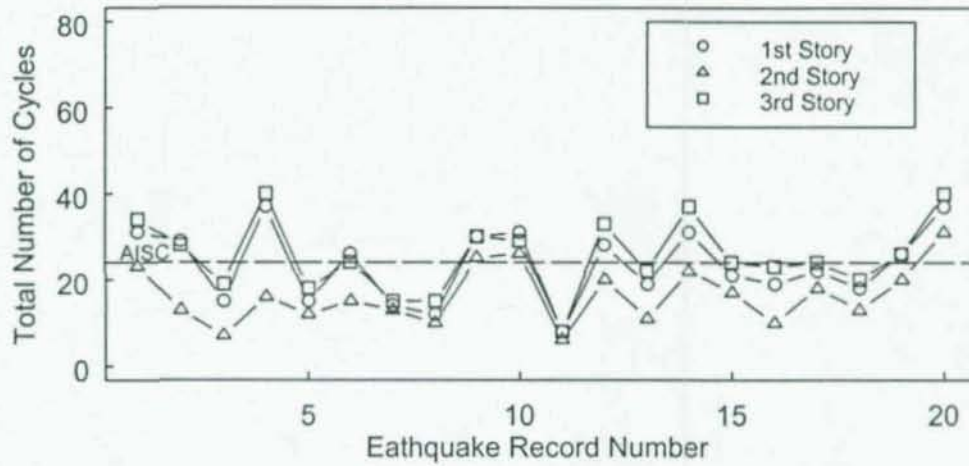
REFERENCES

- AISC. (2002). *Seismic Provisions for Structural Steel Buildings*, American Institute of Steel Construction, Chicago, IL.
- Arce, G. (2002). "Impact of Higher Strength Steels on Local Buckling and Overstrength of Links in Eccentrically Braced Frames." *Masters Thesis*, University of Texas at Austin, Austin, TX (advisor: M.D. Engelhardt).
- Engelhardt, M. D., and Popov, E. P. (1989). "Behavior of Long Links in Eccentrically Braced Frames." *Report No. UBC/EERC-89/01*, Earthquake Engineering Research Center, University of California at Berkeley, Richmond, CA.
- FEMA. (2000). "Prestandard and Commentary for the Seismic Rehabilitation of Buildings." *FEMA 356*, Federal Emergency Management Agency, Washington, D.C.
- Gupta, A., and Krawinkler, H. (1999). "Prediction of Seismic Demands for SMRFs with Ductile Connections and Elements." *Report No. SAC/BD-99/06*. SAC Joint Venture, Sacramento, CA.
- Hjelmstad, K. D., and Popov, E. P. (1983). "Seismic Behavior of Active Beam Links in Eccentrically Braced Frames." *Report No. UBC/EERC-83/15*, Earthquake Engineering Research Center, University of California at Berkeley, Richmond, CA.
- ICBO (1997). *Uniform Building Code*. International Conference of Building Officials, Whittier, CA.
- ICC (2000). *International Building Code*. International Code Council, Inc., Whittier, CA.
- Kasai, K., and Popov, E.P. (1986). "A Study of Seismically Resistant Eccentrically Braced Steel Frame Systems." *Report No. UCB/EERC-86/01*, Earthquake Engineering Research Center, University of California at Berkeley, Richmond, CA.
- Krawinkler, H., Gupta, A., Medina, R., and Luco, N. (2000). "Loading Histories for Seismic Performance Testing of SMRF Components and Assemblies." *Report No. SAC/BD-00/10*. SAC Joint Venture, Sacramento, CA.
- Krawinkler, H., Medina, R., and Alavi, B. (2003). "Seismic Drift and Ductility Demands and Their Dependence on Ground Motions." *Engineering Structures*, 25(5), 637-653.

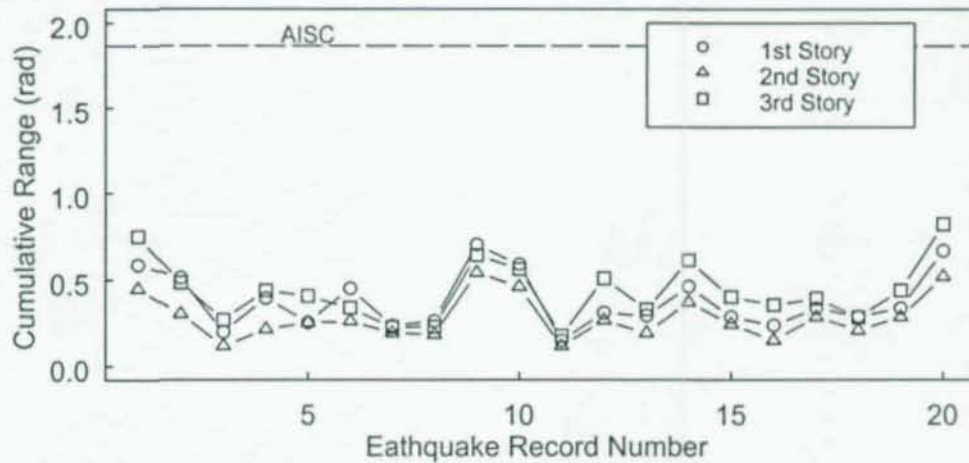
- Malley, J. O., and Popov, E. P. (1983). "Design Considerations for Shear Links in Eccentrically Braced Frames." *Report No. UBC/EERC-83/24*, Earthquake Engineering Research Center, University of California at Berkeley, Richmond, CA
- Medina, R. A. (2003). "Seismic Demands for Nondeteriorating Frame Structures and Their Dependence on Ground Motions." *Ph.D. Dissertation*, Department of Civil and Environmental Engineering, Stanford University, Palo Alto, CA.
- Popov, E.P., Ricles, J.M., and Kasia, K. (1992). "Methodology for Optimum EBF Link Design," *Proceedings*, Tenth World Conference of Earthquake Engineering, Vol. 7, pp. 3983-3988, Balkema, Rotterdam.
- Prakash, V., Powell, G.H., and Campbell, S., (1993). "DRAIN-2DX: Base Program Description and User Guide." *Report No. UCB/SEMM-93/17*, Department of Civil Engineering, University of California, Berkeley, CA.
- Ramadan, T., and Ghobarah, A. (1995). "Analytical Model for Shear-Link Behavior." *Journal of Structural Engineering*, 121(11), 1574-1580.
- Richards, P., and Uang, C-M. (2002). "Evaluation of Rotation Capacity and Overstrength of Links in Eccentrically Braced Frames (Phase 1)." *Report No. SSRP-2002/18*, Department of Structural Engineering, University of California at San Diego, La Jolla, CA.
- Ricles, J. M., and Popov, E. P. (1987). "Experiments on Eccentrically Braced Frames with Composite Floors." *Report No. UBC/EERC -87/06*, Earthquake Engineering Research Center, University of California at Berkeley, Richmond, CA.
- Ricles, J.M., and Popov, E.P., (1994). "Inelastic Link Element for EBF Seismic Analysis." *Journal of Structural Engineering*, 120(2), 441-463.
- Roeder, C. W., and Popov, E. P. (1977). "Inelastic Behavior of Eccentrically Braced Steel Frames under Cyclic Loadings." *Report No. UCB/EERC-77/18*, Earthquake Engineering Research Center, University of California at Berkeley, Richmond, CA.
- Somerville, P., Smith, N., Punyamurthula, S., and Sun, J. (1997). "Development of Ground Motion Time Histories for Phase 2 of the FEMA/SAC Steel Project." *Report No. SAC/BD-97/04*. SAC Joint Venture.
- Whittaker, A. S., Uang, C-M., and Bertero, V. V. (1987). "Earthquake Simulation Tests and Associated Studies of a 0.3-scale Model of a Six-story Eccentrically Braced Steel Structure." *UBC/EERC Report No. 87-02*, Earthquake Engineering Research Center, University of California at Berkeley, Richmond, CA.

APPENDIX A—Results from Time-History Analyses Using Simplified Models

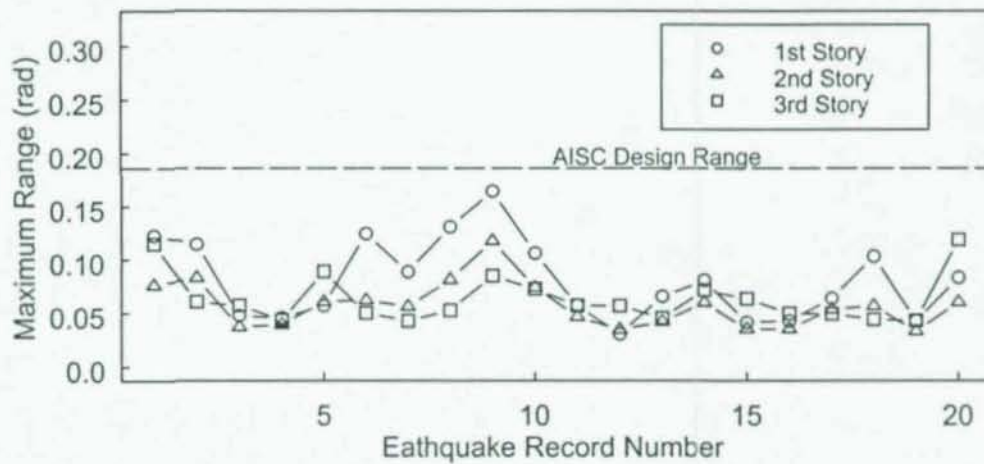
Models were developed using the simplified technique that Whittaker et al. (1987) used. The same data reduction techniques were used and results are presented in the following pages in the same manner as in the body of the report. Results are very similar, and the same loading protocol would be developed based on the simplified models.



(a) Total Number of Cycles

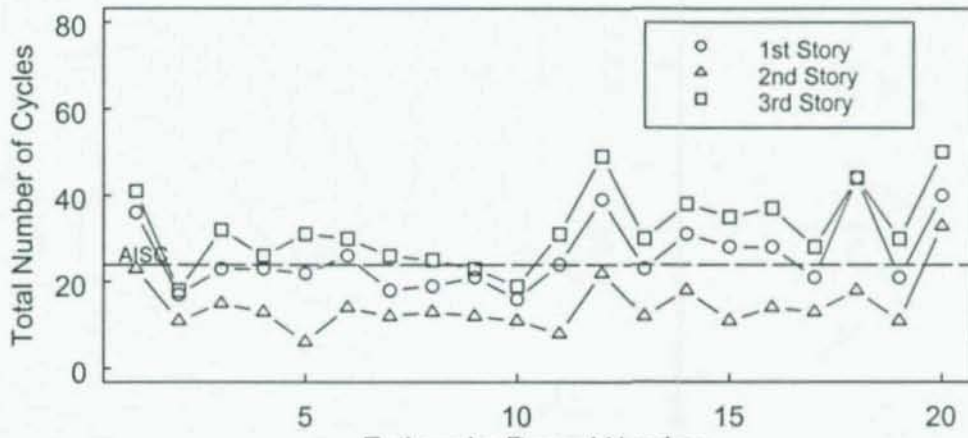


(b) Cumulative Range

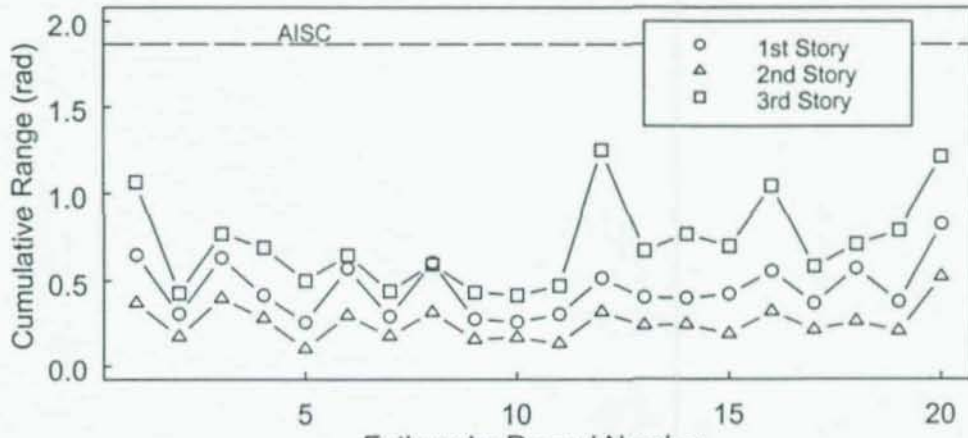


(c) Maximum Range

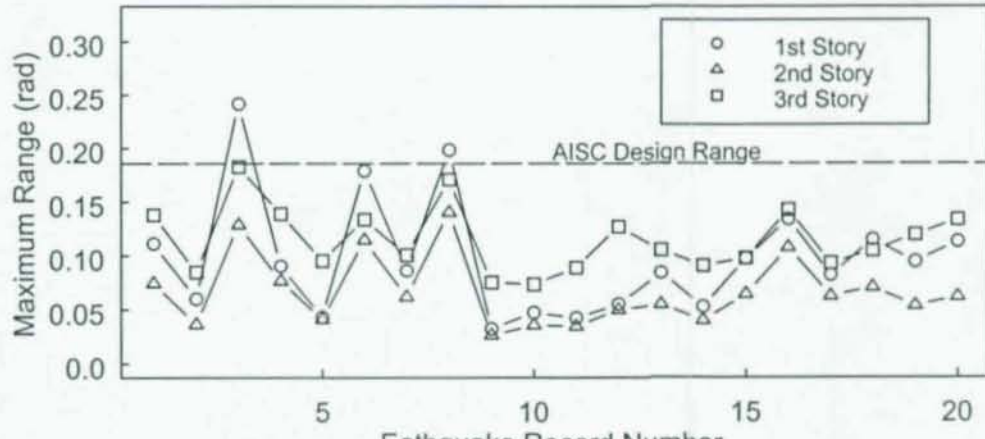
Figure A.1 Demand Parameter Values for Links in Frame 3L
(Cycles with Range > 0.0075 rad Considered)



(a) Total Number of Cycles



(b) Cumulative Range



(c) Maximum Range

Figure A.2 Demand Parameter Values for Links in Frame 3T
(Cycles with Range > 0.0075 rad Considered)

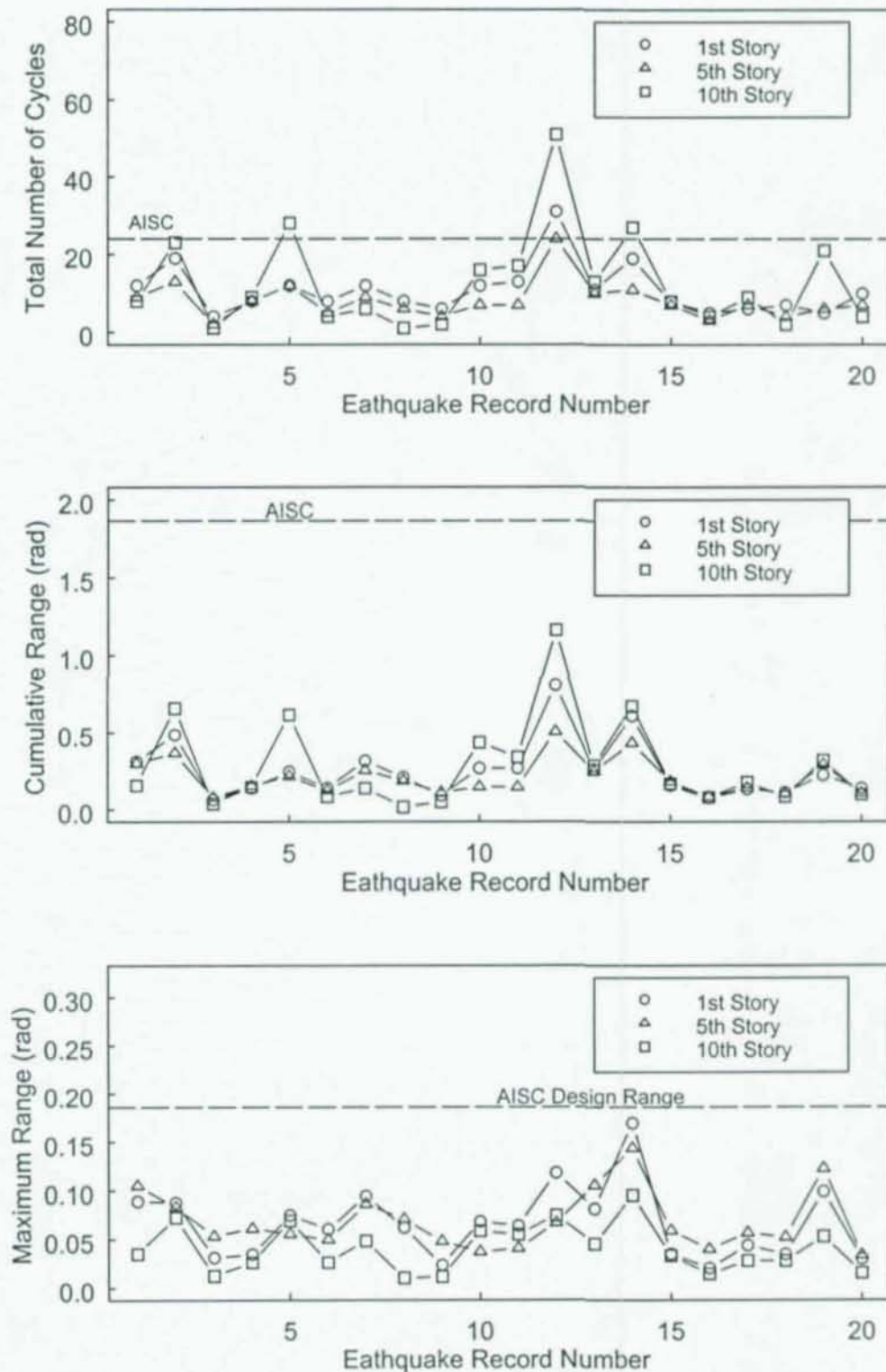


Figure A.3 Demand Parameter Values for Links in Frame 10
(Cycles with Range > 0.0075 rad Considered)

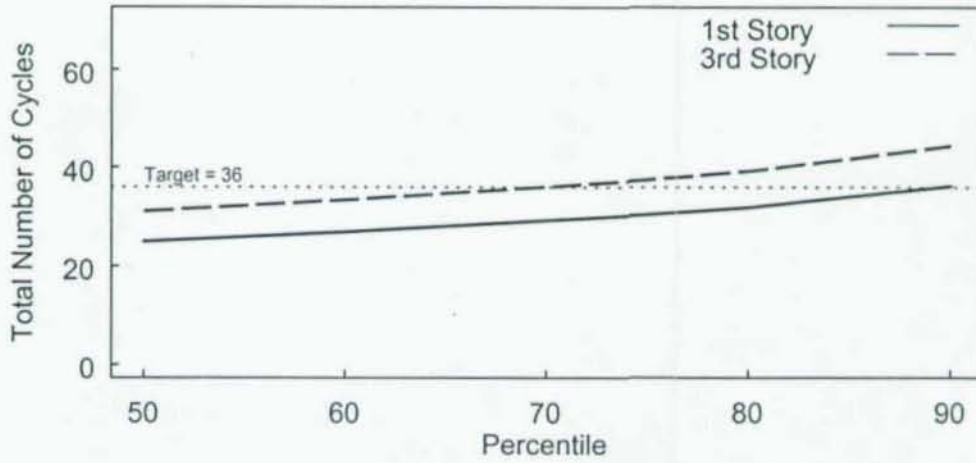


Figure A.4 Percentile Placing of the Total Number of Cycles, N_t
(Cycles with Range > 0.0075 rad)

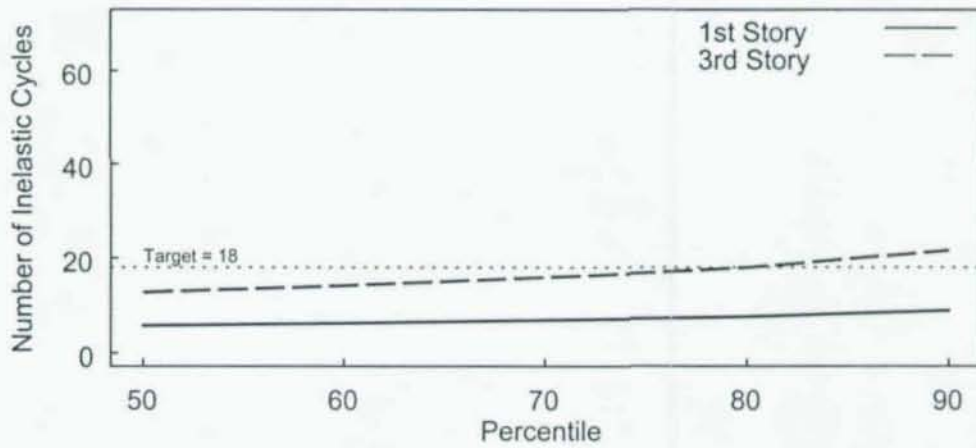


Figure A.5 Percentile Placing of the Number of Inelastic Cycles, N_p
(Cycles with Range > 0.015 rad)

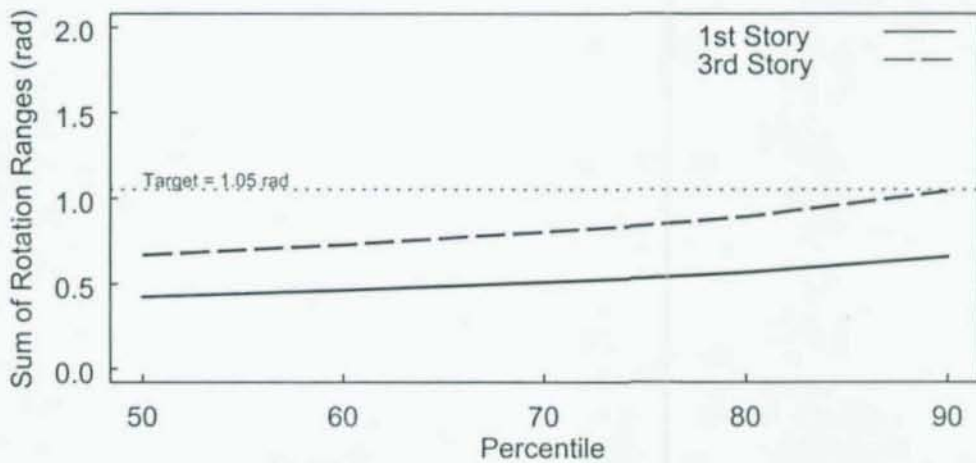


Figure A.6 Percentile Placing of the Sum of the Rotation Ranges, $\Sigma\Delta\gamma_i$
(Cycles with Range > 0.0075 rad)

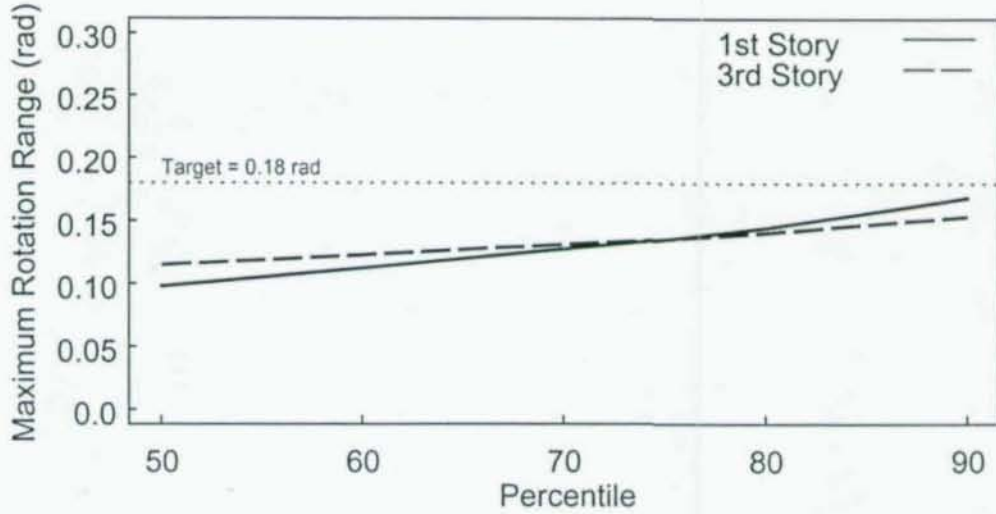


Figure A.7 Percentile Placing of the Maximum Rotation Range, $\Delta\gamma_{\max}$

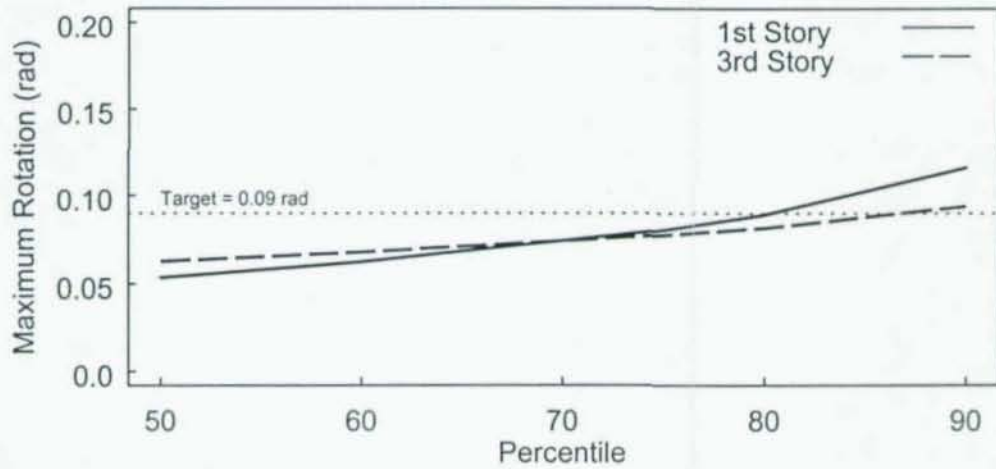


Figure A.8 Percentile Placing of the Maximum Rotation, γ_{\max}

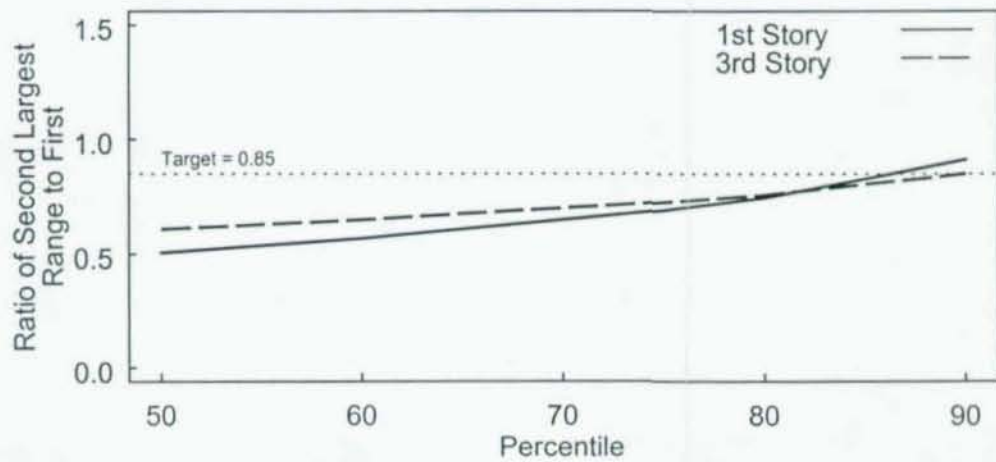


Figure A.9 Percentile Placing of the Ratio of $\Delta\gamma_2$ to $\Delta\gamma_{\max}$

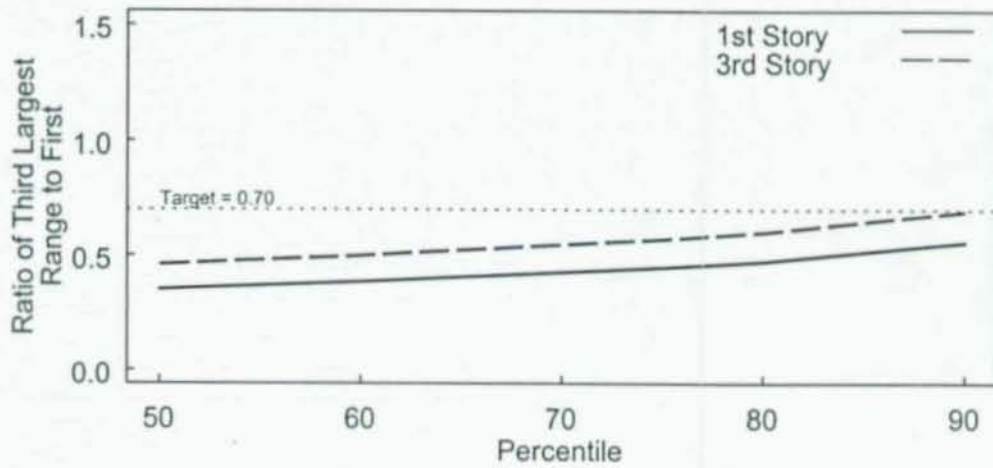


Figure A.10 Percentile Placing of the Ratio of $\Delta\gamma_3$ to $\Delta\gamma_{max}$

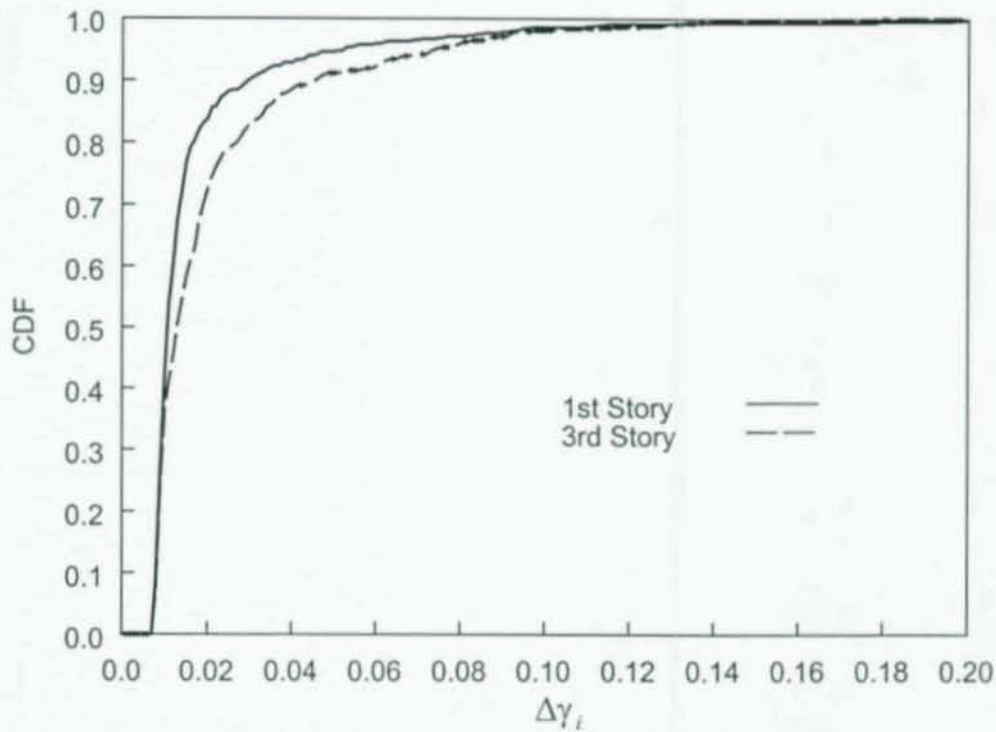


Figure A.11 Cumulative Distribution Function of Cycle Ranges, $\Delta\gamma_i$
 (Cycles with Range > 0.0075 rad, for Links in Frame 3T under all Ground Motions)

APPENDIX B—Results from Time-History Analyses Using SAC LA 10/50 Records

Analyses were also performed on the simplified models using the SAC Los Angeles ground motions with 10 percent probability of exceedance in 50 years. Figure B.1 shows these ground motions (already scaled for the SAC project) with name and PGA indicated in each plot. Figure B.2 shows the spectral accelerations with 2 percent damping. Also included in the plots is the 2 percent design spectra used in the study (see Section 2.4.1 and Figure 2.13).

Analysis results for the key parameters are shown for the three frames in Figures A.3 to A.5. Based on these plots, the 1st and 3rd story links in Frame 3T were the critical links. Figures A.6 to A.12 show the percentile values for the protocol parameters for the critical links. Figure A.13 shows the CDFs for the critical links. Table A.1 compares the target values obtained from these results with those from the runs under the PEER records (see Section 3.3.2). The PEER records resulted in a higher number of cycles, both elastic and inelastic, but the cumulative range was only slightly higher.

The significant difference between the SAC records and the PEER suite was the presence of near fault records in the SAC suite. This resulted in high 90th percentile values for $\Delta\gamma_{\max}$ and γ_{\max} . These secondary protocol parameters would end up being dictated by the design range of the links (0.18 rad), so very similar protocols would have developed from the SAC and PEER data.

Table B.1 Comparing Protocol Demands with Target Values

Protocol Demand Parameter	PEER Records	SAC Records
N_t	36 cycles	32 cycles
N_p^a	18 cycles	15 cycles
$\Sigma\Delta\gamma_i$	1.10 rad	1.02
$\Delta\gamma_{\max}$	0.18 rad	0.18
γ_{\max}	0.09 rad	0.09
$\Delta\gamma_2$	0.10 rad	0.14
$\Delta\gamma_3$	0.08 rad	0.10
$\Delta\gamma_i$	CDF (Figure 3.11)	CDF (Figure B.13)

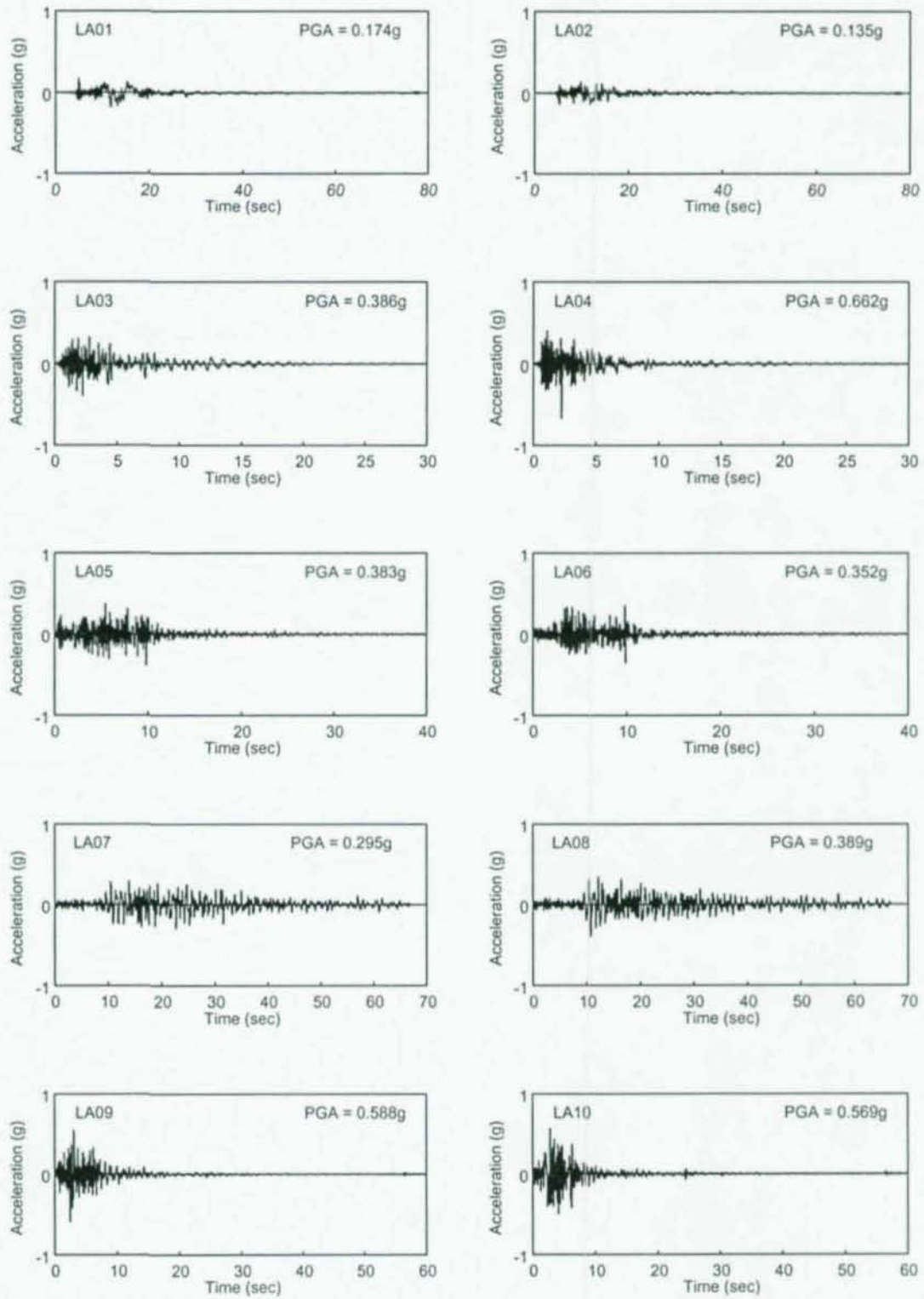


Figure B.1 SAC Los Angeles 10/50 Ground Motion Acceleration Time Histories

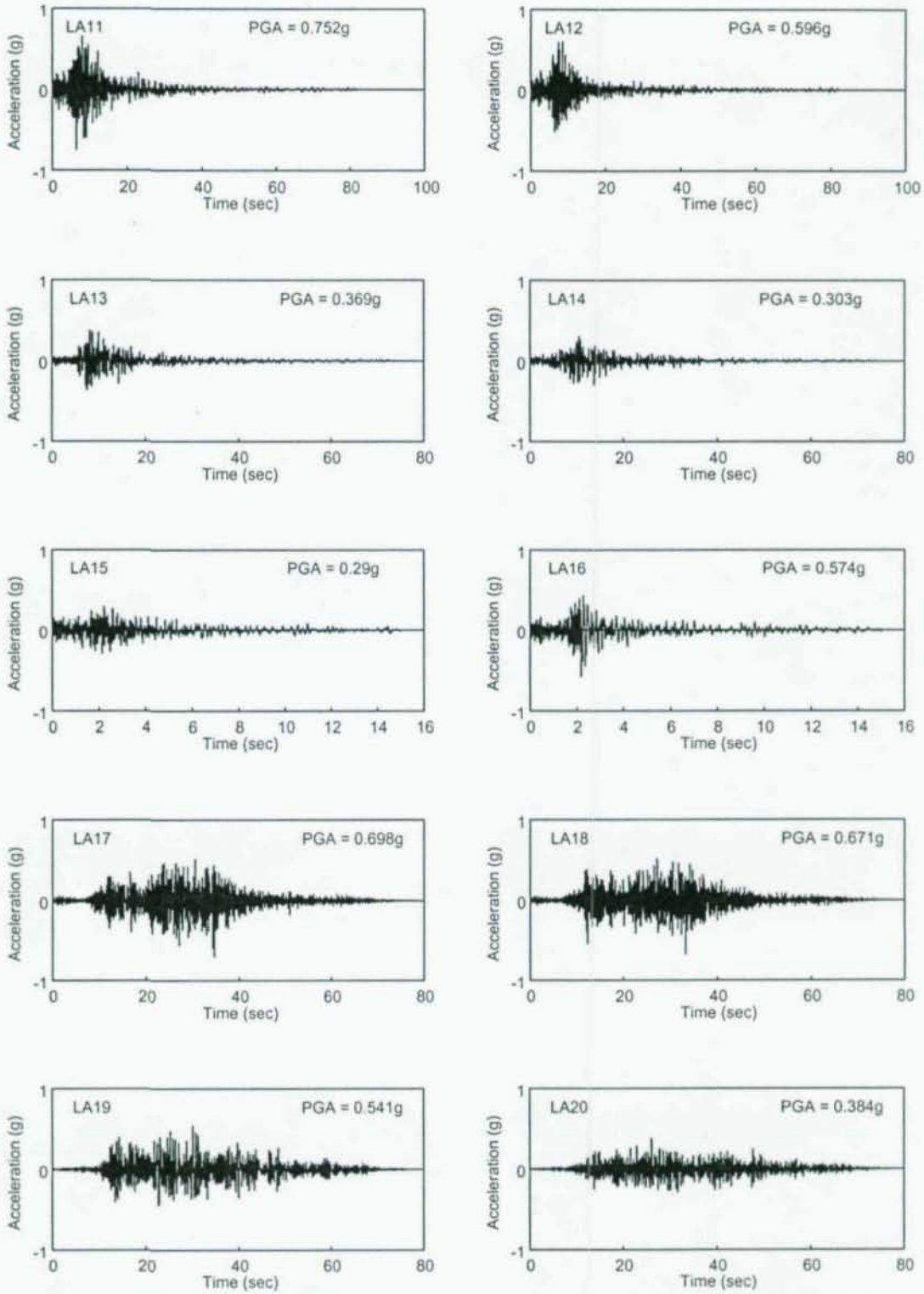


Figure B.1 SAC Los Angeles 10/50 Ground Motion Acceleration Time Histories (con't)

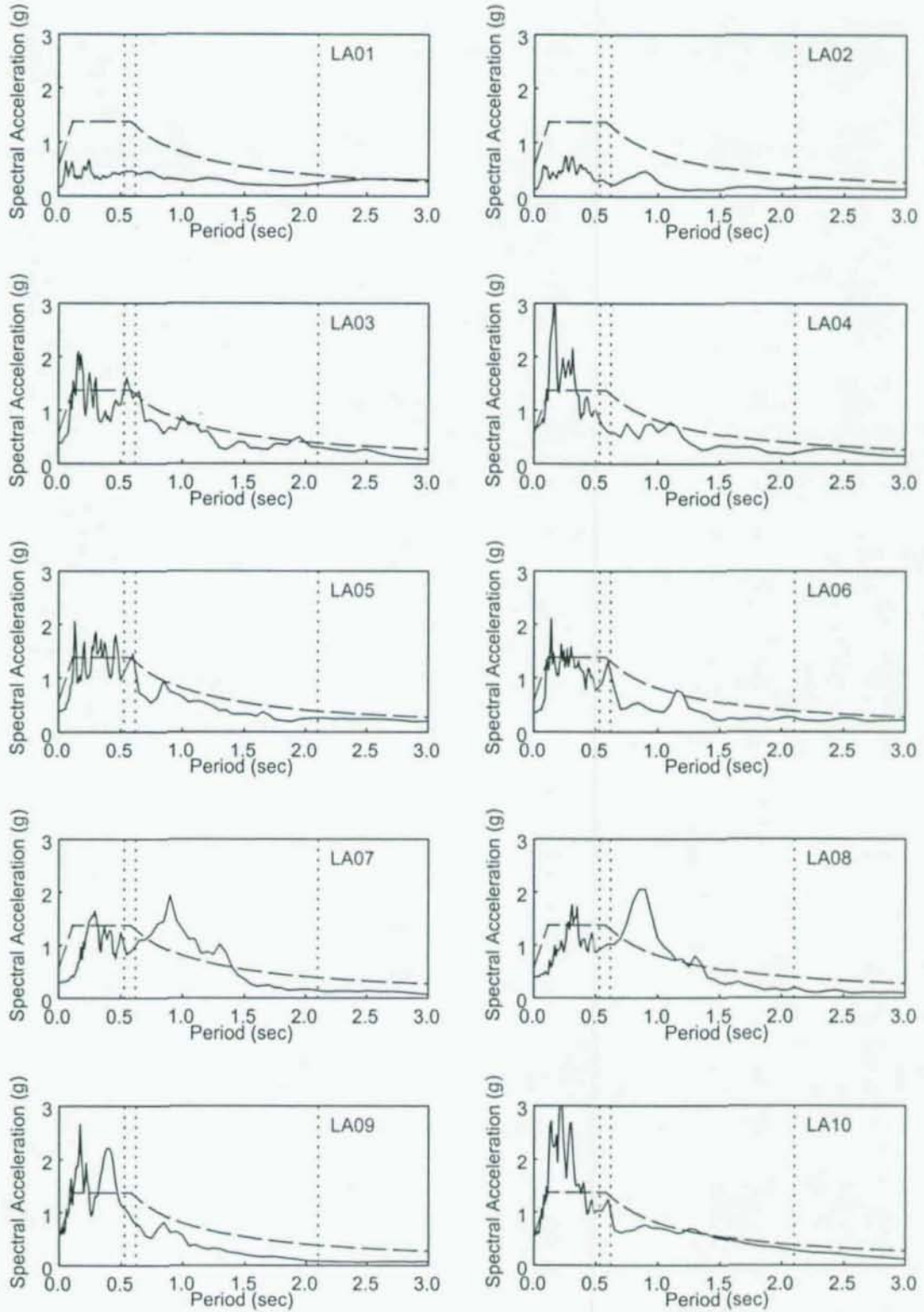


Figure B.2 Response Spectra for SAC Los Angeles Ground Motions (2 percent damping)

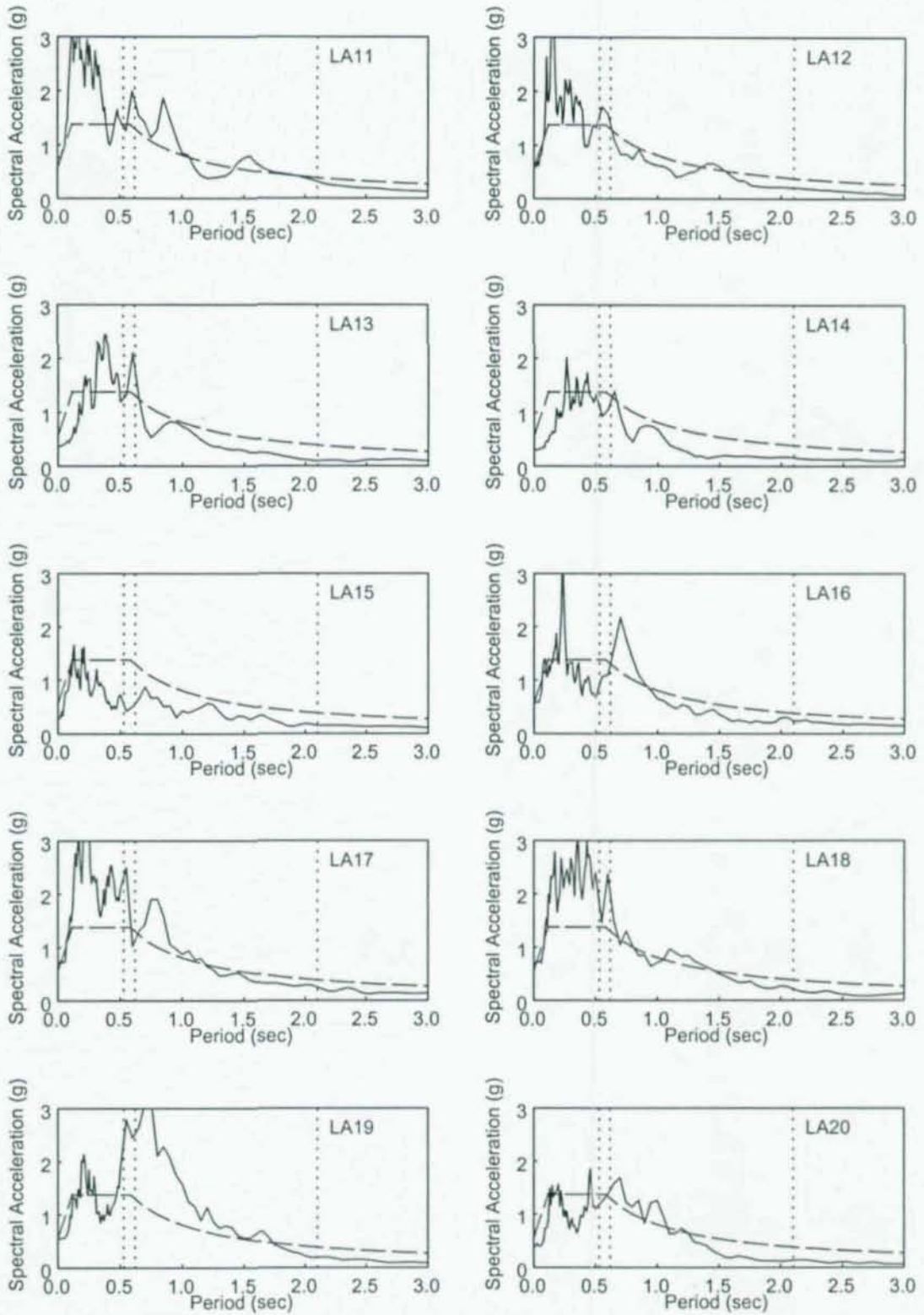
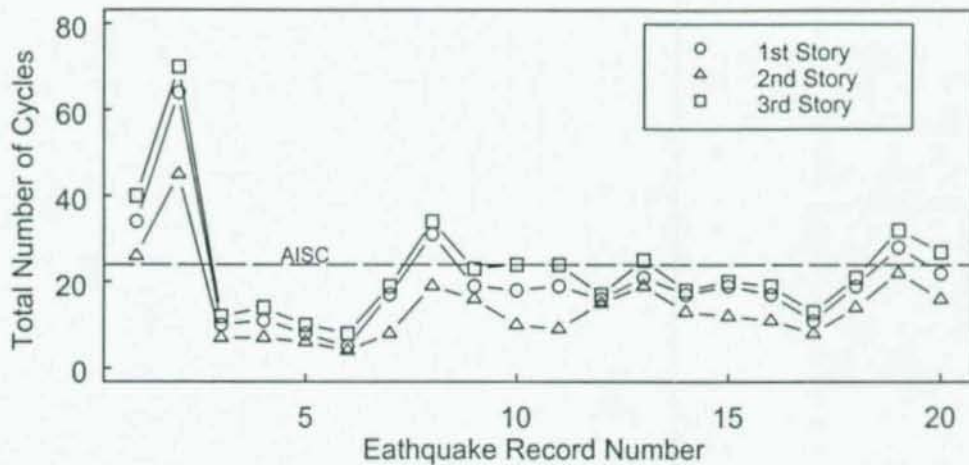
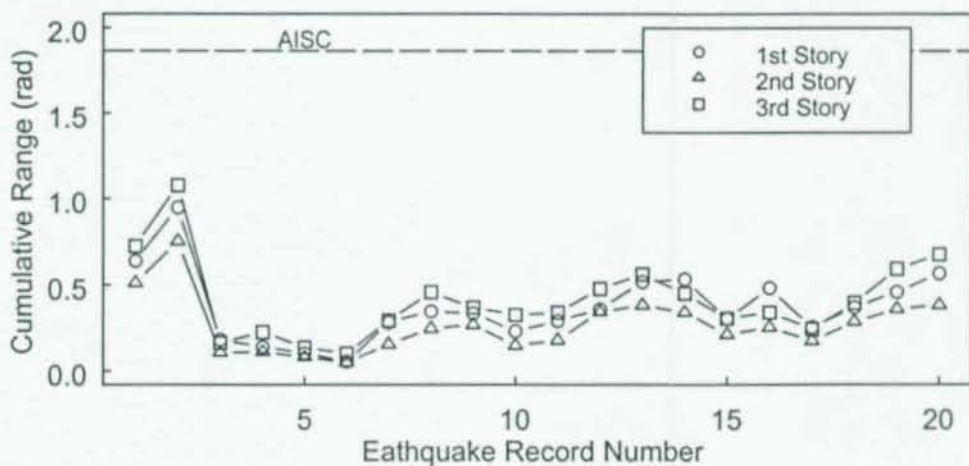


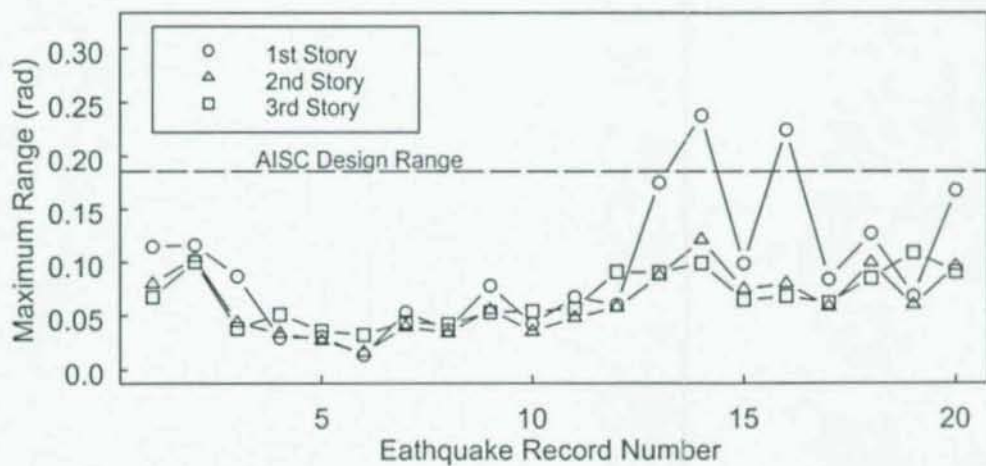
Figure B.2 Response Spectra for SAC Los Angeles Ground Motions (con't)



(a) Total Number of Cycles



(b) Cumulative Range



(c) Maximum Range

Figure B.3 Demand Parameter Values for Links in Frame 3L
(Cycles with Range > 0.0075 rad Considered)

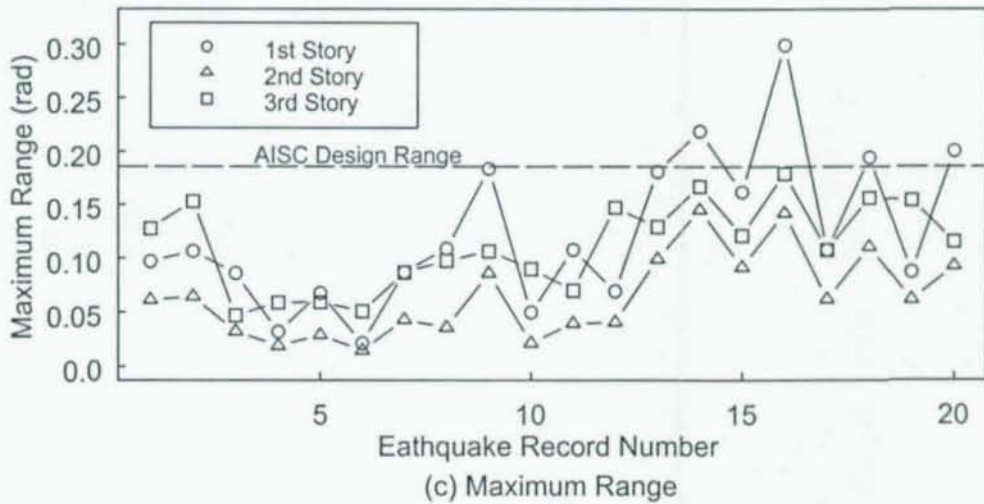
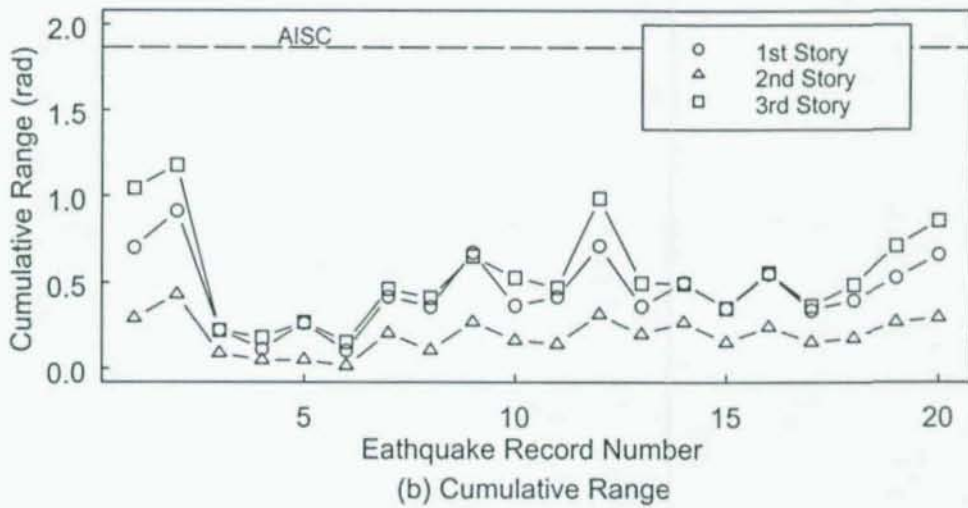
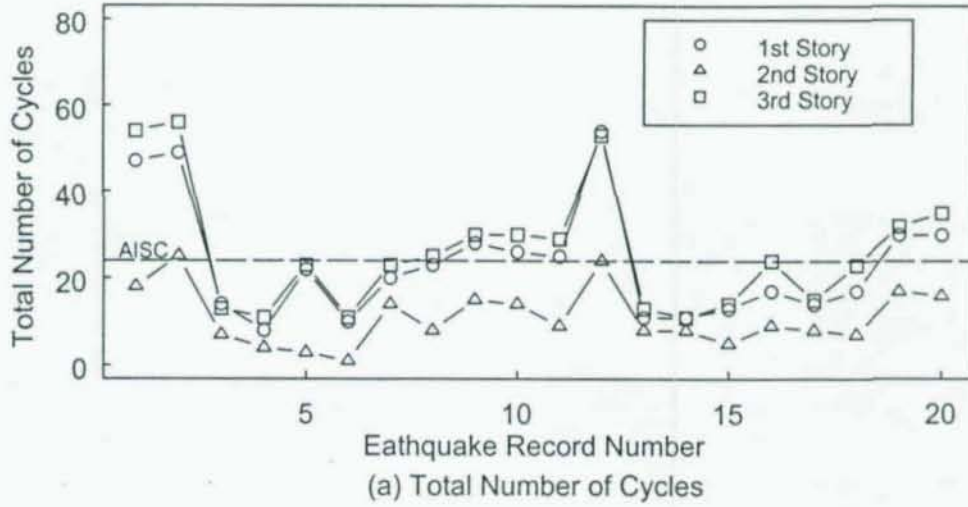


Figure B.4 Demand Parameter Values for Links in Frame 3T
(Cycles with Range > 0.0075 rad Considered)

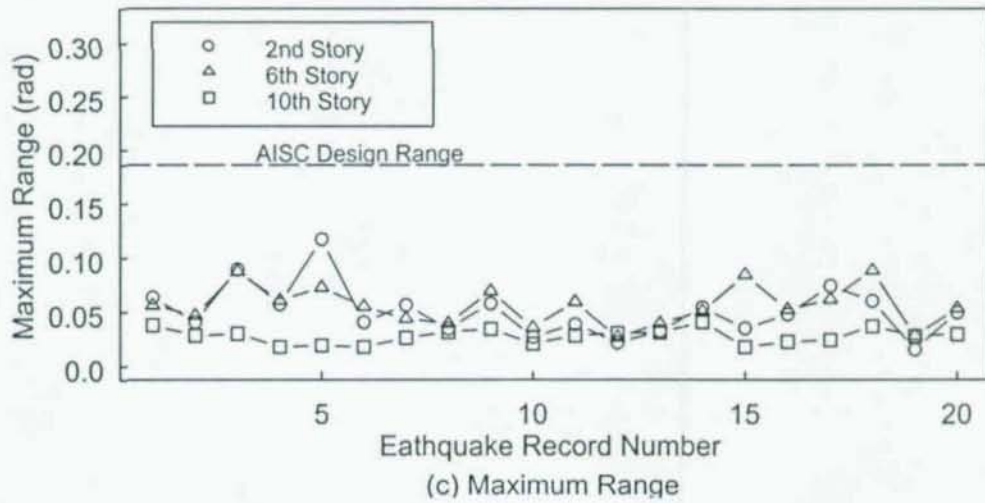
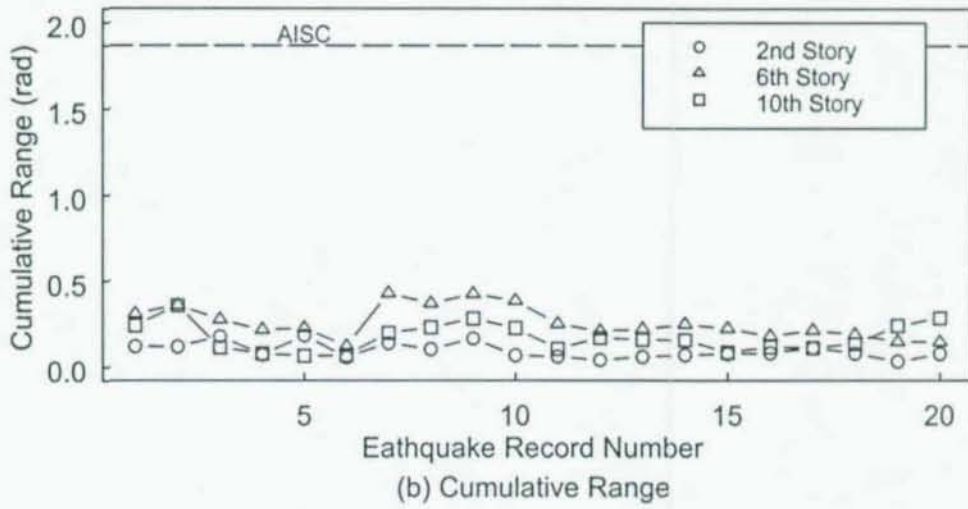
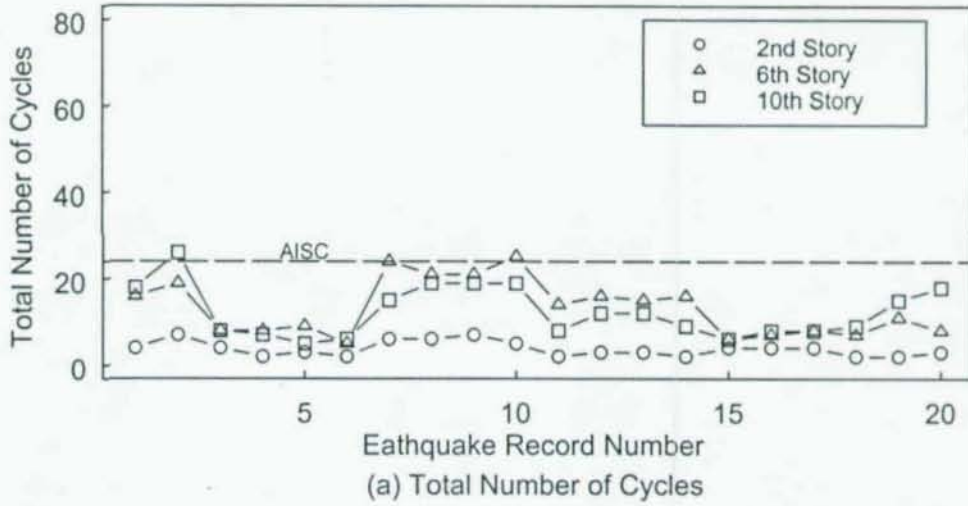


Figure B.5 Demand Parameter Values for Links in Frame 10
(Cycles with Range > 0.0075 rad Considered)

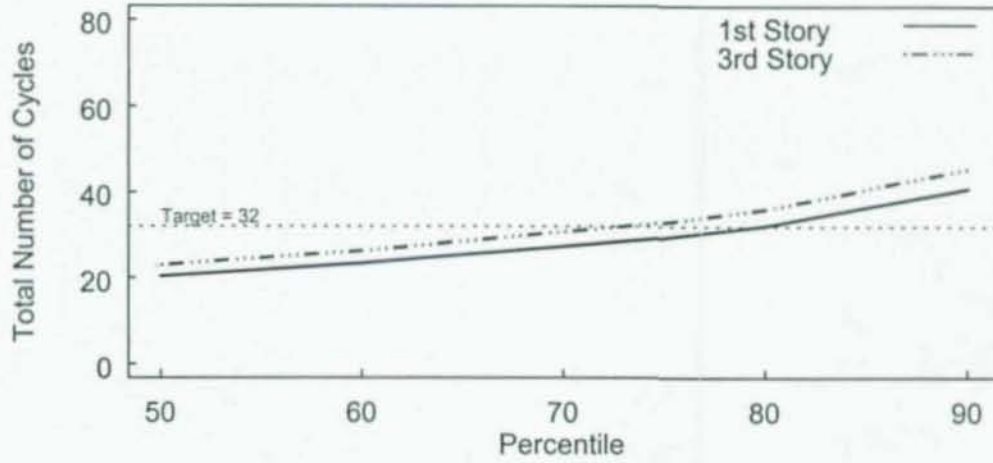


Figure B.6 Percentile Placing of the Total Number of Cycles, N_t

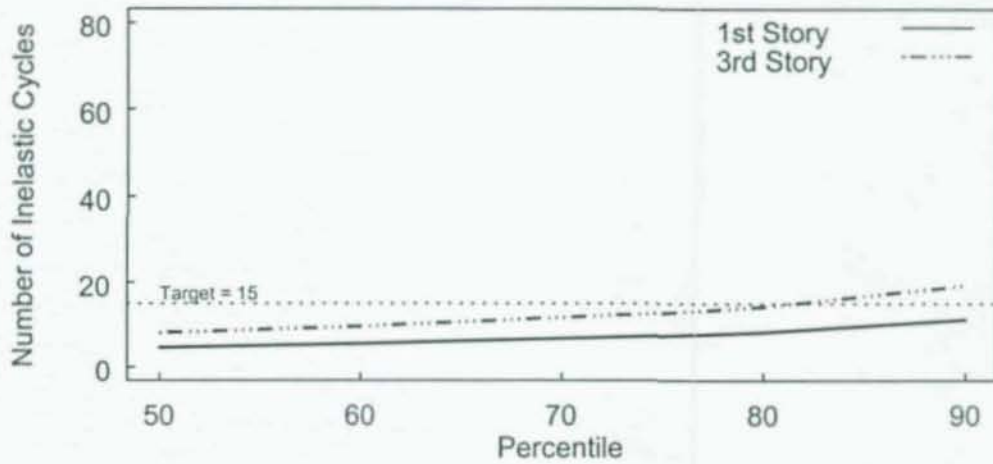


Figure B.7 Percentile Placing of the Number of Inelastic Cycles, N_p

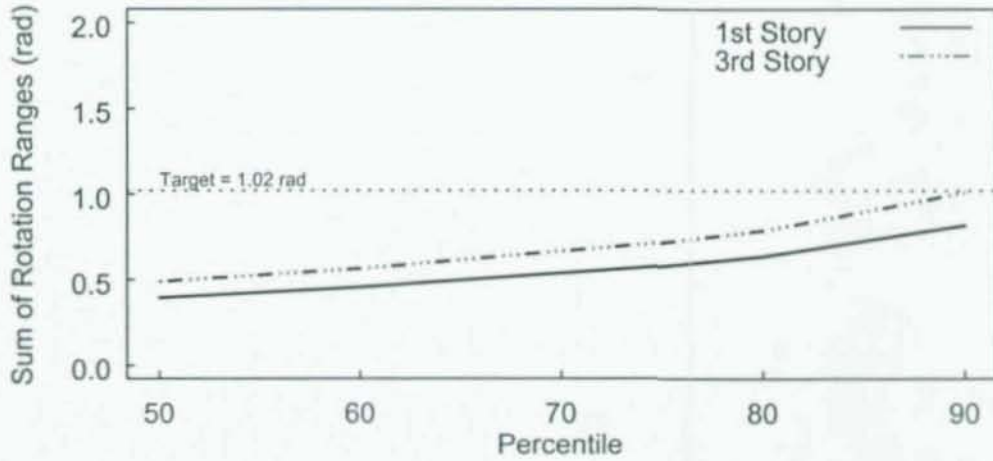


Figure B.8 Percentile Placing of the Sum of the Rotation Ranges, $\Sigma\Delta\gamma_i$

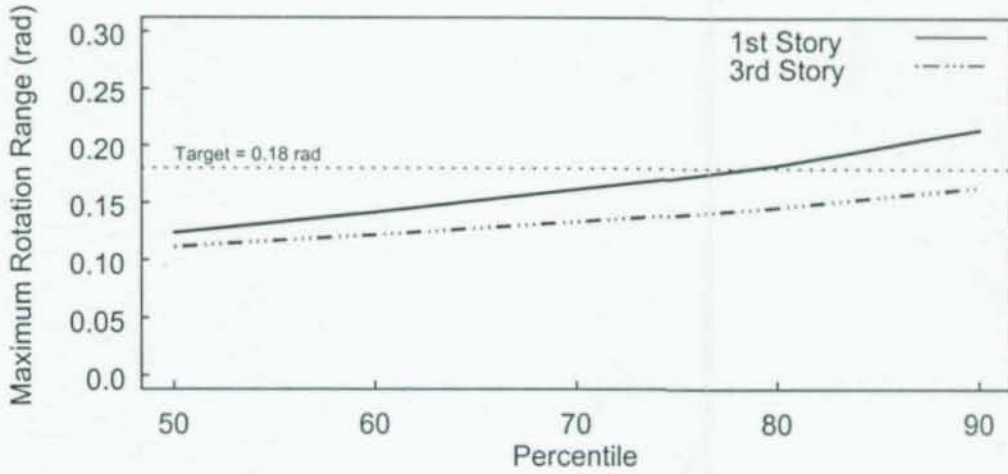


Figure B.9 Percentile Placing of the Maximum Rotation Range, $\Delta\gamma_{max}$

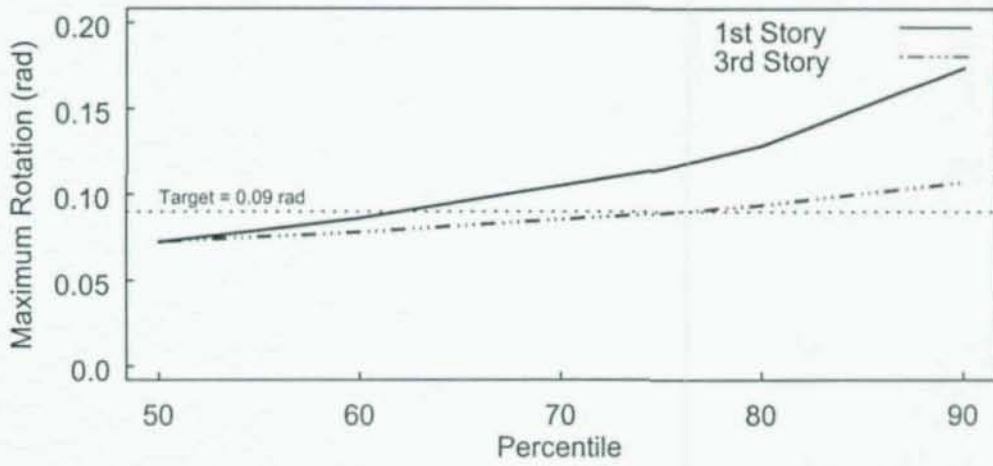


Figure B.10 Percentile Placing of the Maximum Rotation, γ_{max}

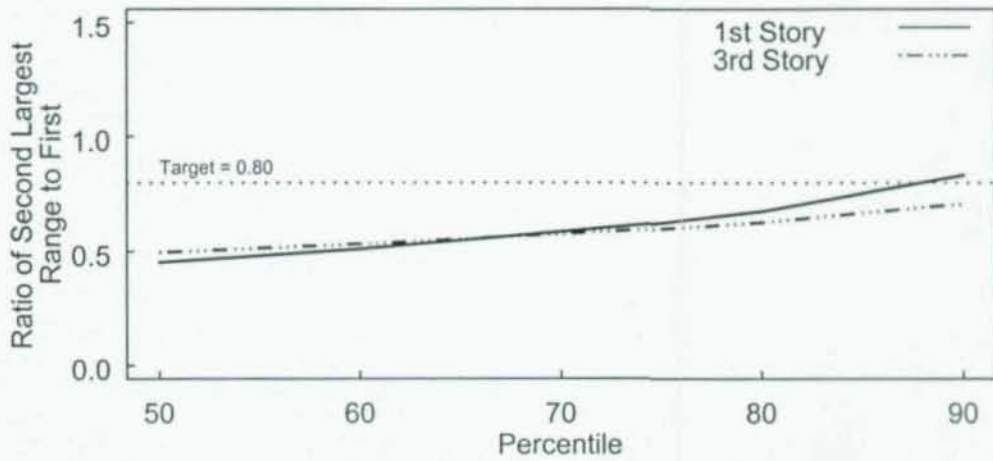


Figure B.11 Percentile Placing of the Ratio of $\Delta\gamma_2$ to $\Delta\gamma_{max}$

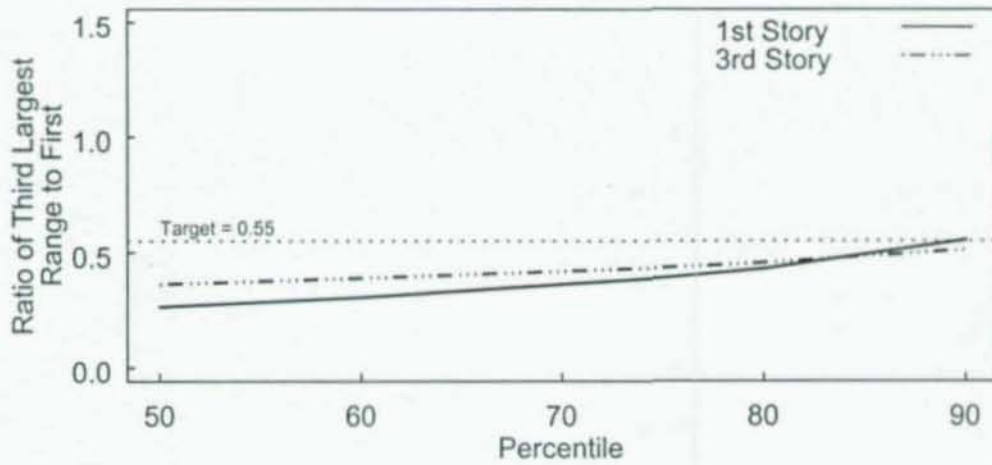


Figure B.12 Percentile Placing of the Ratio of $\Delta\gamma_3$ to $\Delta\gamma_{max}$

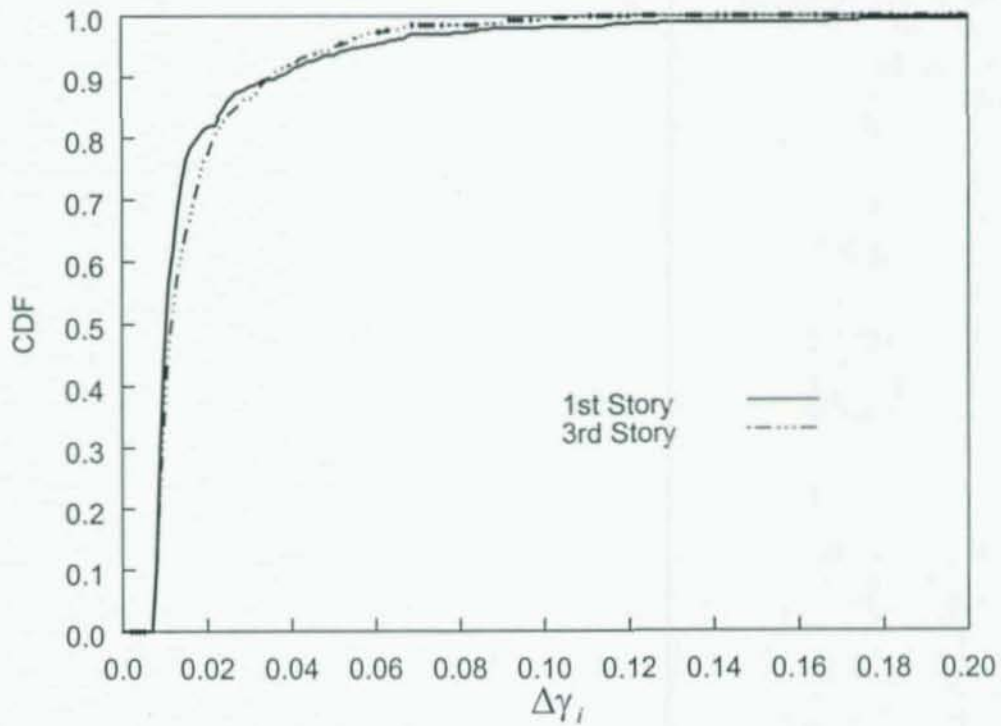


Figure B.13 Cumulative Distribution Function of Cycle Ranges, $\Delta\gamma_i$,
(Cycles with Range > 0.0075 rad, for Links in Frame 3T under all Ground Motions)

APPENDIX C–Rainflow Cycle Counting Procedure

Cycle counting is needed to convert a link rotation time history into a series of cycles from which a loading history can be developed. The rainflow cycle counting procedure used in this study (Krawinkler et al. 2000) is described below and illustrated in an example.

1. First the rotation time history is drawn so as to begin and end at the greatest rotation, to eliminate the counting of half cycles,. This is done by moving the portion of the time history that follows the maximum amplitude point to the front of the history. The end of the original time history is then artificially connected to the beginning of the time history [implications discussed in Krawinkler et al. (2000).]
2. All of the peaks and valleys are identified in the time history.
3. Cycle counting starts at the beginning of the time history. Once a cycle is counted and recorded, the peak and valley associated with the cycle are not considered for further cycle counting purposes. A cycle is counted when the *second range* in a peak-valley-peak or valley-peak-valley combination is *greater than the first range*. The cycle counted is defined by the *first* peak-valley or valley-peak combination (see example on next page). The range of the cycle is the difference in rotation between the peak and valley. The mean value associated with the cycle is the average of the rotation values at the peak and valley associated with the cycles. Counting continues from left to right and starts again at the beginning when the end is reached. Counting continues until the entire history is exhausted.
4. Cycles are arranged from greatest range to least. Mean effects are not considered for basic loading history development, so symmetric cycles result.

An example of the rainflow cycle counting technique follows. A short rotation time history with some residual drift is shown below in Figure C.1.

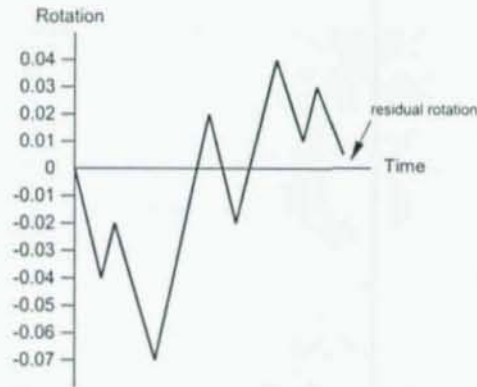


Figure C.1 Example Rotation Time History

In Step 1, the part of the history following the maximum rotation is identified and moved to the beginning (Figure C.2). The original end of the record is artificially connected to the original beginning of the record.

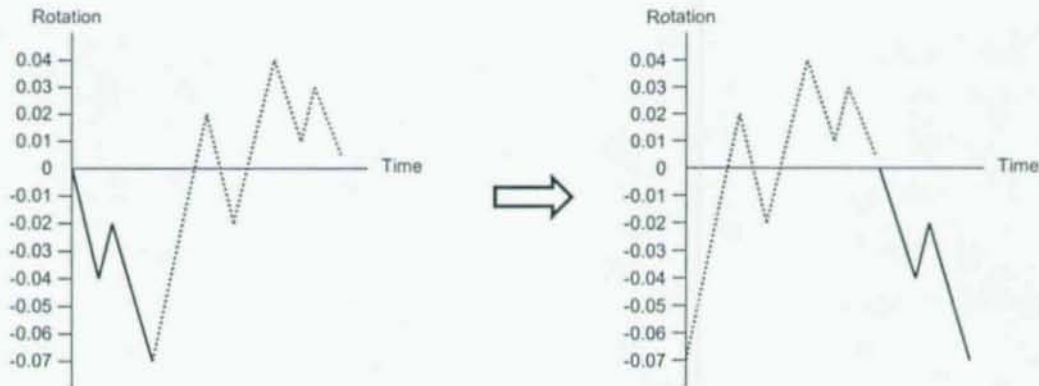


Figure C.2 Reordering Rotation Time History

In Step 2 peaks and valleys are identified (Figure C.3).

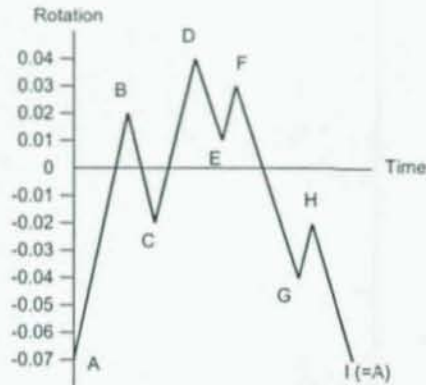


Figure C.3 Identification of Peaks and Valleys

In Step 3, cycles are counted as the record is read from left to right. The first peak-valley-peak or valley-peak-valley combination to be read is A-B-C. Since the second leg of the combination B-C is *not* greater than or equal to A-B, *no* cycle is counted (Figure C.4). The next peak-valley-peak or valley-peak-valley to be considered is B-C-D. Since second leg D-C is *greater* than the first leg B-C, the cycle B-C is counted, and points B and C are not considered anymore. Similarly, continuing to the right, cycle E-F is counted since F-G is greater than or equal to E-F; and cycle G-H is counted since H-I is greater than or equal to G-H.

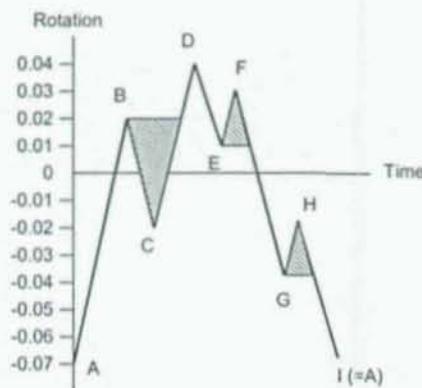


Figure C.4 Counting Cycles in Record

After reading through the record once, and removing the peaks and valleys that were "counted", the only remaining points are A, D, and I (Figure C.5). When the record is read a second time, cycle A-D is counted since D-I is greater than or equal to D-A. Since there are no peak-valley-peak or valley-peak-valley combinations remaining, the record is exhausted and the process is finished.

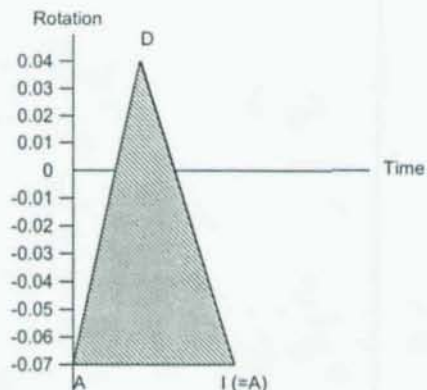


Figure C.5 Counting Final Cycle

The results of the cycle counting are tabulated, with cycles arranged from greatest range to least as shown in Table C.1. The ranges define the resulting cycles. For a basic loading history mean effects are not considered, so the set of cycles are symmetric (mean value of zero). Figure C.6 shows the resulting symmetric cycles from the original time history. The maximum rotation (0.05 rad) is equal to half of the maximum range (0.11 rad).

Table C. 1 Rainflow Counting Results

Cycle No.	Range (rad)	Mean (rad)
1 (A-D)	0.11	-0.015
2 (B-C)	0.04	0.0
3 (E-F)	0.02	0.02
4 (G-H)	0.02	-0.03

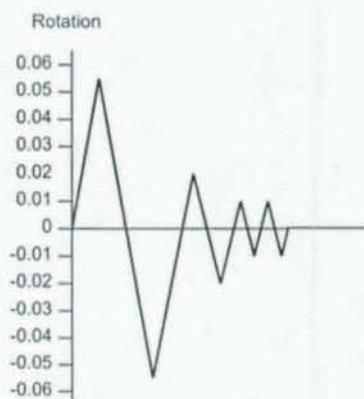


Figure C.6 Resulting Symmetric Cycles from Rainflow Counting

01005